AFCRL-66-211

AD631046

AFCRL-66-211

61(052)-490

December 1965

FINAL SCIENTIFIC REPORT

ON THE PROPAGATION OF VLF WAVES IN SOLIDS

DR. W. BITTERLICH

INNSBRUCK

AUSTRIA

The research reported in this document has been sponsored by the:

UNITED STATES GOVERNMENT

under Contract 61(052)-490

ZUSAMMENFASSUNG

In diesem Bericht wird in Experiment und Theorie die Art der Ausbreitung von VLF-Wellen im festen Medium für das Nahfeld und die anschließende Übergangszone zum Fernfeld beschrieben.

Die maßgebenden Parameter σ (Leitfähigkeit) und ε (Dielektrizitätskonstante) werden durch unabhängige Meßverfahren bestimmt. Die notwendigen, vielfach selbst konstruierten Geräte werden beschrieben. Durch eine Vielzahl von Messungen in geologisch verschiedenen Gebieten wird die Theorie des strahlenden magnetischen Dipols überprüft und modifiziert.

ABSTRACT

In the present report, the propagation of VLF waves in solid media is described by theory and experiment for the near field and for the subsequent transition zone to the far field.

The decisive parameters σ (conductivity) and ε (dielectric constant) are determined by independent methods of measurement. The required instruments, largely designed by our team, are described. The theory of a magnetic transmitting dipole is checked and modified by a number of measurements in regions of different geological conditions.

TABLE OF CONTENTS

INTRODUCTION

The propagation of electromagnetic waves in air, i.e., in the earth - ionosphere cavity as well as outside the ionosphere has been studied sufficiently in the region from long waves to ultrashort waves. Also the studies on the propagation mechanism of very long (VLF) to extremely long (ELF) waves in the atmosphere have almost been concluded in the past few years. The behavior of VLF waves passing through homogeneous or inhomogeneous media was studied only as far as these problems were of geophysical interest. The studied frequencies mainly lay in the long wave region or short wave region, i.e., at frequencies above 50 kcps.

The VLF project Dr. W. Bitterlich which was founded in autumn 1960 under the sponsorship of the US Government, had the aim of studying the propagation mechanism of long electromagnetic waves (< 20 kcps) passing through the interior of the earth. At the same time the resulting possibilities of underground communication had to be studied as well as the possibilities of their practical application in geophysics, geology and mining.

The present report gives a review of all VLF studies made between December 1960 and December 1965. The principal directions of this work were the following:

1. Investigation of the propagation of VLF waves in rock by means of our own transmitters; preferred frequencies: 3 and 10 kcps. The field strengths of measuring distances given at various points were determined and evaluated as functions of the transmitter - receiver distance and the angle of direction of the axes of transmitting antennas and receiving antennas.
2. Studies of the penetration of electromagnetic waves of remote VLF transmitters into the ground.
3. The directivity pattern of a magnetic dipole was determined as a function of conductivity of the surrounding medium of

the transmitter - receiver distance and of the frequency.

4. Determination of the electrical conductivity of natural rock with various direct current and alternating current methods by direct contact, and studies on the frequency dependence of the dielectric constant of rock samples.
5. Detailed theoretical studies of problems regarding pos. 1-4.

At the end of the present report, the titles of the previous 16 Scientific Reports are given as well as the tables of contents of the four Technical Annual Summary Reports.

During the entire period of project work, Dr. O. Gröbner, Dr. O Wörz, W. Gradl, G. Tinhofer and N. Nessler were my closest collaborators. The above gentlemen contributed decisively to the results and I herewith thank them cordially for their collaboration.

The measurements in the mines were made possible owing to the generious support by Bergrat Dipl. Ing. P. Kettner, Director of the Montanwerke Brixlegg who permitted us the establishment of a mine laboratory, and the friendly assistance of the Berghauptmannschaft of the province of Tyrol. Let me now express my sincere gratitude to the concerned gentlemen and above all to Univ. Prof. Dr. R. Steinmaurer, Head of the Physics Institute of the University of Innsbruck.

December 1965

Dr. Wolfram Bitterlich

1. Apparatus

1.1. General information

At the beginning of our studies in 1961, a considerable number of instruments that are now being produced in series were not on the market. Especially battery-fed power amplifiers of low weight and high efficiency as well as mains-independent selective level meters for the VLF region were not available. We therefore had to rely on our own developments and special designs. The development and testing of suitable, i.e., small antennas required great efforts in time and work.

Instruments used for measurements below ground are exposed to much harder conditions than those used in the laboratory. Transportation to the sites of measurement is troublesome, as it is only in the main galleries that instruments can be transported with a mine railway, and even there they are exposed to hard shocks and rough handling. The actual region of measurement should be far away from tracks, tubes and cables, it is therefore only accessible on foot through rather difficult terrain. Occasionally, remote sites are only reached by means of ladders, manshafts or by crawling. The extremely high water content in the atmosphere (100%, numerous galleries are dripping wet with water running over the bottom of the gallery) makes special demands to insulation and anticorrosion.

From these requirements result the partly contradictory conditions for developing and constructing special instruments for our experiments. The devices must be strong, shockproof, protected against dripping water and provided with a waterproof base. Yet they must be light and sufficiently small or collapsible as to pass through narrow passages in the form of single parts.

1.2. Transmitter

In order to make the efficiency as high as possible, we used transistorized push-pull amplifiers, except for a preliminary LF experiment. Fig. 1.1 shows the device used for our final measurements. A transistorized RC generator serves as an oscillator. The driver is designed as usual. The output-stage in C-operation works on an autotransformator, thus keeping the transfer losses low and yet offering a good possibility of antenna adaptation. The attained compensating power was 50 w, the cut-off frequency was 10 kcps. The antenna current is indicated on a built-in instrument via a control transformer. For tuning the antenna, a multistage capacitor is built in which consists of mica capacitors with a maximum dielectric strength of 2000 volts. In order to protect the power transistors against voltage peaks that may occur at the moment when the antenna is switched over, the collectors are short-circuited with powerful silicon diodes as limiters.

Because of the weight restriction of the individual parts, the available battery capacitance is limited to about 75 ah. With an output of approximately 50 w and an efficiency of about 50% we have a working time of 7 hours which is quite sufficient for long-time experiments (description see [3]).

For attaining a higher transmitter power, we have set up a 1 kw - IF amplifier (Bryan Savage) type KM2Z in our laboratory in the mine of St. Gertraudi. The amplifier has a frequency ranging from 20 cps to 10 kcps at full output. The matching impedance can be chosen between 0.6 and 40 Ω.

In order to extend the frequency range toward higher values we used a stereoamplifier (McIntosh) type MC275 for our recent measurements. It has an output of 150 w up to 40 kcps and 75 w up to 100 kcps, with change-over output impedances of 4 to 600 Ω.

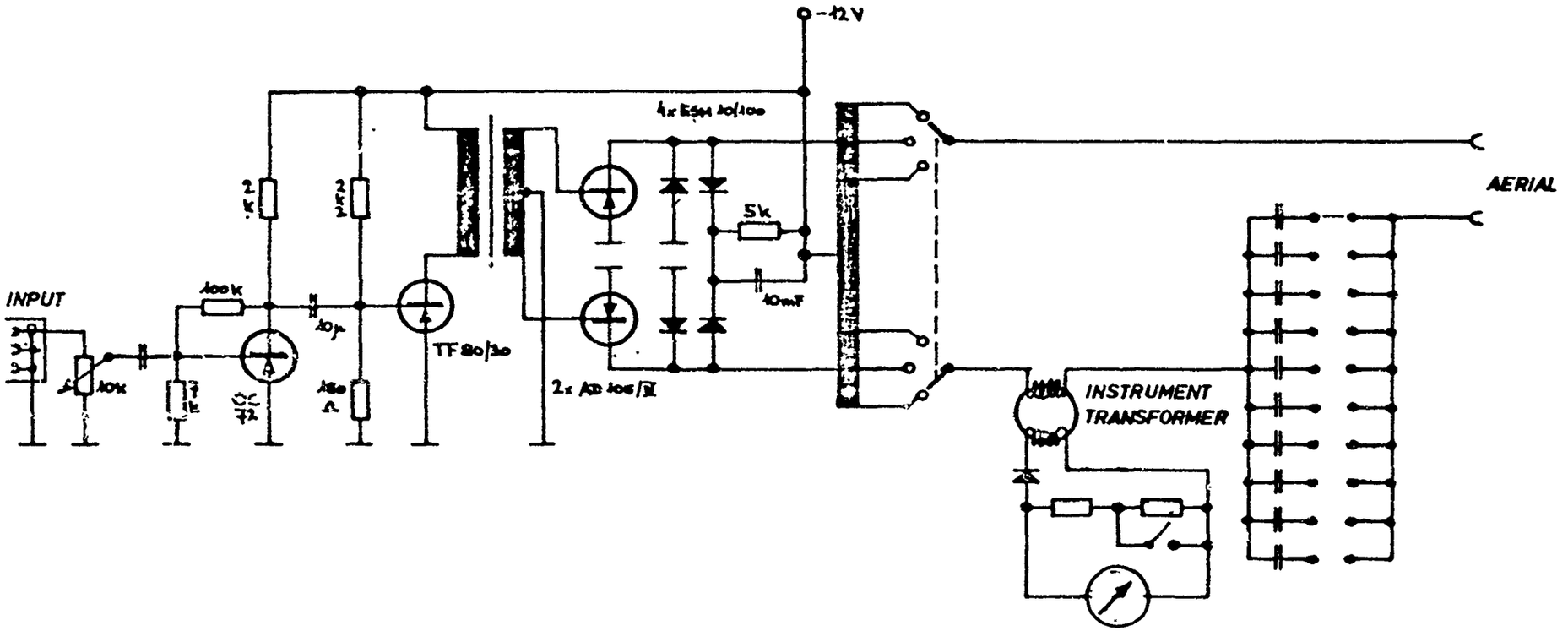

TRANSMITTER

FIG. 1.1

1.3. Transmitting antennas

Based upon practical and theoretical considerations, especially with respect to power adaptation and dimensions, we have used magnetic dipoles as transmitting antennas right from the beginning ([1] chapter 1.2 and 1.3, [3] chapter 2.3, [24]). At first, rod antennas with iron cores made of transformer sheet metal with center-tapped windings, were connected directly to the power transistors of the push-pull stage without output transformer. The magnetic moment of this array, however, was too small because of the small turn-area. We therefore used air coils with possibly large diameters instead of the above coils. As described in [1] , they were chosen in accordance with the given power of amplifier and the possible weights and dimensions.

Data of the transmitting antennas that were specially suited for propagation measurements:

SA VI [2] square frame, area 1.4 m^2.
60 turns of copper-stranded wire, 2.5 mm^2 cross section, 15 mH, 2.1 Ω.
In this antenna, the copper-stranded wire is welded as a bunch in a flexible plastic hose. Thus, the winding can be removed from the frame and folded up, the frame itself being collapsible. Transportation of the antenna is thus very easy. The majority of measurements with this antenna were made by means of a battery-fed transmitter, above all those in the German and Dutch mines (cf. chapter 2).

SA VII [3] Rectangular frame, area 17 m^2.
2 x 15 turns, 1.5 mm^2 copper-stranded wire, 12 mH, 13.5 Ω. This antenna is suspended in the "Bunte Kluft" in the St. Gertraudi mine and can be rotated about its vertical axis. It has been used for numerous measurements with the 1 kw transmitter.

SA VIII [3] An approximately square loop having an area of 1600 m^2, 3 turns, 2.5 mm^2 copper, 20 mH, 3 Ω. In order to attain these dimensions, the antenna had to be firmly established at a suitable site at St. Gertraudi in two shafts with a vertical distance of approximately 40 m and in two connecting galleries having a vertical interval of 40 m.

SA IX As described in [4], the SA VIII had been reconstructed. The number of turns was increased to 10 and the cross section to 135 mm^2 (aluminum). Thus it was possible to get antenna currents of up to 40 a.

The transmitting antennas were tuned to series resonance so that the apparent power can be reached by means of the tuning capacitor, thus only the active power (which almost completely was consumed in the wire in the form of ohmic losses) being attained by the transmitter. Because of the necessary alternating voltage strength and the high reactive currents, mica capacitors were used for lower powers and oil capacitors for the 1 kw amplifier.

1.4. Field strength meters

In order to keep the dimensions and weights as low as possible, only transistorized receivers were developed [1 - 4]. Figs. 1.2 - 1.5 show the circuit of a highly suited instrument. The input stage is equipped with two low-noise transistors in emitter circuit and a silicon transistor in collector circuit, serving as impedance transformer for the stage attenuator. The input voltage on the first transistor is limited to a maximum of approximately 100 mv by means of the OA 71 diodes in order to avoid overloading of the input stage. The range of measurement is switched over with S 1 .

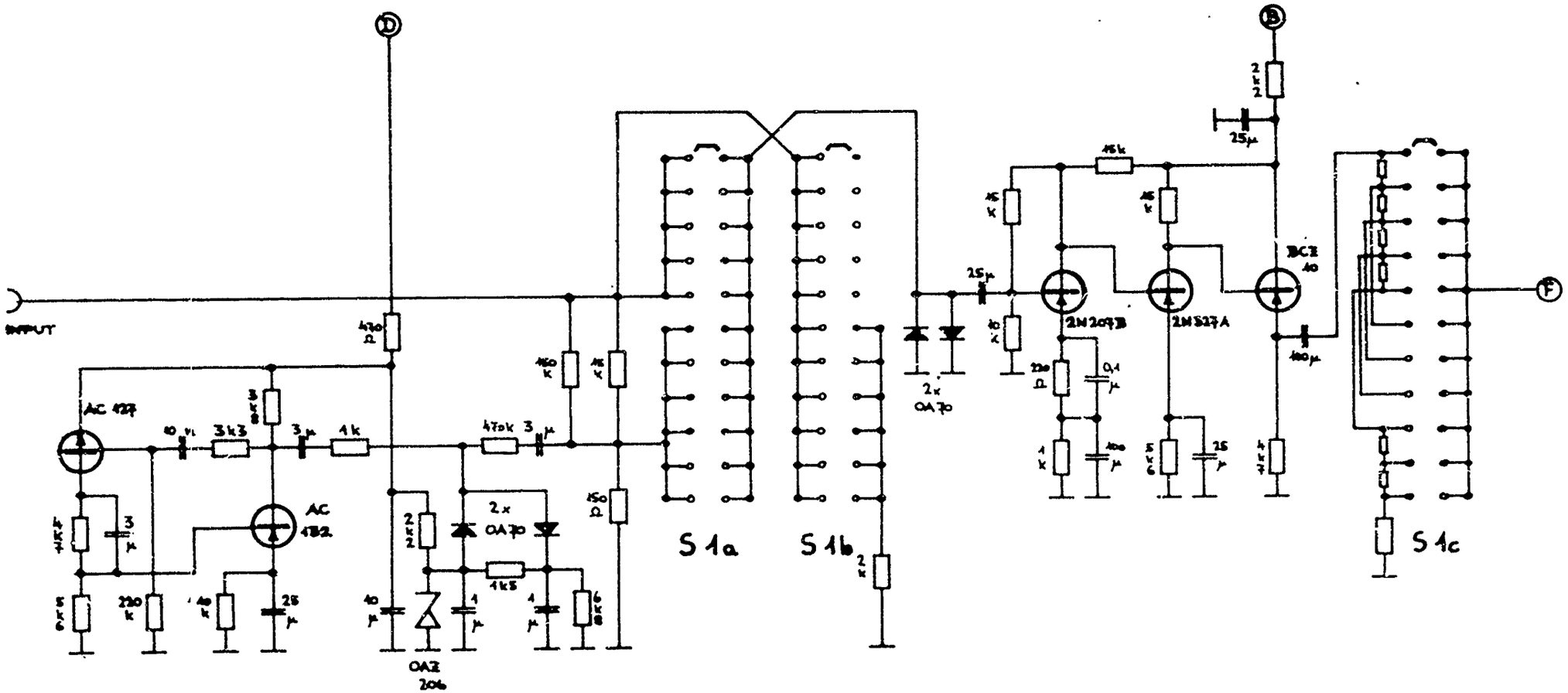

PART 2: PREAMP + OSZILLATOR

FIG. 1.2

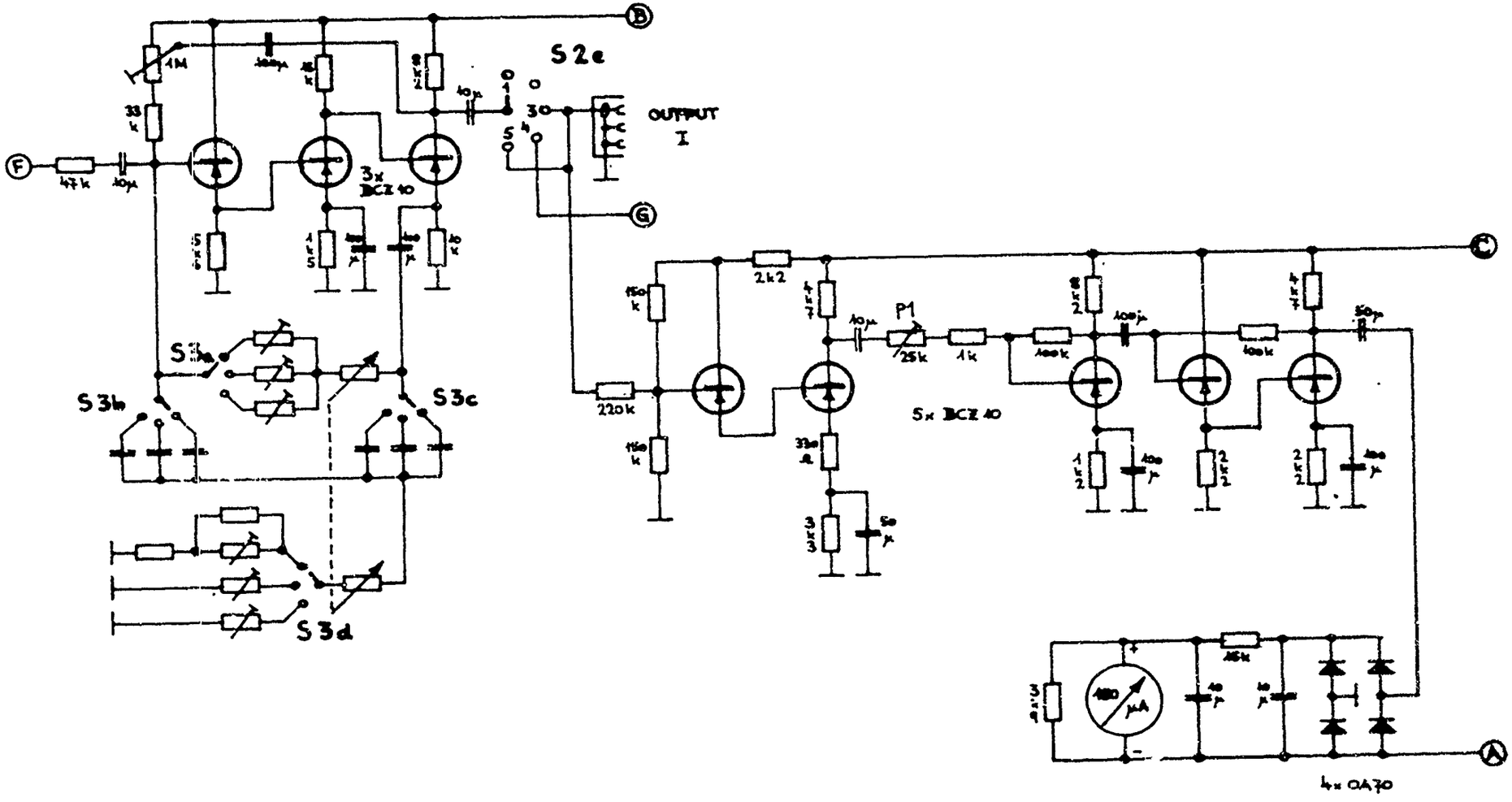

PART 3: SELECTIVE CIRCUIT + METER AMP

FIG: 13

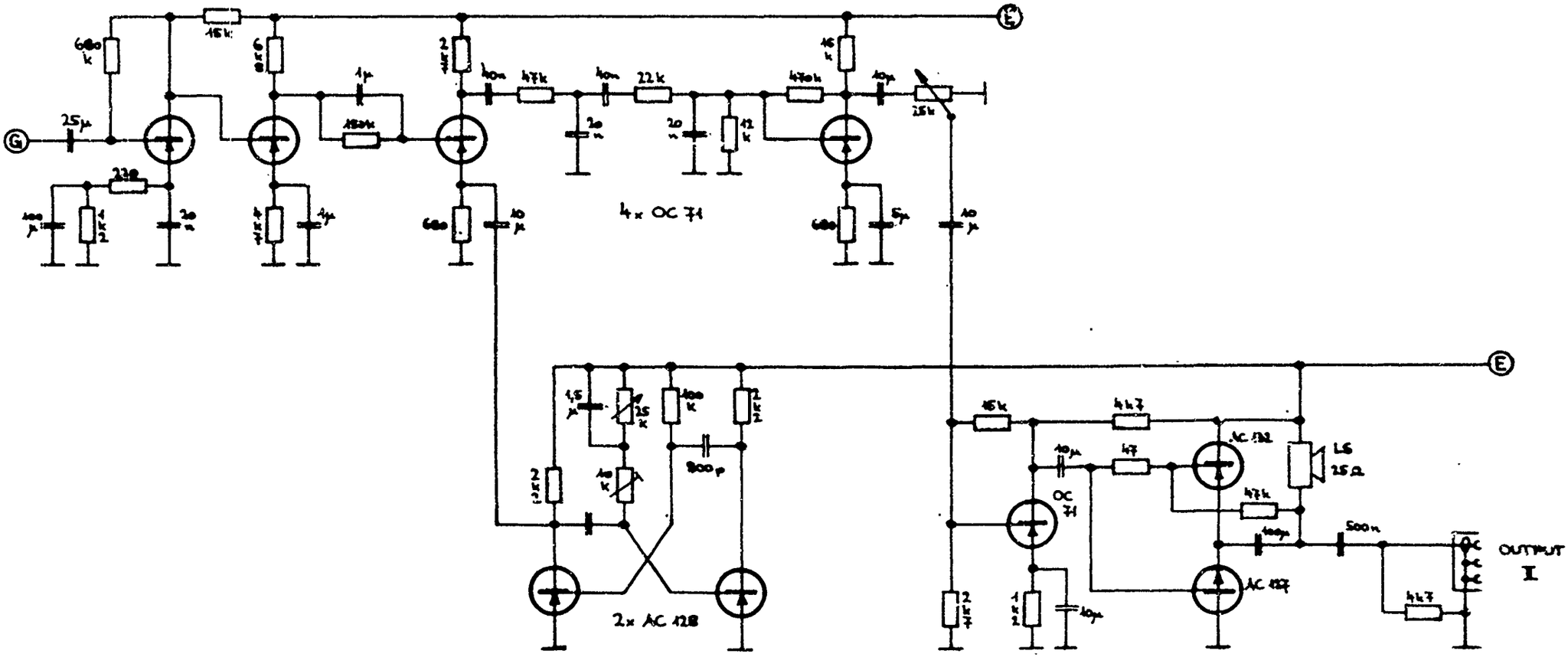

PART 4: HETERODYNE CIRCUIT

FIG.1.4

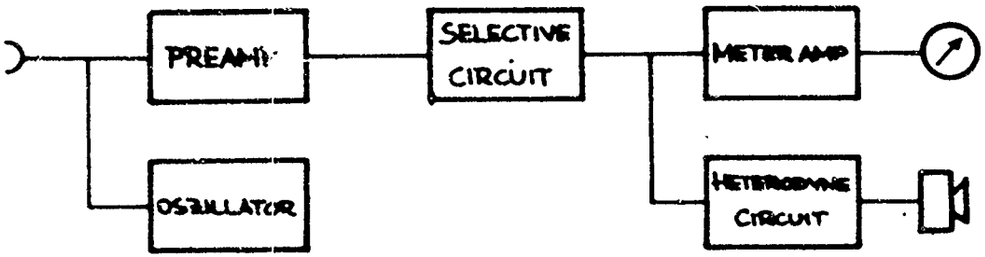

SCHEME S2:

1 OFF
2 SUPPLY
3 METER
4 HETERODYNE
5 CALIBRATE

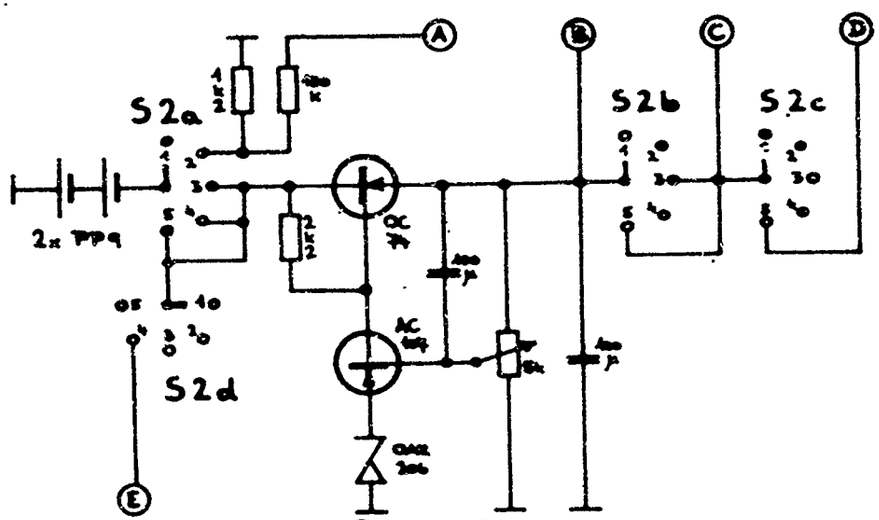

PART 1: POWER REGULATOR

FIG. 1.5

VLF FIELD STRENGTH METER

such that attenuation before the input stage is 40 dB and behind it 10 dB. The input resistance is kept constant by the switch plane S1b. The second attenuator is connected with a selective amplifier. A bridged T-type section has a frequency-dependent negative feed-back with three stages. Tuning is performed in stages 1 : 10 : 100 by switching over the capacitors, and continuously 1 : 10 by a 10-turn helical potentiometer with two sections. The band width can be adjusted by changing a feedback which is independent of the frequency. At sufficient stability, a relative bandwidth of $\frac{\Delta f}{f}$ = 5 - 10% was attained. The selective amplifier is followed by an indicating amplifier feeding an instrument which is calibrated directly in μv or mv. For controlling the voltage calibration, a calibration oscillator is built in whose calibration voltage stabilized with a diode circuit is sufficiently constant at temperatures between +5°C and + 35°C. A superheterodyne supplement permits the acoustic control of nonmodulated or keyed transmitters. The operating voltage of most stages is stabilized electronically.

Technical data: Measuring range 1 μv to 100 mv full deflection
accuracy of measurement ± 5%
noise voltage of input 0.1 μv_{eff}
input resistance 1.9 kΩ
frequency range 20 cps to 30 kcps
relative band width 5%,
detailed description in [3].

Nuvistorized field strength meter:

For further improvement of the sensitivity and the signal-to-noise ratio, nuvistors were substituted for the transistors. Thus, a very high input resistance was attained which on the one hand kept the high quality of a ferrite antenna tuned to parallel resonance as well as its high selectivity and induced voltage, and on the other hand permits the useful application of high quality resonant circuits in

the subsequent circuits too.

An input stage according to Fig. 1.6, an improved version of [12], is fixed to the antenna. It consists of a cascode connection with a triode and a pentode followed by another triode as impedance transformer. The antenna coil is symmetrical, its center tap being grounded. Coupling with the non-symmetrical cascode input is made with a transducer. Antenna and transducer are jointly tuned to resonance. The device contains a calibration oscillator for adjusting the amplification by means of the potentiometer R 1. Low-ohmic output voltage is collected on Bu2 and further amplified and measured by separate instruments. Current supply is provided either jointly with our own field strength meter discussed in [12], or separately with a 6 v lead battery and a 120 v nickel-cadmium battery. Following such an input stage, the selective measuring amplifier described in detail in [12] was built. It is also nuvistorized using an LC series resonant circuit as a means of selection which is connected between the output cathode follower of the input stage and the input of the meter amplifier such that the considerable voltage increase due to the high quality is fully utilized. Technical data of the input stage of Fig. 6:

Maximum input voltage on Bu 1: 200 mv
Amplification factor: 50
noise on the short-circuited antenna input: 0.2 μv_{eff},
frequency range: 2.4 - 26 kcps,
band width of the antenna FA 7 with input stage alone
at 10 kcps: 75 cps, at 3 kcps: 10 cps.

Together with the transmission level meter Marcony TF 2330 a maximum sensitivity range of 0.6 µv full deflection is reached. Besides our own meters, commercial devices were used in the course of our studies. We used the following instruments:

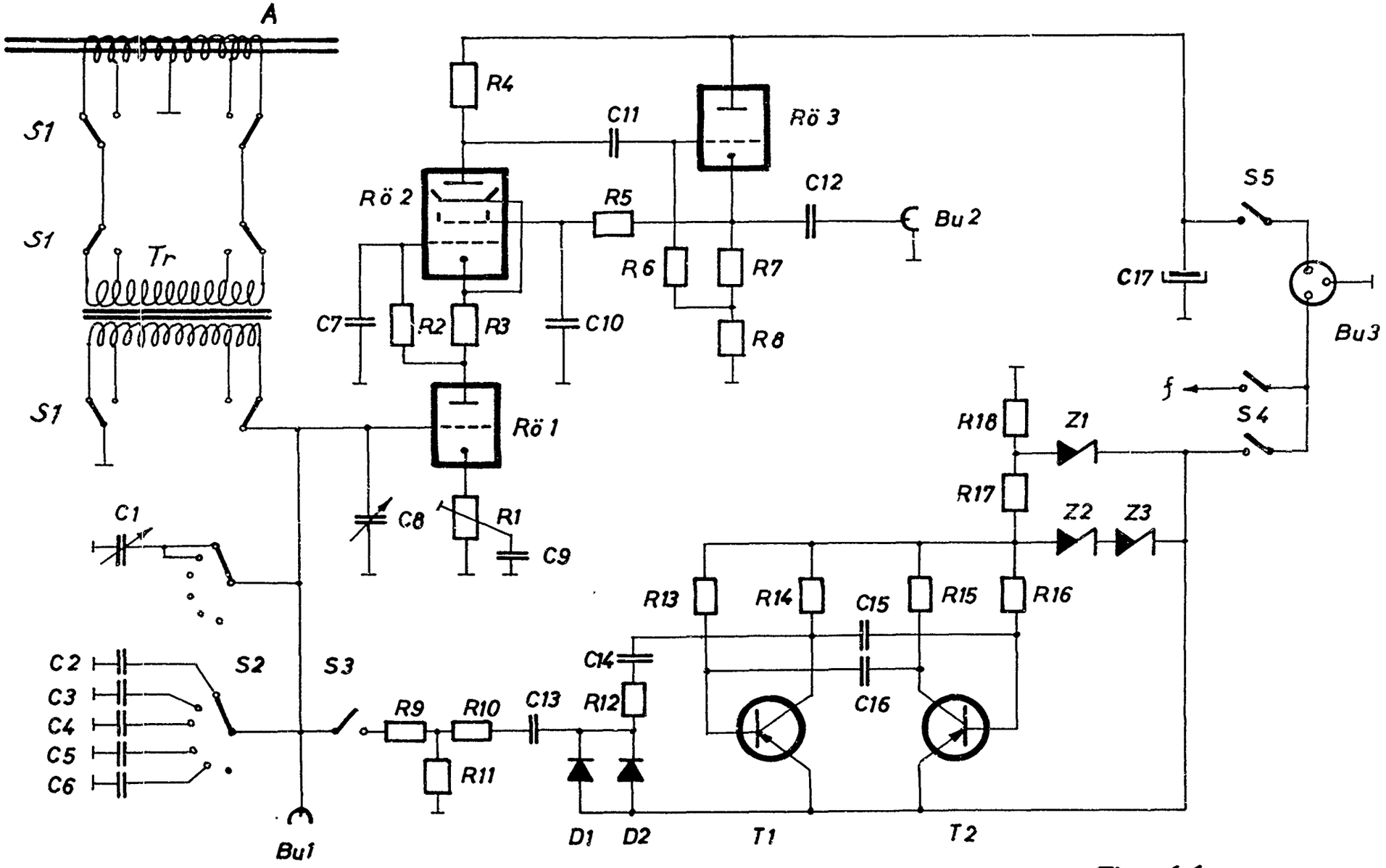
A
S1
S1
S1
S1
Tr
R4
C11
Rö 3
Rö 2
R5
C12
Bu 2
R6
R7
R8
C7
R2
R3
C10
Rö 1
C8
R1
C9
C1
C2
C3
C4
C5
C6
S2
S3
Bu1
R9
R10
C13
R11
C14
R12
D1
D2
R13
R14
C15
R15
R16
C16
T1
T2
R18
Z1
R17
Z2
Z3
S5
C17
Bu3
f
S4

Fig.: 1,6

Wave Analyzer TF 2330, Marconi Instruments Ltd, Great Britain
Frequency range 20 cps - 50 kcps.
Measuring range 30 μv - 300 v full deflection,
Measuring accuracy 5%,
Input resistance 100 kΩ/1MΩ
Band width: 3.5 cps,
Battery-fed.

Wave Analyzer KLA 48, Wandel und Goltermann, Germany
Frequency: 30 cps - 50 kcps,
Measuring range: 0.25 mv - 8v full deflection
Band width changeable, 5.5 and 15 cps, respectively.

Wave Analyzer SPM 2, Wandel und Goltermann, Germany
Frequency region 4 - 600 kcps,
Band width: 200 cps,
Measuring range 2 mv - 7 v full deflection.
Battery-fed.

Oscilloscope 421, Tektronix, USA.

1.5 Receiving antennas

It has already been shown in [4] and [14] that preferably magnetic receiving antennas should be used for our present problems, mainly because of their easy transportation. For the induced voltage U_e on a coil tuned to resonance, the following relation is valid:

$$U_e = \omega \cdot n \cdot F \cdot B \cdot \mu_{eff} Q \cdot k$$

ω = angular frequency
n = number of turns
F = turn area (in air coils) or core cross section (ferrite rods)
μ_{eff} = effective permeability for the used core shape
k = form factor which depends on the coil array, lies between approximately 0.5 and 1.

In air coils, $\mu_{eff} = 1$ and the induced voltage can only be increased by increasing the turn area nF. Apart from the desired restriction in size, the coil losses thus increase considerably so that the reduction of Q obstructs the desired effect. By means of rod cores of highly permeable ferrites which are well suited for VLF, a μ_{eff} of about 50 to 100 can be attained. A high permeability involves high inductance and thus also a large L/C ratio. Together with the small diameter of winding which yields short wire length and small coil losses, a high Q (usually above 100) is obtained which can only be used if the input resistance of the connected amplifier input circuit is correspondingly high as for example in the field strength meter E4 described in [12].

Of all tested antennas, the most typical and preferred types are described hereinafter:

EA I: [1] ferrite rod, length 47.5 cm, diameter 1.5 cm, inductance 0.8 H, ohmic resistance 135 Ω.

EA III: [1] cylinder coil without iron core, diameter 45 cm, 1000 turns.

Both antennas are tuned to parallel resonance, the receiver [1] (10 kΩ input resistance) is always connected with a tap..

At first, the antenna EA III was used for numerous measurements.

EA IV: [2] five ferrite rods of 2 cm diameter and 80 cm length each, arranged as the edges of a regular pentagonal prism. 5 x 1600 turns, 5 x 50 Ω, always in the rod center; total inductance has a maximum of 8 H.

EA V: [2] a ferrite rod of 2 cm diameter and 65 cm length, 3000 turns in the middle, 135 Ω, 2 H.

EA VI: [2] a laminated iron core made of metal sheet strips (0.35 mm thick and 30 mm wide), total iron cross section 8 cm^2, length 100 cm, material Hyperm 766 by Krupp-Widia, Essen, with a very high ring core permeability of μ_{tor} = = 80000.

The improved transistor receivers had a smaller input resistance (E 3: 1.9 kΩ). The antennas were operated in series resonance. At the receiver input E 2 [2] they yielded a voltage of 1 μv at a field strength of

	f = 3 kcps	f = 10 kcps
EA IV	$2.32 \cdot 10^{-12}$	$0.73 \cdot 10^{-12}$ Wb·m^{-2}
EA V	$6.8 \cdot 10^{-12}$	$2.42 \cdot 10^{-12}$ "
EA VI	$3.25 \cdot 10^{-12}$	$2.63 \cdot 10^{-12}$ "

The input voltage of 1 μv at the receiver E 3 [24] was reached at:

	f = 3 kcps	f = 10 kcps
EA IV	$0.26 \cdot 10^{-12}$	$0.15 \cdot 10^{-12}$ Wb·m^{-2}
EA VI	$1.3 \cdot 10^{-12}$	$0.55 \cdot 10^{-12}$ "

FA V: Ferrite rod of 2 cm diameter and 48 cm length; in the middle 1200 turns, 450 mH.

This antenna is installed as a direction-finder antenna in Cardanic suspension so that the value as well as the direction of the field strength can be measured accurately. Fig. 1.9 shows the principle of the array that can be rotated in all three space axes. In order to avoid a field distortion by metal parts, the construction was entirely made of plastics. The antenna is also tuned to parallel resonance and operates on an impedance transformer which although having a voltage amplification < 1, permits the high quality of the antenna circuit to be utilized. The impedance transformer (Fig. 1.10) consists of two collector stages in cascade, equipped with HF transistors. A considerable reduction of pickup from electrical stray fields was attained by tapping and grounding the coil center of the antenna and by connecting the impedance transformer symmetrically via a transformer with symmetrical input and nonsymmetrical output. The transformer transforms upward at 1 : 1.8 and is tuned to resonance together with the antenna. At 10 kcps, this improved antenna yields a voltage of

1 μv at $7.75 \cdot 10^{-14}$ Wb·m^{-2} at the output of the impedance transformer. The calibration curves for different frequencies and field strengths are shown in Fig. 1.8.

FA 7: Ferrite rod of 2 cm diameter and 98 cm length. 1200 turns in the middle.

This antenna was originally developed for the E 4 receiver, for details see [12] and [14]. Together with the improved input stage as shown in Fig. 1.6, the FA 7 was changed in the same way as FA 5 with respect to symmetrical winding and transformer connection. At the output of the first stage (Bu 2, Fig. 1.6), FA 7 yields a voltage of 1 mv at $6.6 \cdot 10^{-13}$ Wb·m^{-2} at 10 kcps. Fig. 17 shows the calibration curves as dependent on the frequency. Here, the increase in LC ratio at higher frequencies becomes especially evident. The discontinuity at 5 kcps corresponds to the impedance switch-over with S 1 of Fig. 1.6.

For the antennas EA IV and EA V as well as FA 5 and FA 7, the material 1100 N22 of Siemens und Halske, Munich was used.

1.6 Calibration of field strength meters

As the voltage induced in the antenna depends on the frequency, calibration curves of the used antennas together with the receivers were made as a function of frequency. For this purpose, a calibration field was produced according to Biot-Savart's law. A circular calibration coil with an area of 1290 cm^2 and 10 turns was fed by an RC generator, the current being measured with a clip-on a-c current probe. A series resistor of 150 Ω between the generator and the coil inductance of 75 μH made the coil current sufficiently independent of the frequency up to about 20 kcps, up to which frequency the maximum impedance of the coil is no more than 1/15 of the chosen value of the barrier resistance. The

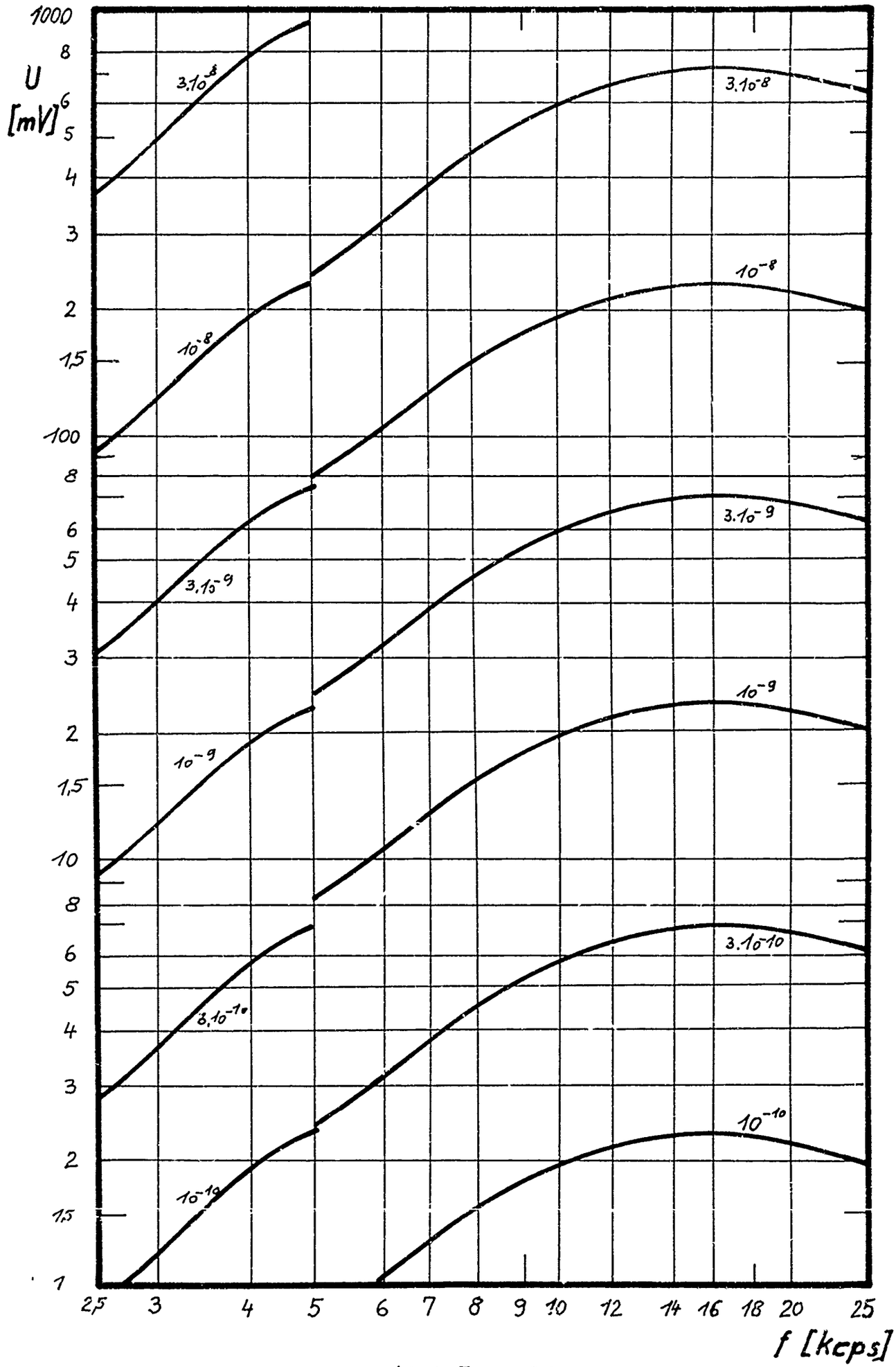

Parameter $|H|$ [Vs/m²]

Fig.: 1.7

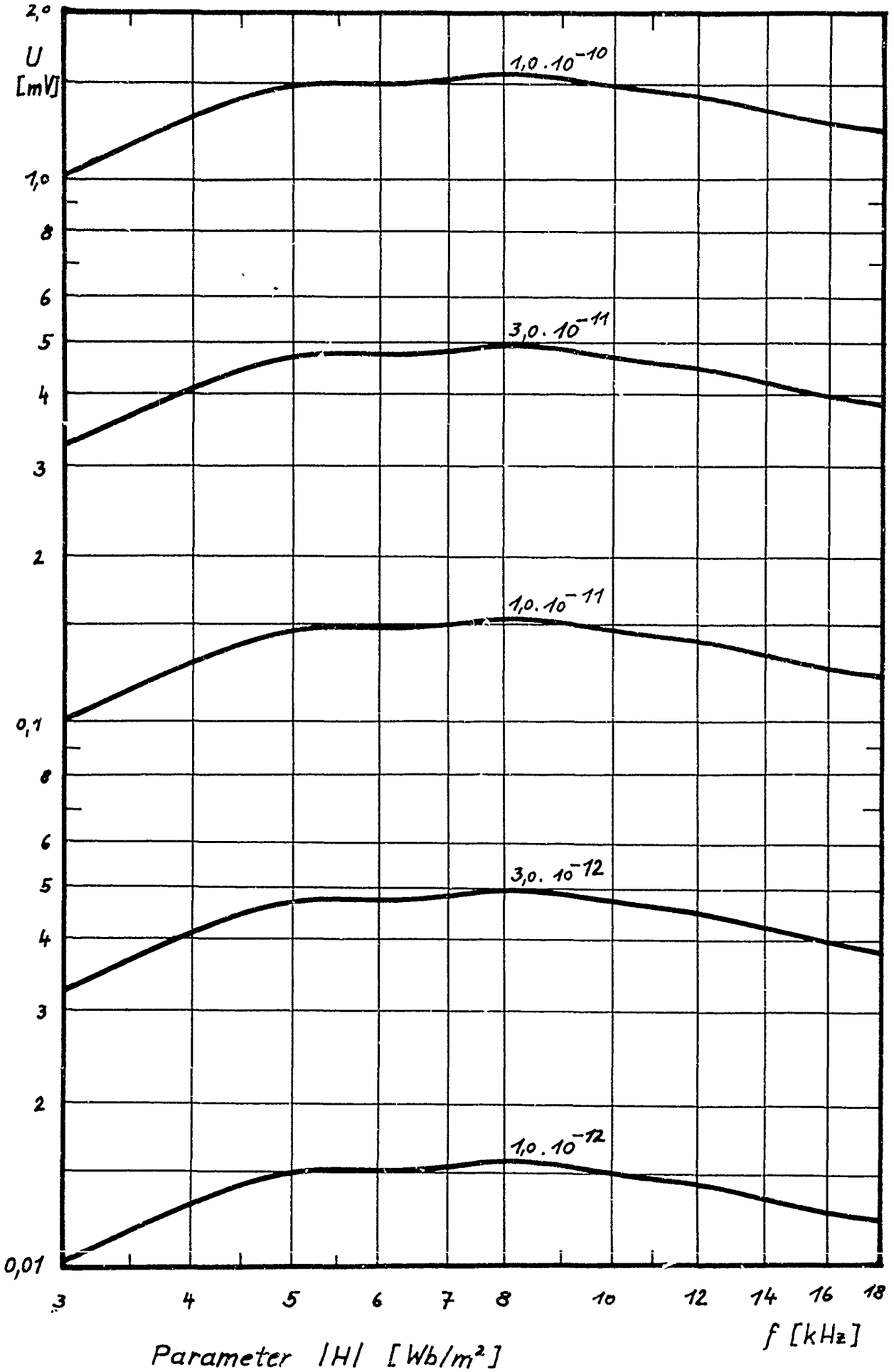
2,0
U
[mV]
1,0
8
6
5
4
3
2
0,1
8
6
5
4
3
2
0,01
1,0 . 10⁻¹⁰
3,0 . 10⁻¹¹
1,0 . 10⁻¹¹
3,0 . 10⁻¹²
1,0 . 10⁻¹²
3
4
5
6
7
8
10
12
14
16
18
f [kHz]
Parameter |H| [Wb/m²]

Fig.: 1,8

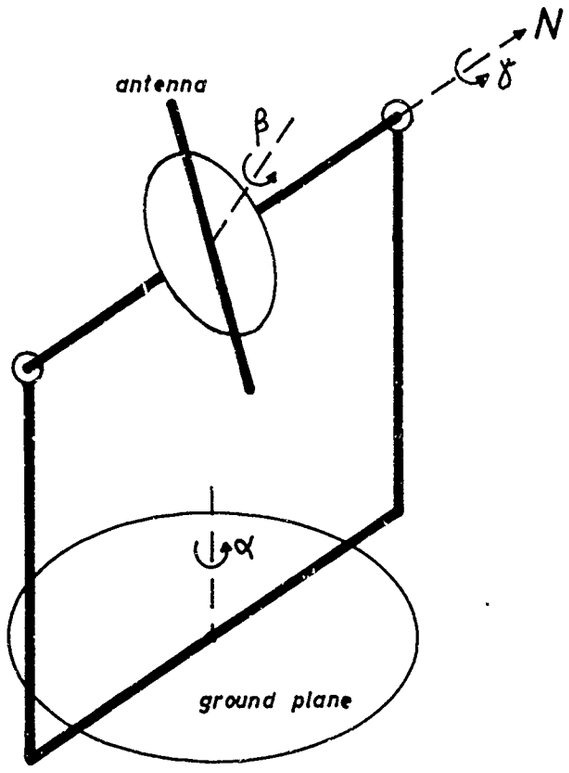

FIG. 1.9

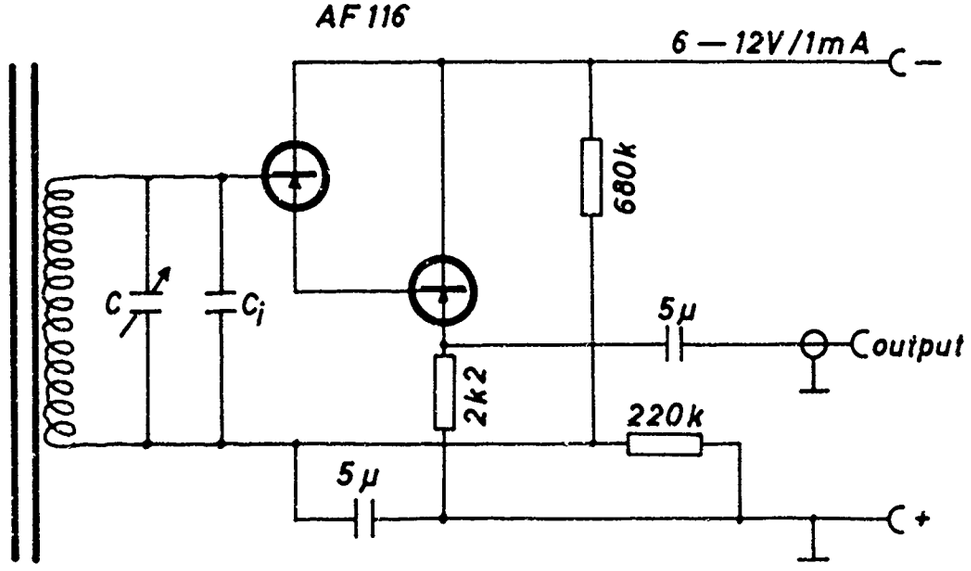

FIG. 1.10

receiving antenna to be calibrated was set up at a sufficient distance which is well known, coaxially to the calibration coil. Under the condition that the field distortion due to the introduction of a receiving antenna is negligible, the following relation holds for the field strength at the site of the receiving antenna :

$$H = 2\pi\mu_o \cdot I \cdot n \cdot \frac{a^2}{(r^2 + a^2)^{3/2}}$$

H = field strength in Vb/m^2,
n = number of turns of the calibration coil
r = distance between the plane of the calibration coil and the end of the receiving antenna facing the calibration coil, m,
I = coil current, a,
a = radius of the calibration coil.

In general, the radius a is small as compared to the distance r, therefore the expression is simplified as follows:

$$H = \frac{2\mu_o \cdot I \cdot n \cdot F}{r^3} \quad .$$

For practical reasons, the distances used for the calibration varied between 5 and 15 m, the coil current reached about 6 ma. Used instruments:
Decade RC generator TG 66, Levell, England
Clip-on a-c current probe 456 A, Hewlett-Packard Company, USA.
Calibration was controlled by small receiving calibration coils described in [2] , to guarantee that the field change of the calibration field caused by introducing the receiving antennas was definitely kept below the admissible limits.

Figs. 1.7 and 1.8 show examples of the calibration curves obtained in the above manner.

2. Experimental studies in the mine

2.1 Introduction

Measurements below ground were made for the purpose of determining the manner of VLF-wave propagation in a solid medium and the effect and quantity

of the parameters ε, μ, σ (dielectric constant, permeability, conductivity) in connection with it, as well as the relation between

the transmitter power (value of the magnetic moment of the transmitting coil m) and

the transmitter position (angle α between the transmitting dipole and the radius vector with respect to the point of measurement),

distance between transmitter and receiver and the angularity of the receiving antenna (angle ψ).

The permeability μ with good approximation was found to be un ity for all types of rock. Measurements showed this to be valid with sufficient accuracy also for hematitic and sideritic ores. The dielectric constant ε was measured on cylindrical laboratory samples. The results are summarized in a special chapter of the present report. On measuring the conductivity σ it was soon found out that the conditions of measurement influence the results in a rather complex way. σ was therefore determined by two completely separate methods: by direct measurement on solid rock by the Wenner method (see section 3) and by measuring the propagation of VLF waves.

The propagation measurements were made in different ways, in accordance with the numerous problems that arose.

It has already been said above that the transmitter (voltage source, generator of accurate frequency, amplifier

and transmitting antenna) were set up in a suitable cavern of the mine, the transmitting antenna being aligned under a defined angle by means of a geological compass. In most cases, the axis of the transmitting frame and thus also of the magnetic dipole has a horizontal position. The frame (in rotating antennas) is moved about a perpendicular axis (angle ϑ, see Fig. 2.1).

The measurement can thus be made in the same manner as a profile measurement, i.e., the field strength is measured by means of the receiver as rectilinearly as possible, at suitable distances from the transmitter. The antenna position and antenna current, i.e., the efficiency of the transmitting dipole were kept constant. The measured values were then plotted in a diagram over the distance r. Important conclusions with respect to propagation and the decisive factors can be made from this field strength profile.

Another possibility which shall be discussed in detail in another section is the measurement of an antenna diagram.

Based on the results of these measurements, the theoretical team developed a theory attempting to describe the propagation of VLF waves in a dissipative medium. In order to describe the method of measurement and its results, the theoretical results described in chapter 4 shall be discussed in brief.

For a simpler mathematical treatment of the given problem, the following assumptions were made for the theoretical investigation:

homogeneous, isotropic, unbounded medium surrounding the transmitting antenna and the receiver;

let the transmitting antenna be considered as a magnetic dipole;

let the distance between the transmitter and receiver be so large that both may be looked upon as being point-shaped;

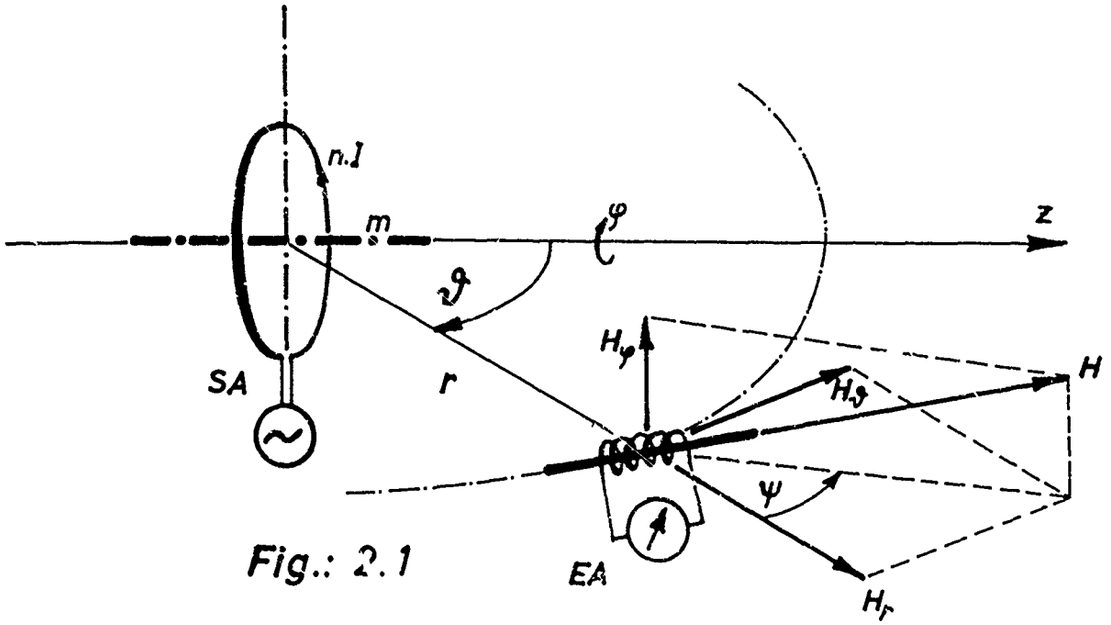
n.I
m
φ
z
ϑ
SA
r
H_φ
H_ϑ
H
ψ
EA
H_r

Fig.: 2.1

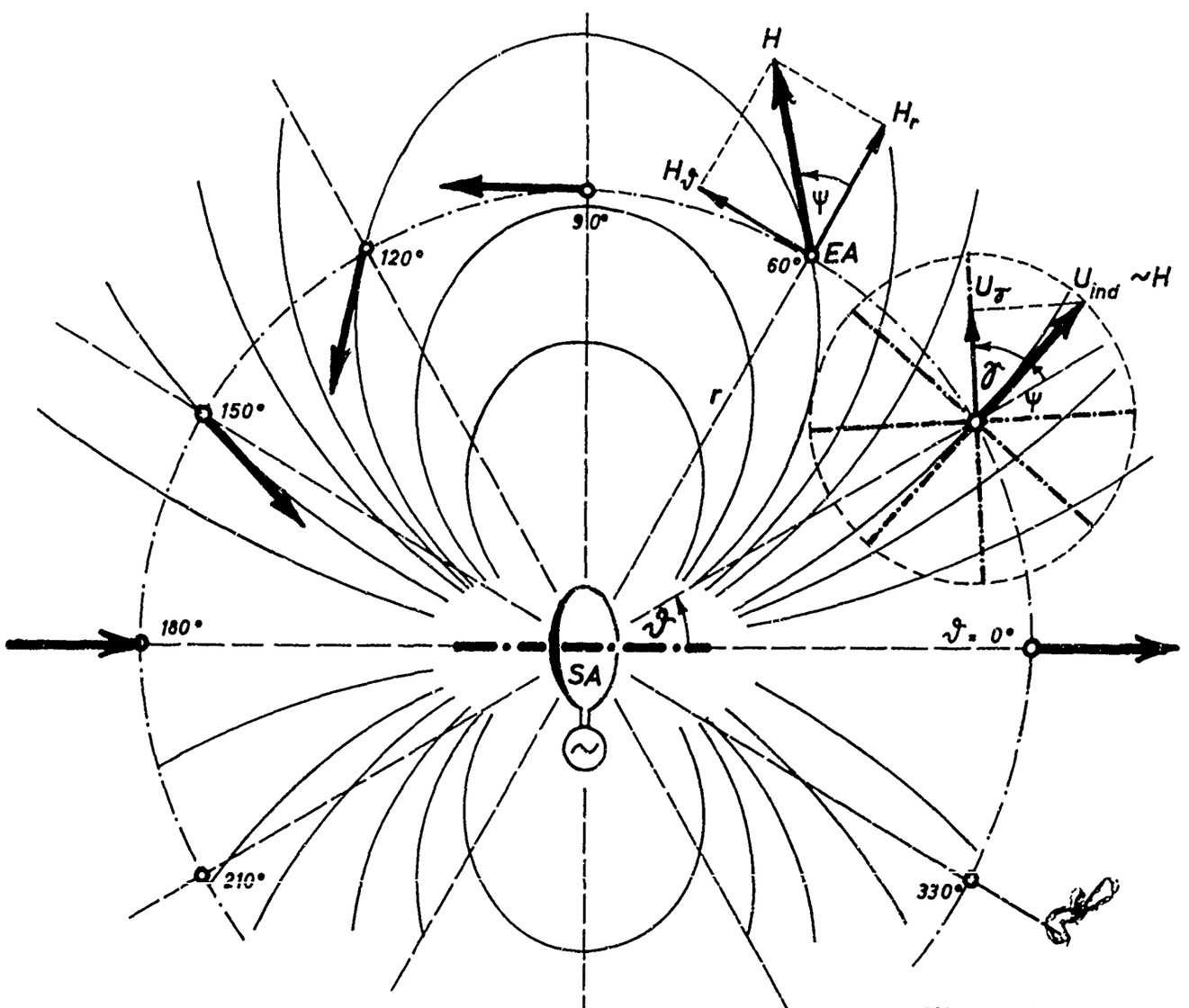
H
H_r
H_ϑ
ψ
90°
120°
60°
EA
U_ϑ
U_{ind} ~H
ϑ
150°
r
180°
ϑ_1
$\vartheta = 0°$
SA
210°
330°

Fig.: 2.2

let us furthermore assume the decisive parameters ε and σ to be constant and independent of the frequency.

The materialization of some requirements, especially that of an unbounded medium involves considerable difficulties; thus, theoretical attempts were made, e.g., of considering the influence of the earth's surface.

Since both, transmitter and receiver, had to be set up in adequate caverns (shafts, galleries) of the mine, the influence of these caverns theoretically was estimated as being spherically idealized and in most cases negligibly small [2].

From the theory of a transmitting magnetic dipole, the magnetic field strength was calculated which under these conditions is the only factor of interest. The geometry of the problem is placed in spherical coordinates, with the dipole axis coinciding with the z-axis (cf. Fig. 2.1).

With $m = \mu_o \cdot n \cdot I \cdot F$ .... magnetic moment of the transmitting dipole

n, I, F ..... number of turns, antenna current, area of the transmitting frame,

ϑ ..... angle between the dipole and the radius vector with respect to the point of measurement,

r ..... distance between transmitter and receiver

β^* ..... complex material constant containing $\varepsilon, \varepsilon_o, \mu, \mu_o, \sigma$ and $\omega = 2\pi\nu$ (frequency),

we thus have

$$\vec{H}_r = 2m \cdot e^{-i\beta^* r} \cdot \cos\vartheta \cdot \left(\frac{1}{r^3} + \frac{i\beta^*}{r^2}\right) \qquad (2.1)$$

$$\left|\vec{H}_r\right| = \cos\vartheta \cdot h_r \qquad (2.1a)$$

;

$$\vec{H}_\varphi = 0 \qquad (2.2)$$

$$\vec{H}_\vartheta = -m \cdot e^{-i\beta^* r} \cdot \sin\vartheta \left(\frac{1}{r^3} + \frac{i\beta^*}{r^2} - \frac{\beta^{*2}}{r}\right) \qquad (2.3)$$

$$|\vec{H}_\vartheta| = \sin \vartheta \cdot h_\vartheta . \qquad (2.3a)$$

From $\vec{H}_\varphi = 0$ we obtain the symmetry about the z-axis (dipole axis) in accordance with the geometry of the transmitting antenna which is assumed to be circular. The field lines thus all lie in meridional planes. Hence the problem of space becomes somewhat simpler, the measurement of one meridional plane is quite sufficient for describing in detail the radiation picture.

Only the field strength value at the respective point of measurement which is vectorially composed of $\vec{H}_r$ and $\vec{H}_\vartheta$, is accessible to measurement. The voltage U_{ind} which is induced in the coil of the receiving antenna is measured with suitably dimensioned instruments (no overload, linear part of the hysteresis curve of the ferrite material); it is proportional to the field strength.

$$U_{ind} \sim |\vec{H}| = (\vec{H}_r^2 + \vec{H}_\vartheta^2)^{1/2} . \qquad (2.4)$$

The direction of the field strength maximum according to Fig. 2.2 is given by

$$\tan \psi = \frac{|\vec{H}_\vartheta|}{|\vec{H}_r|} . \qquad (2.5)$$

Similarly to the Gaussian positions, the measurements for $\vartheta = 0^\circ$ and $\vartheta = 90^\circ$ are of special interest.

From the Eqs. (2.1a), (2.3a) and (2.4a) it follows that

$$|\vec{H}|_{\vartheta=0^\circ} = h_r \qquad (2.6)$$

$$|\vec{H}|_{\vartheta=90^\circ} = h_\vartheta . \qquad (2.7))$$

From the relation

$$G = \frac{h_r}{h_\vartheta} \qquad (2.8)$$

conclusions can again be drawn as to the decisive parameters. In order to be able to compare the measured curves with the theoretical results, a large array of field strength values was calculated for the entire range of parameters under consideration, using an electronic computer of the Zuse Z 23 V type; the field strength values were also graphically represented. The curves shown in Figs.2.3 - 2.8 were plotted according to a profile measurement. The constant factor m (dipole moment) was arbitrarily taken as 10^5 (in accordance with the calculated and tabulated values). The circle diagrams in Figs. 2.9 - 2.12 correspond to the well-known antenna diagrams for certain distances and conductivities. These circle diagrams were drawn for the most frequently used frequency of 3 kcps.

2.1.1. Methods of measurement

Profile measurement

This very simple possibility of measuring a VLF field has already been described at the beginning. From it results the magnitude of the decrease in field strength with increasing distance r.

Antenna diagram

An antenna diagram is measured in the well-known manner by finding the field strength values at a constant distance around the transmitting antenna; if necessary also their direction is measured. As such measurements are impossible in a mine, the transmitting antenna was turned instead, and the receiving antenna was left at its place. The rotation of the transmitting antenna may be seen from the angle ϑ in Fig. 2.2. The direction-finder antenna FA 5 (for details see Chapter 1) was developed for the purpose of measuring the field strength values at the point of measurement, as well as for a precise angular measure-

ment of the field direction. The ferrite rod is mounted on a turn-table so as to rotate perpendicularly to its axis. The turn-table in turn swivels in any direction; for field strength measurements it is adjusted so that its plane contains the field strength maximum. The latter determines the angle ψ (see Fig. 2.2). In order to reduce the errors in reading and adjusting the angles, another circle diagram is recorded with the use of th receiving antenna: The ferrite rod is rotated through 10° each time starting from the maximum direction ($\gamma = 0^{\circ}$), and the respective voltage values are read; between the latter and the field strength maximum there exists the following relation:

$$U_{\gamma} = U_{ind} \cdot \cos \gamma . \qquad (2.9)$$

U_{ind} is determined for every ϑ by a balancing calculation (method of least squares) and from it the antenna characteristics are concluded by another balancing calculation.

This antenna characteristic having the form of a circle diagram (Figs. 2.9 - 2.12) also contains the radial field strength h_r for $\vartheta = 0^{\circ}$ and for $\vartheta = 90^{\circ}$ the tangential field strength h_{ϑ} . The ratio $G = h_r : h_{\vartheta}$ is a near field - - far field measure depending considerably on the conductivity [3], [4]. In the extreme near field (r very small). $G = 2$ (cf. Eqs. (2.1) and (2.3)). The relation shifts toward smaller G values as the distance increases. From $G < 1$ onward we may speak of a far field. In connection with it, the maximum field strength of reception in its vicinity can be expected at an angle of $\vartheta = 0^{\circ}$, at greater distances (the boundary varies depending on the conductivity and frequency) the principal radiation direction is $\vartheta = 90^{\circ}$, a minimum occurring at $\vartheta = 0^{\circ}$. For $G = 1$, the radiation characteristic is spherical.

Measurement of angle

In the method described so far, the propagation para-

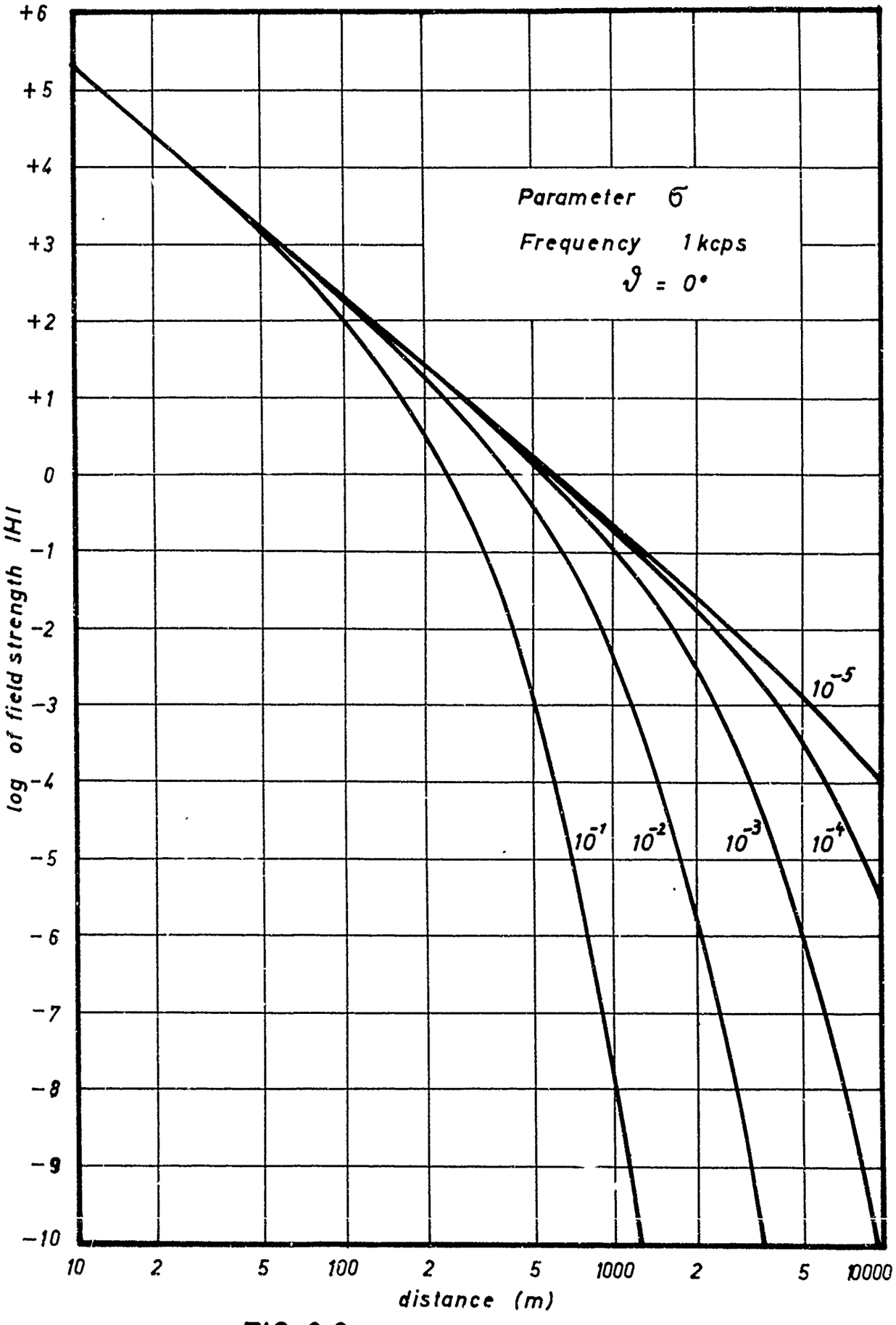
+6
+5
+4
+3
+2
+1
0
−1
−2
−3
−4
−5
−6
−7
−8
−9
−10
log of field strength |H|
Parameter σ
Frequency 1 kcps
ϑ = 0°
10⁻⁵
10⁻¹
10⁻²
10⁻³
10⁻⁴
10
2
5
100
2
5
1000
2
5
10000
distance (m)

FIG. 2.3

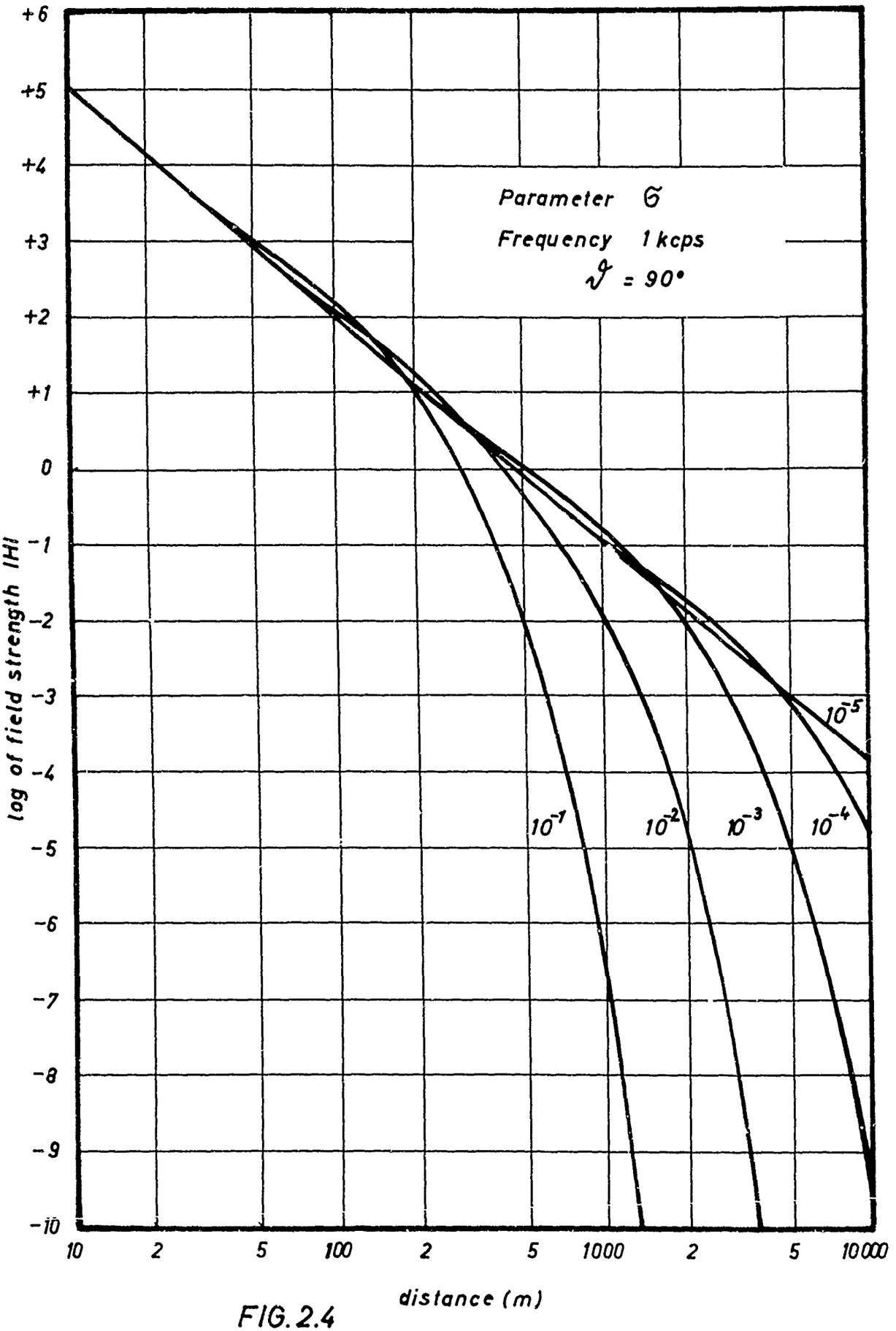
+6
+5
+4
+3
+2
+1
0
-1
-2
-3
-4
-5
-6
-7
-8
-9
-10
log of field strength |H|
Parameter σ
Frequency 1 kcps
ϑ = 90°
10^-5
10^-1
10^-2
10^-3
10^-4
10
2
5
100
2
5
1000
2
5
10000
distance (m)

FIG. 2.4

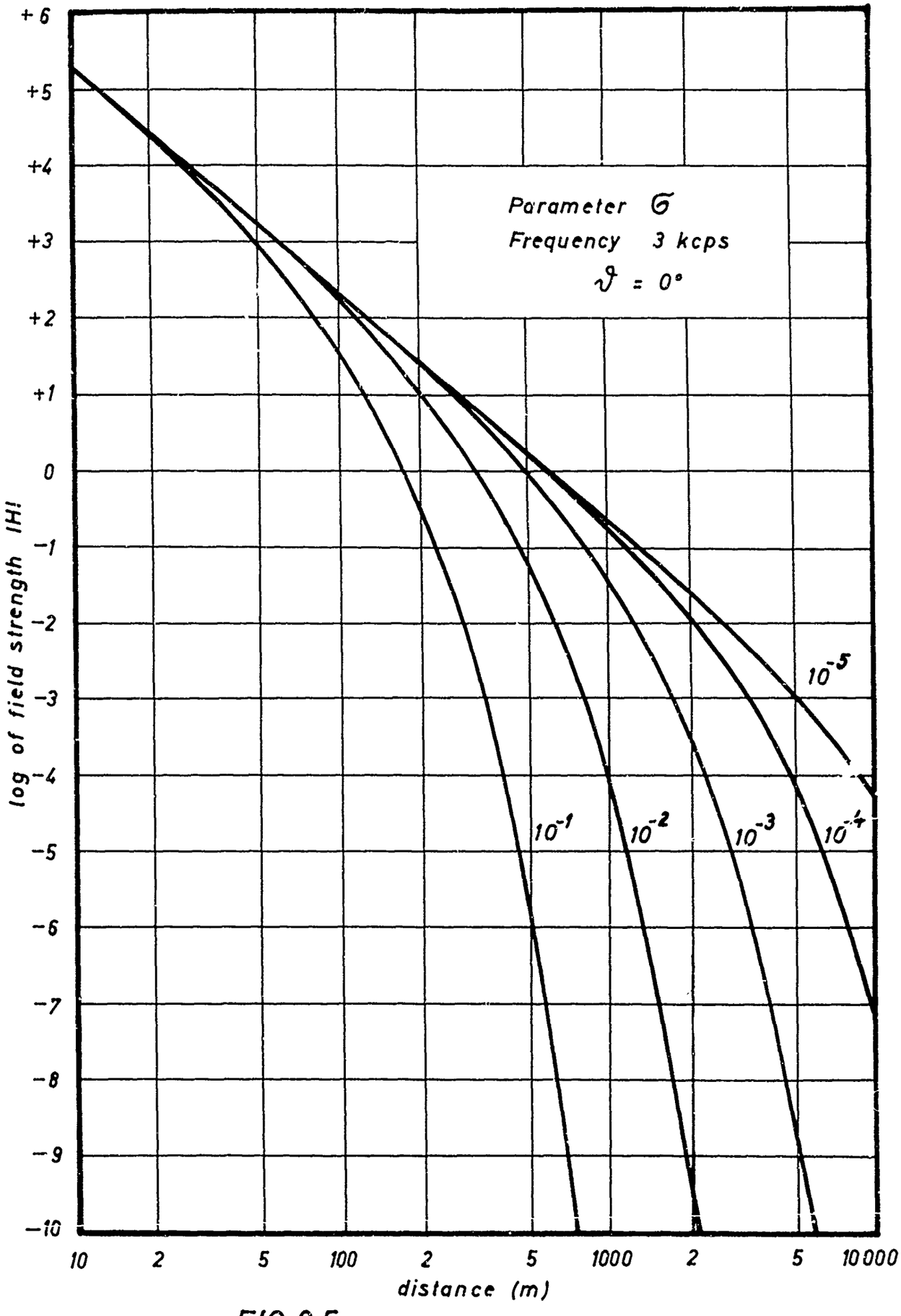
+6
+5
+4
+3
+2
+1
0
−1
−2
−3
−4
−5
−6
−7
−8
−9
−10
log of field strength |H|
Parameter σ
Frequency 3 kcps
ϑ = 0°
10⁻⁵
10⁻¹
10⁻²
10⁻³
10⁻⁴
10
2
5
100
2
5
1000
2
5
10000
distance (m)

FIG. 2.5

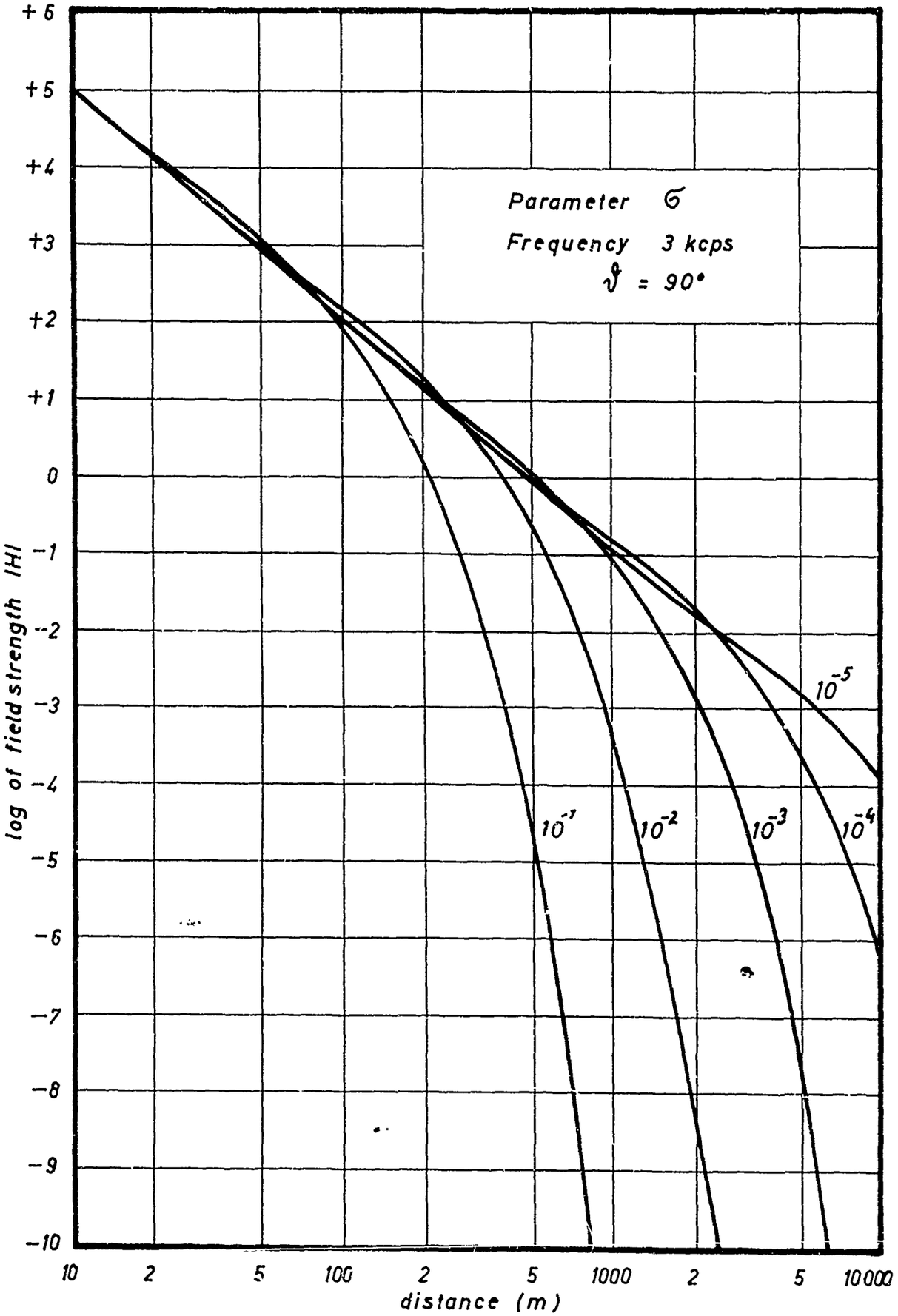
+6
+5
+4
+3
+2
+1
0
−1
−2
−3
−4
−5
−6
−7
−8
−9
−10
log of field strength |H|
Parameter σ
Frequency 3 kcps
ϑ = 90°
10⁻⁵
10⁻¹
10⁻²
10⁻³
10⁻⁴
10
2
5
100
2
5
1000
2
5
10000
distance (m)

FIG. 2.6

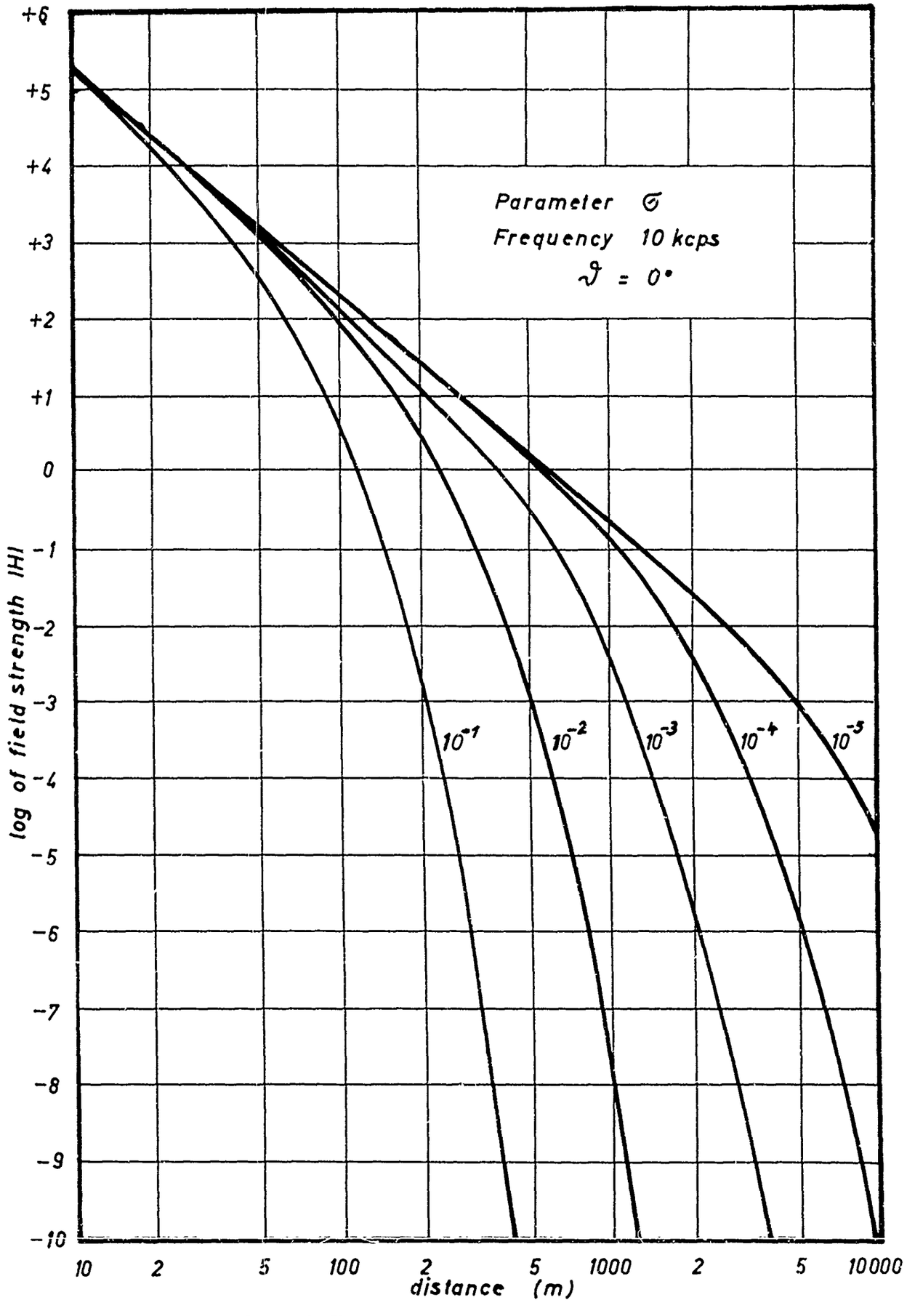
+6
+5
+4
+3
+2
+1
0
-1
-2
-3
-4
-5
-6
-7
-8
-9
-10
log of field strength |H|
Parameter σ
Frequency 10 kcps
ϑ = 0°
10^-1
10^-2
10^-3
10^-4
10^-5
10
2
5
100
2
5
1000
2
5
10000
distance (m)

FIG.2.7

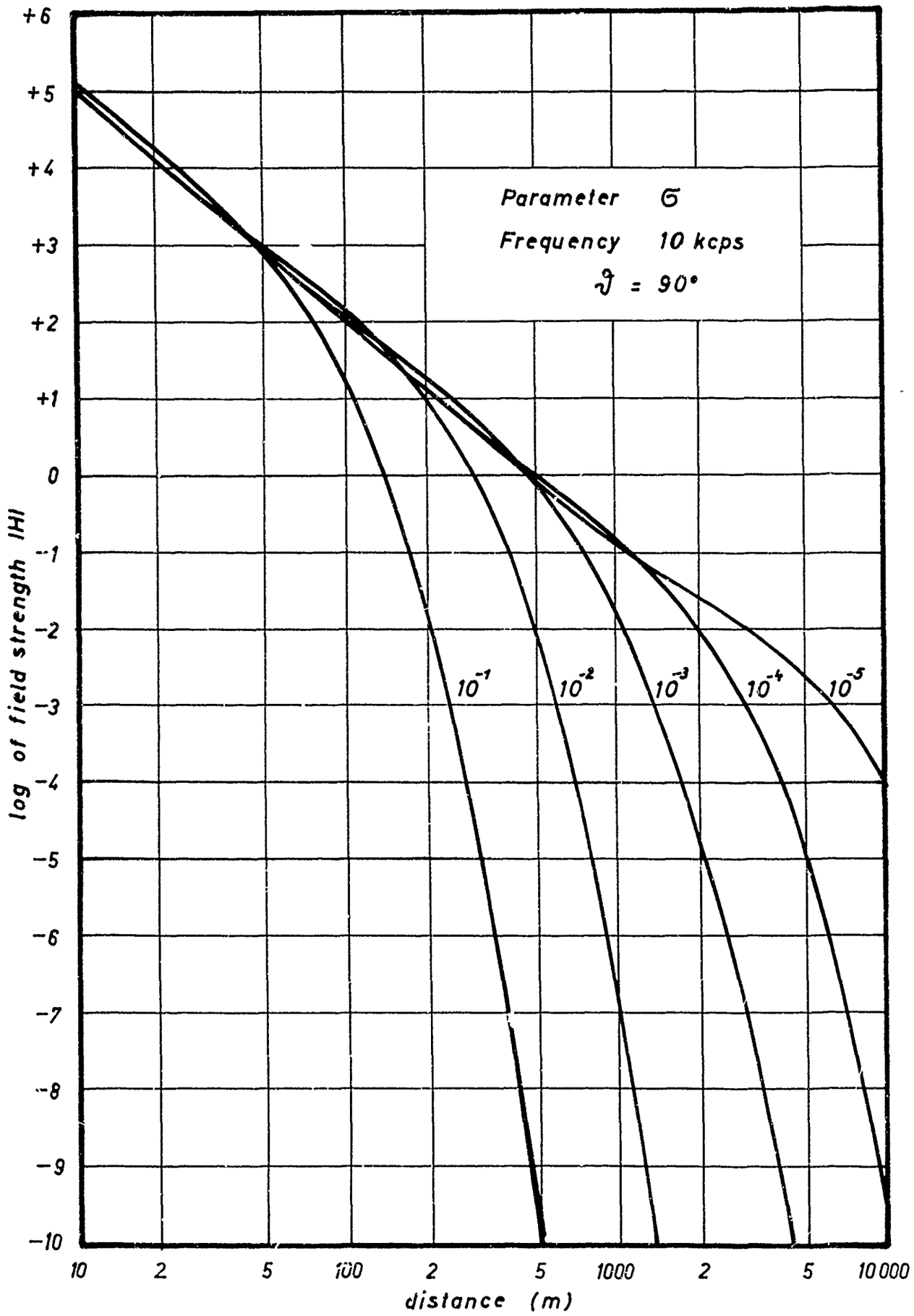
+6
+5
+4
+3
+2
+1
0
−1
−2
−3
−4
−5
−6
−7
−8
−9
−10
log of field strength |H|
Parameter σ
Frequency 10 kcps
ϑ = 90°
10⁻¹
10⁻²
10⁻³
10⁻⁴
10⁻⁵
10
2
5
100
2
5
1000
2
5
10 000
distance (m)

FIG. 2.8

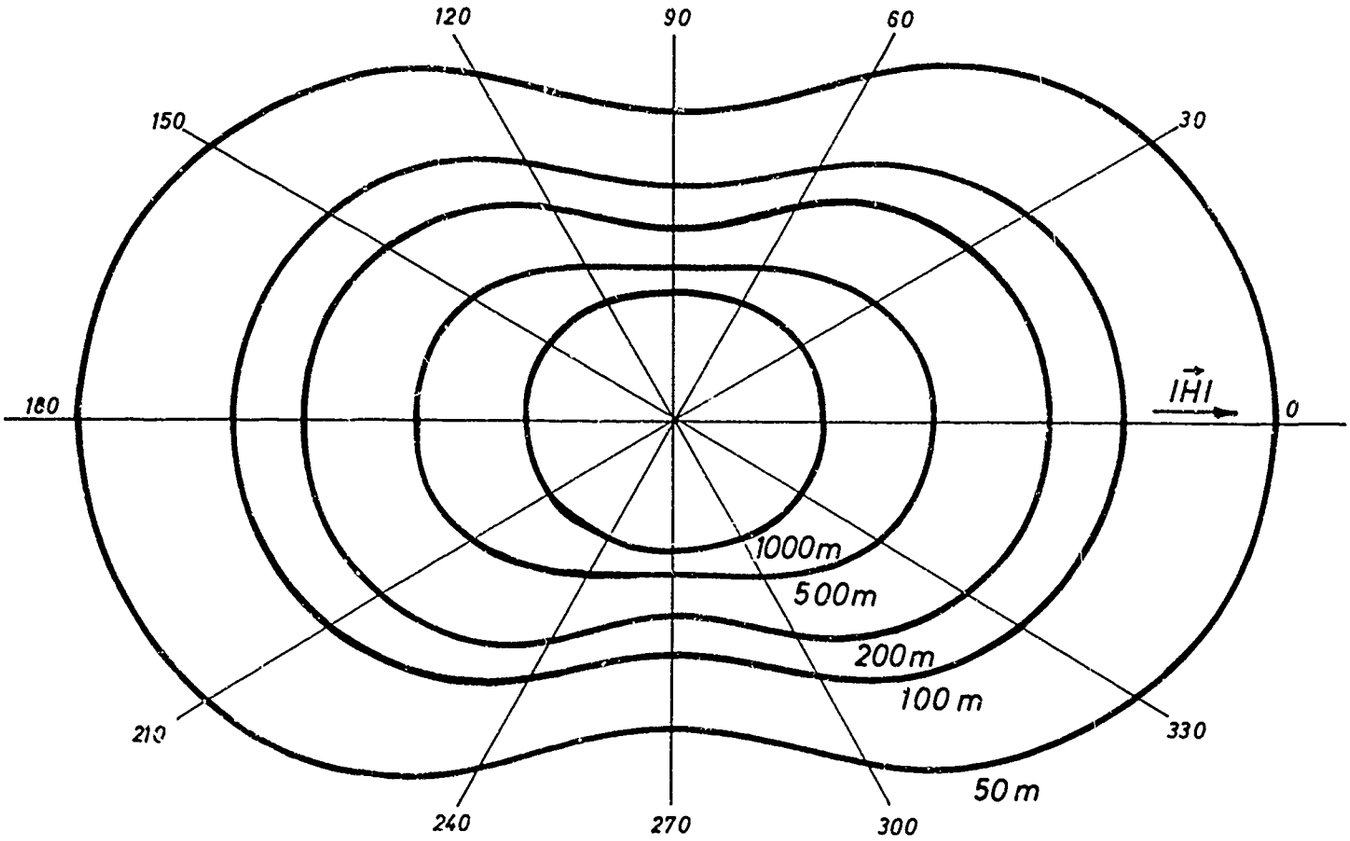

$f = 3$ kcps

$\sigma = 10^{-4}$ S/m

scale for .....

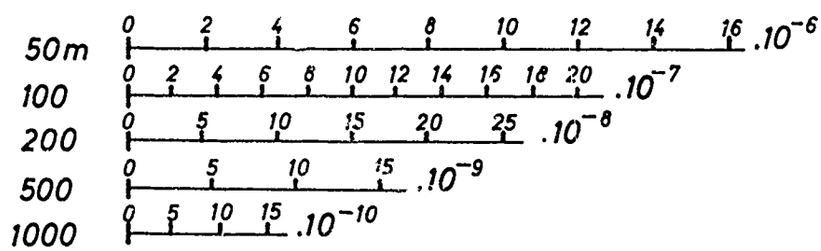

$f = 3$ kcps

$\sigma = 10^{-3}$ S/m

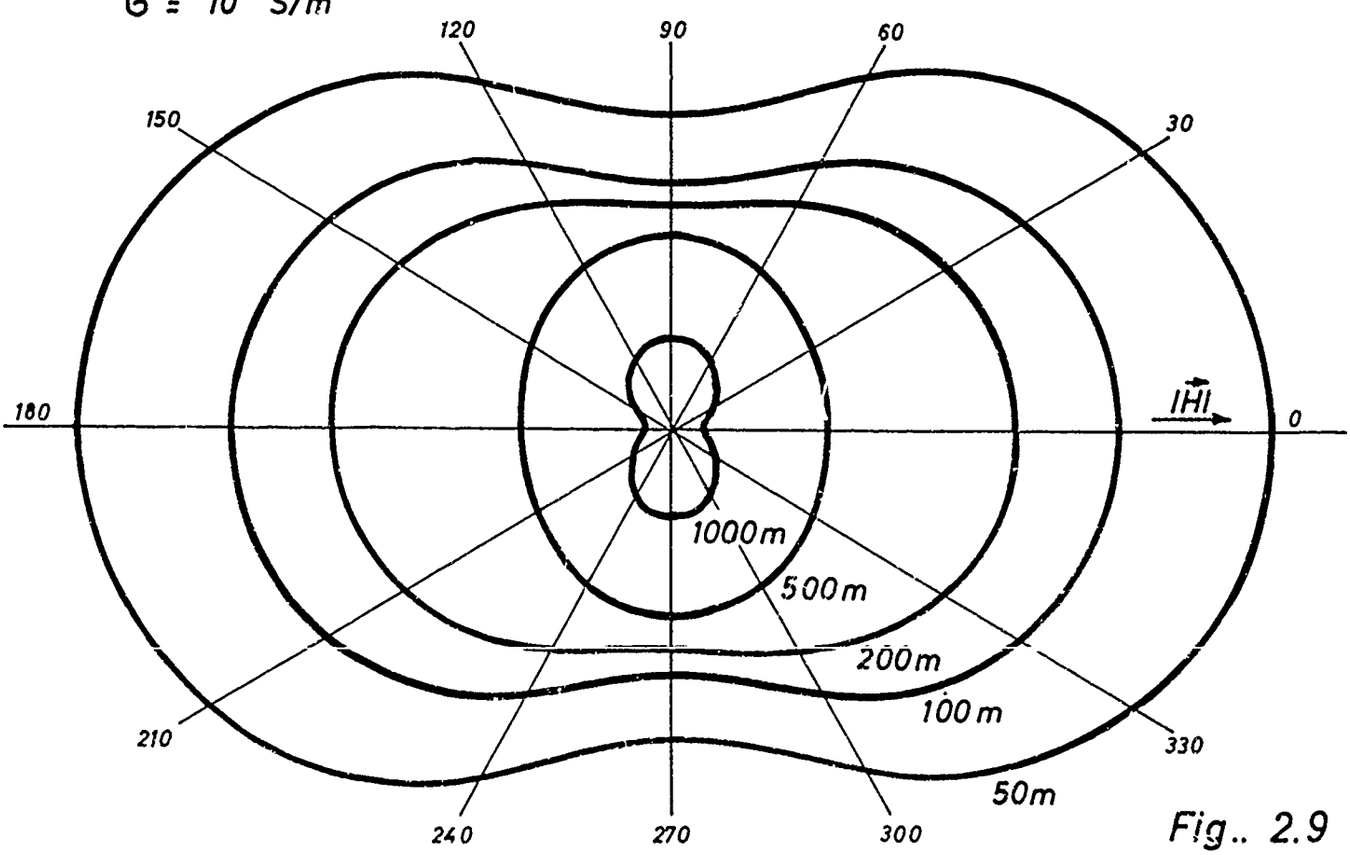

Fig.. 2.9

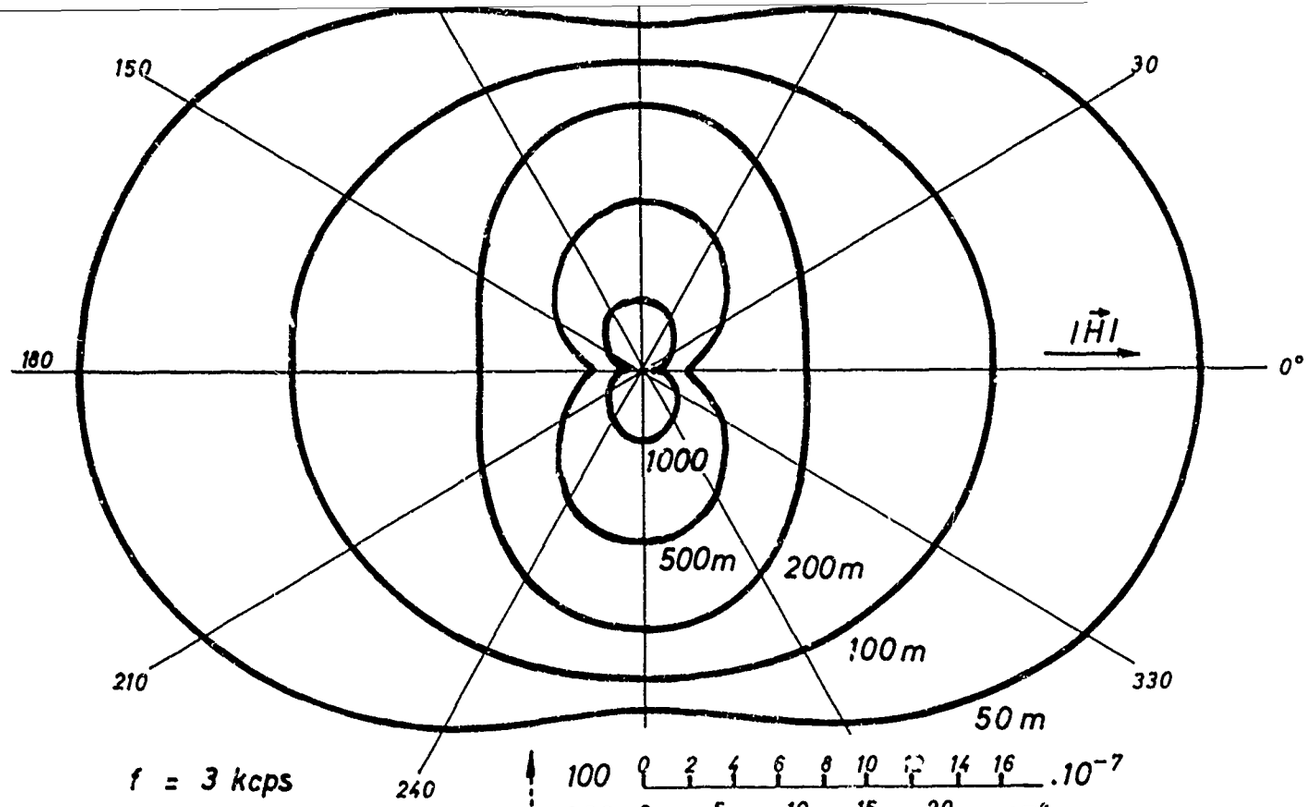

180

f = 3 kcps

$\sigma = 10^{-2}$ S/m

scale for....

100	0 2 4 6 8 10 12 14 16	$.10^{-7}$
200	0 5 10 15 20	$.10^{-9}$
500	0 1 2 3	$.10^{-9}$
1000	0 5	$.10^{-12}$
50 m	0 2 4 6 8 10 12 14 16	$.10^{-6}$
100	0 2 4 6 8 10	$.10^{-7}$
200	0 5 10 15	$.10^{-9}$
500	0 2	$.10^{-13}$

f = 3kcps

$\sigma = 10^{-1}$ S/m

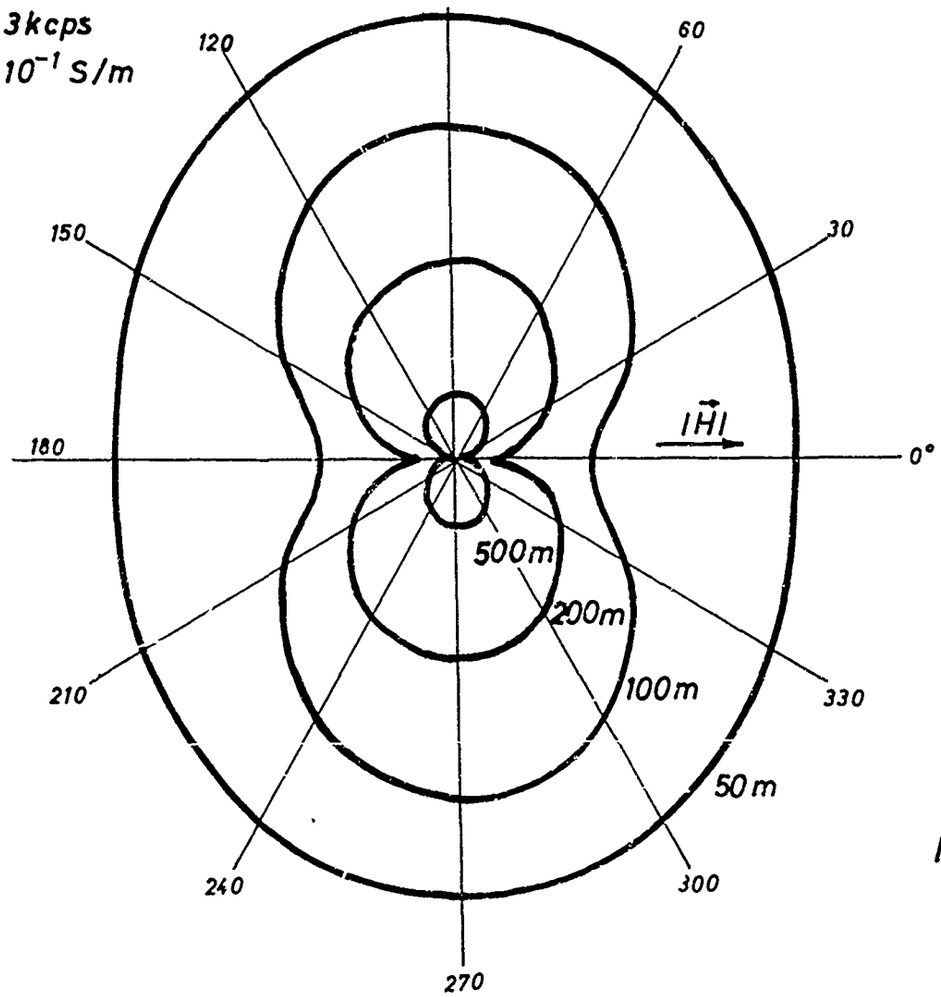

180

Fig.: 2.10

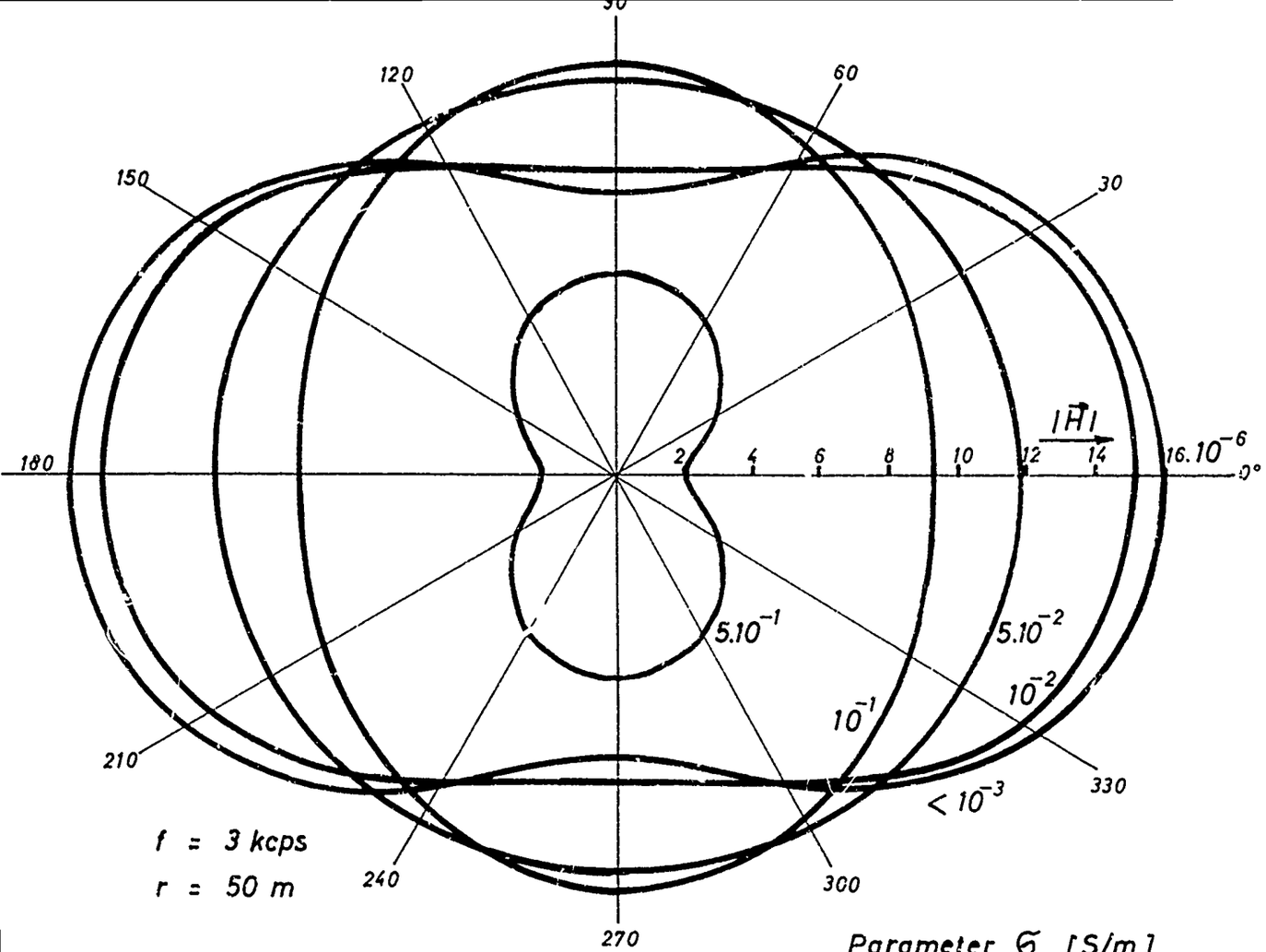

Parameter σ [S/m]

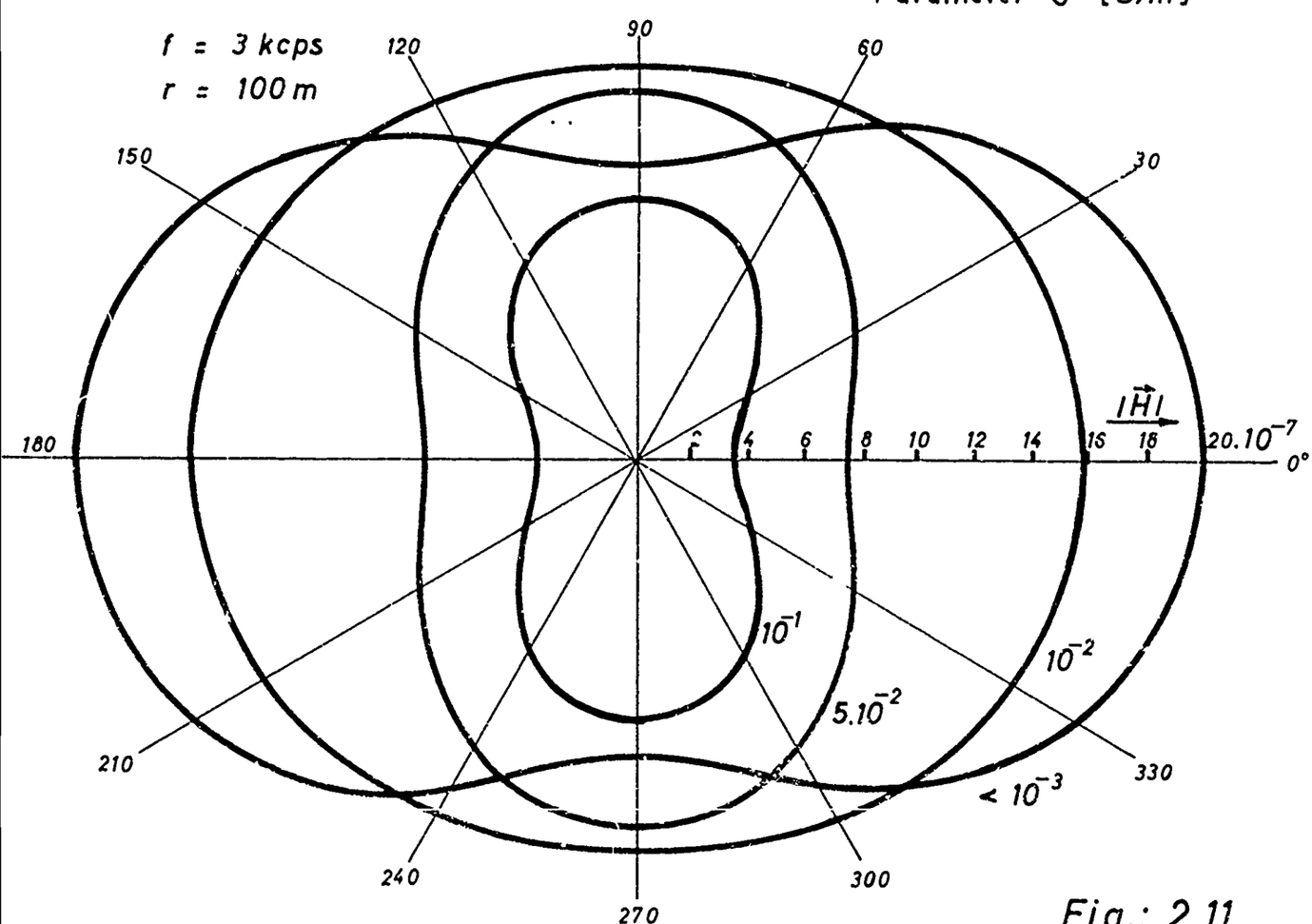

Fig.: 2.11

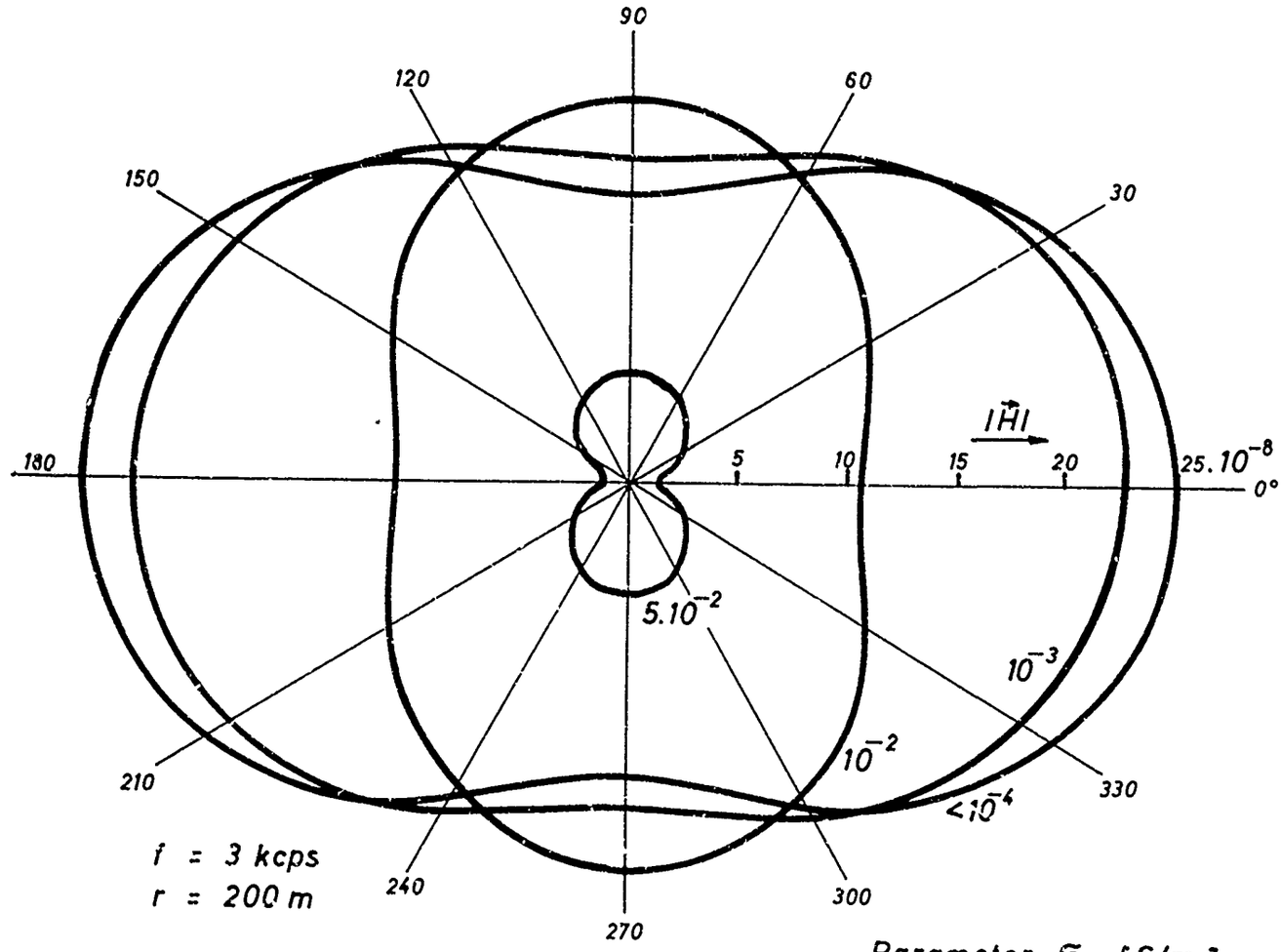

Parameter G [S/m]

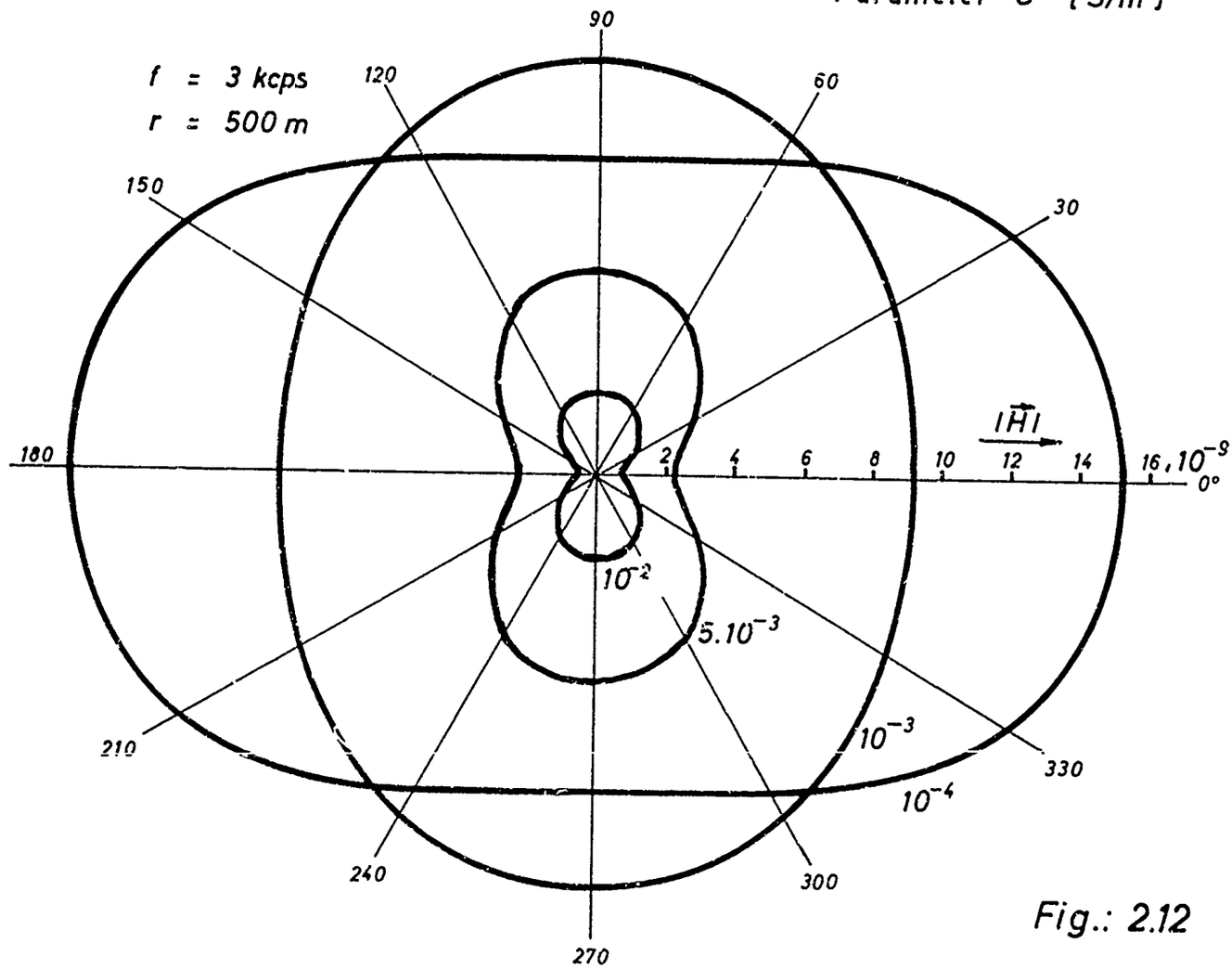

Fig.: 2.12

meters (the most important one being the conductivity σ) in general are determined only as a value integrated over the entire range of measurement. For various purposes of application it is desirable that disturbances even smaller than that be detected which integration over the entire region would be too small as to affect the result noticeably. This is valid especially in those cases where the attenuating effect of the dissipative medium at the distance in question is not noticed (cf. also Figs. 2.3 - 2.8, linear section of the curves) because of the low conductivity.

Disturbances as small as that do not affect the amplitude to a measurable extent, a deviation of the angular position of the maximum, however, may be expected [4] . From Eq. (2.5) (cf. Fig. 2.2) we obtain:

$$\tan \psi = \frac{h_{\vartheta} \cdot \sin \vartheta}{h_r \cdot \cos \vartheta} = \frac{\tan \vartheta}{G} \quad . \qquad (2.10)$$

The dependence of the angle ψ on ϑ for different values of G is shown in Fig. 2.13.

The direction of the maximum is determined not at a weak maximum, but at the clearly adjustable minimum perpendicular to it. The direction-finder antenna FA 5 constructed for this purpose, permits an accuracy of measurement $< 1^{\circ}$.

2.1.2. Modeling tests [5]

Within the framework of experimental studies, modeling tests were also taken into consideration [3, 4, 5] . It would be highly desirous that inhomogeneities in the rock should be avoided and that the conditions of laboratory tests should be accurately expressed by theory. This is of great interest especially in those cases where the earth - air interface is being considered, which in most mines is not sufficiently plane, especially not in the Tyrolean mines.

Another advantage would be the independence of accessible galleries that are suitable for our measurement; the choice being highly restricted above all by the latter condition.

For a modeling test it is by no means sufficient to change all longitudinal dimensions (wavelength and with it the frequency), but the conductivity and the dielectric constant must also be varied [23].

Based on the wave equation we divide all quantities into factors with and without dimensions:

$$\Delta'\vec{E}' - (r^2\mu\varepsilon\omega^2 - i\omega r^2\sigma\mu)\vec{E}' = 0 \qquad (2.11)$$

(dashed quantities being dimensionless).

This dimensionless equation is not changed any further by a gauge transformation, as long as the individual terms are kept constant, which themselves are not dimensionless. Thus we obtain the "modeling condition" (subscript m ... model size):

$$\begin{aligned} &\text{real part: } r^2\mu\varepsilon\omega^2 = r_m^2\mu_m\varepsilon_m\omega_m^2 \\ &\text{imaginary part: } r^2\mu\sigma\omega = r_m^2\mu_m\sigma_m\omega_m \quad . \end{aligned} \qquad (2.12)$$

Since the electrical quantities of the media in question differ widely, we may distinguish two cases:

Case 1:
$$\frac{\sigma}{\varepsilon\omega} \gg 1$$
(Imaginary part of the wave equation prevails, high conductivity, e.g., earth, ionosphere). (2.13)

Case 2:
$$\frac{\sigma}{\varepsilon\omega} \ll 1$$
(Real part prevails, vanishing conductivity, e.g., air). (2.14)

In both cases only one condition (2.12) must be satisfied, which is an essential simplification.

For an earth - air - ionosphere model, the meaningful model factors have an order of 10^6. From it results a model conductivity which can be represented by metal only. "Underground" measurements should therefore be made in boreholes, yet

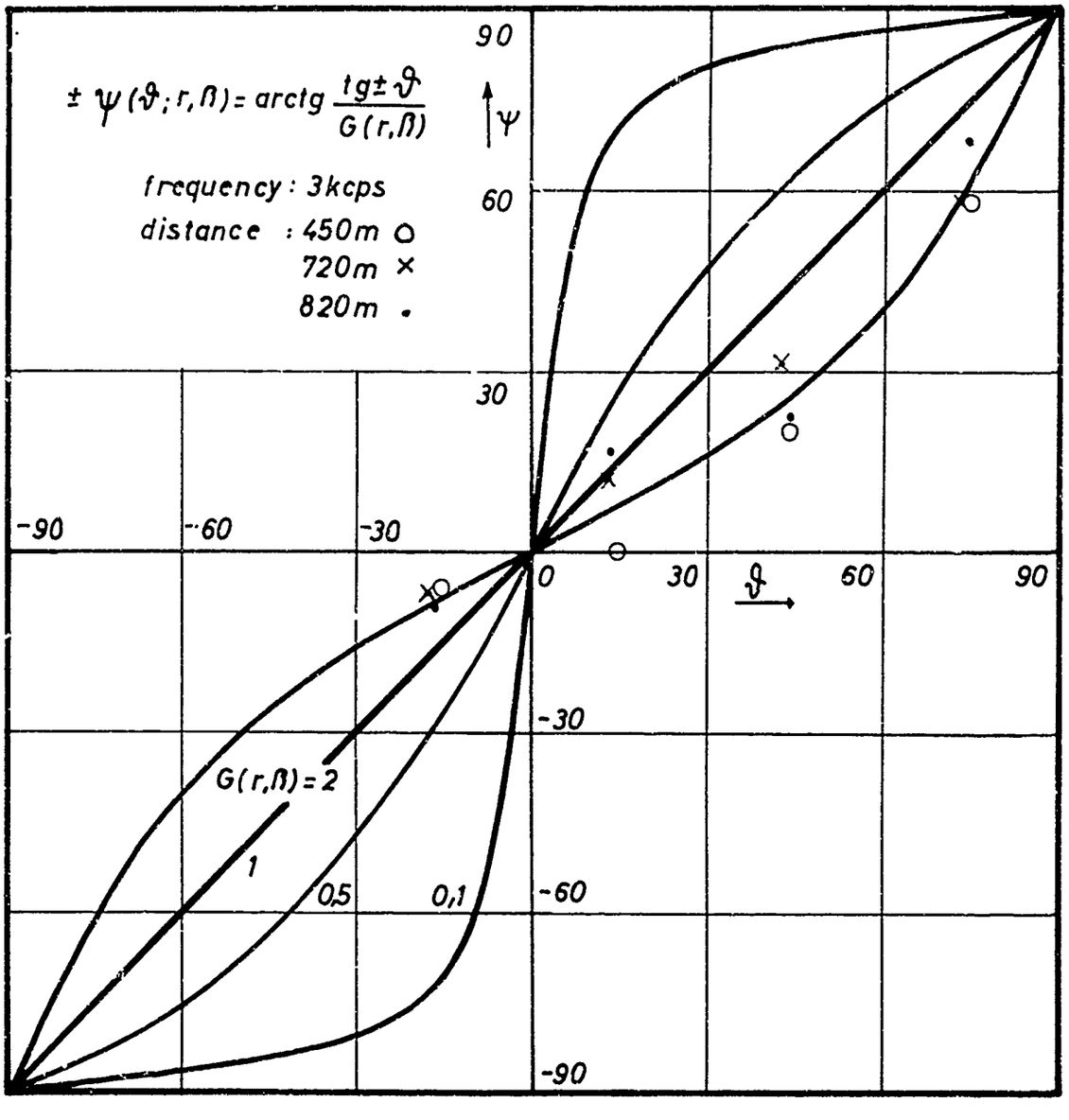
± ψ (ϑ; r, Π) = arctg tg± ϑ / G(r, Π)
frequency : 3kcps
distance : 450m
720m
820m
90
60
30
-30
-60
-90
ψ
ϑ
0
30
60
90
G(r,Π) = 2
1
0,5
0,1

Fig: 2.13

secondary effects (skin effect) occur at the model frequencies (several Mcps), rendering such a measurement impossible. Reducing the model factor such that the earth can be represented by acidified water makes the dimensions unsuitable.

Another field of application would be measuring the antenna directivity patterns under clearly defined conditions. In this case, the model factors are approximately 10^2 to 10^3, thus involving conditions that can be materialized.

Furthermore the possibility was studied of making modeling tests on solid rock in the mine in order to be able to conduct measurements over great distances also at restricted regional dimensions. At constant conductivity, only length and frequency must be changed.

Case 1: The simultaneous fulfilment of Eqs. (2.12) and (2.13) (imaginary part) restricts the number of possibilities. The condition

$$\frac{\sigma}{\varepsilon\omega} = \frac{10^6}{\omega} \gg 1 \qquad (2.13)$$

puts an upper limit of frequency of approximately 10 kc/sec at $\sigma = 10^{-4}$ mhos/m. This, however, lies in the order of magnitude of the actual frequency of measurement. A model of this type is possible only at higher conductivities.

Case 2: The condition (2.12) (real part) is independent of the conductivity.

According to the requirement of (2.14), the latter condition is restricted to conductivity values below 10^{-5} mhos/m and frequencies above 1 Mc/sec.

For the region that lies between case 1 and case 2, which is quite frequent in practical application, the fulfillment of both conditions (2.12) is necessary; this is possible only when length, frequency and conductivity are modeled simultaneously.

The only possibility of conducting laboratory tests at reasonable modeling dimensions (having the order of meters) is the measurement of antenna directivity patterns. Plotting such diagrams proved to be comparatively easy in practice, especially since in numerous cases a distance of less than 1 km was measured so that the expenses for setting up the instruments and for the modeling tests themselves did not appear to be justified.

2.2. Measurements in the mine

The measurements below ground were made in several mines offering various types of rock. Thus it was possible to obtain series of measurements for a large range of decisive parameters which were then compared with the theoretical results obtained for wave propagation in solid media [1],[2].

The conductivity of the surrounding rock varies between approximately 10^{-1} mhos/m in the mine of Konrad I (iron ore) to 10^{-8} mhos/m in the Hansa III mine (dry salt).

The sites of measurement were chosen so that the conditions assumed for theoretical calculation were fulfilled as far as possible. Large iron units such as rails, pipes, mining railways or iron formwork had to be avoided. In order to meet the requirement of a homogeneous medium, there should be no dislocations, cavities or ore inclusions in the region of measurement.

The distances between the individual points of measurement were read from mine charts and the angles were measured with a geological compass. The resulting errors of measurement (inaccurate charts, magnetic disturbance of the compass) are partly corrected by balancing calculations.

The necessary communication between the transmitter and the sites of reception is made possible by a field telephone. The effect of the connecting wire on the measurement can be neglected according to various experiments. In cases

where a telephone communication was impossible because of the great distances, the measurements were made in accordance with an accurate timetable. The distance over which measurements were conducted varied considerably, depending on the conductivity and the possibilities of the respective mine. In many cases, measurements could be made over distances of 800 m, occasionally, however, only 20 to 30 m. In the "home mine" of St. Gertraudi, Tyrol, measurements over a distance of 7000 m with a stationary transmitter erected for this purpose were possible, part of the distance, however, being above ground.

2.2.1. Mine of Lafatsch, Tyrol

(Mining charts see [2])

This mine which at present has been abandoned contains a large deposit of lead and zinc ores in the form of a steep layer, entered at several levels. The transmitter was first set up at the lowest, the sixth level having the largest system of galleries, where the majority of measurements were conducted. The ore is mainly located above the region of measurement.

The conductivity determined on the basis of these measurements by a balancing calculation is approximately 5.10^{-6} mhos/m.

For a second series of measurements, the transmitter was set up at the top end of the ore layer on level 2, the field strength measurements being conducted along the ore deposit down to level 6. As could be expected from the theoretical results, the integrated conductivity was somewhat higher, namely 10^{-5} mhos/m. Both curves together with the theoretical representation belonging to this conductivity value are shown in Fig. 2.14. It is quite evident that the ore deposit swallows more energy because of its higher conductivity (curve 1) so that the curve trend on the whole is somewhat steeper for measurements along the ore deposit.

Although the conductivity during the measurements at Lafatsch was found to differ, the maximum distance of measurement at the given frequency and material constants was too small as to yield a satisafactory accuracy of conductivity values.

2.2.2. Mine at Schwaz, Tyrol

(Mining charts see [2])

In contrast to the Lafatsch measurements, the measurements here covered distances of up to approximately 1300 m. For this distance, the previous transmitter was no longer suited. Another transmitting antenna of about 16 m^2 and 35 turns (for details of SA VII see [2]), was set up for covering this distance. The measured values are plotted in Fig. 2.15. Curve 3 was measured with the small transmitting antenna (SA III), curve 2, however, shows the values obtained with the large frame. The measurements of curve 1 were made through different types of rock (slate wedge, else dolomite). The mean conductivity calculated from it is 10^{-5} mhos/m.

The measurements made so far were almost pure near field measurements owing to the small conductivity and distances. They were consistent with the theory within the measuring accuracy, although the compared values were not absolute, a balancing calculation was made in order to make the measured attenuation consistent with the theory.

2.2.3. Konrad I mine at Salzgitter

The geological structure of this region is characterized by a varied, flat stratification formed by repeated sea floods. The concentration of this oolitic ore is approximately 30%, the average size of the individual brown iron grains is 0.5 mm. The depth of the mine is approximately 1000 m.

Sites suitable for the measurements were difficult to find in the mine, they had to be free of iron formwork, rails,

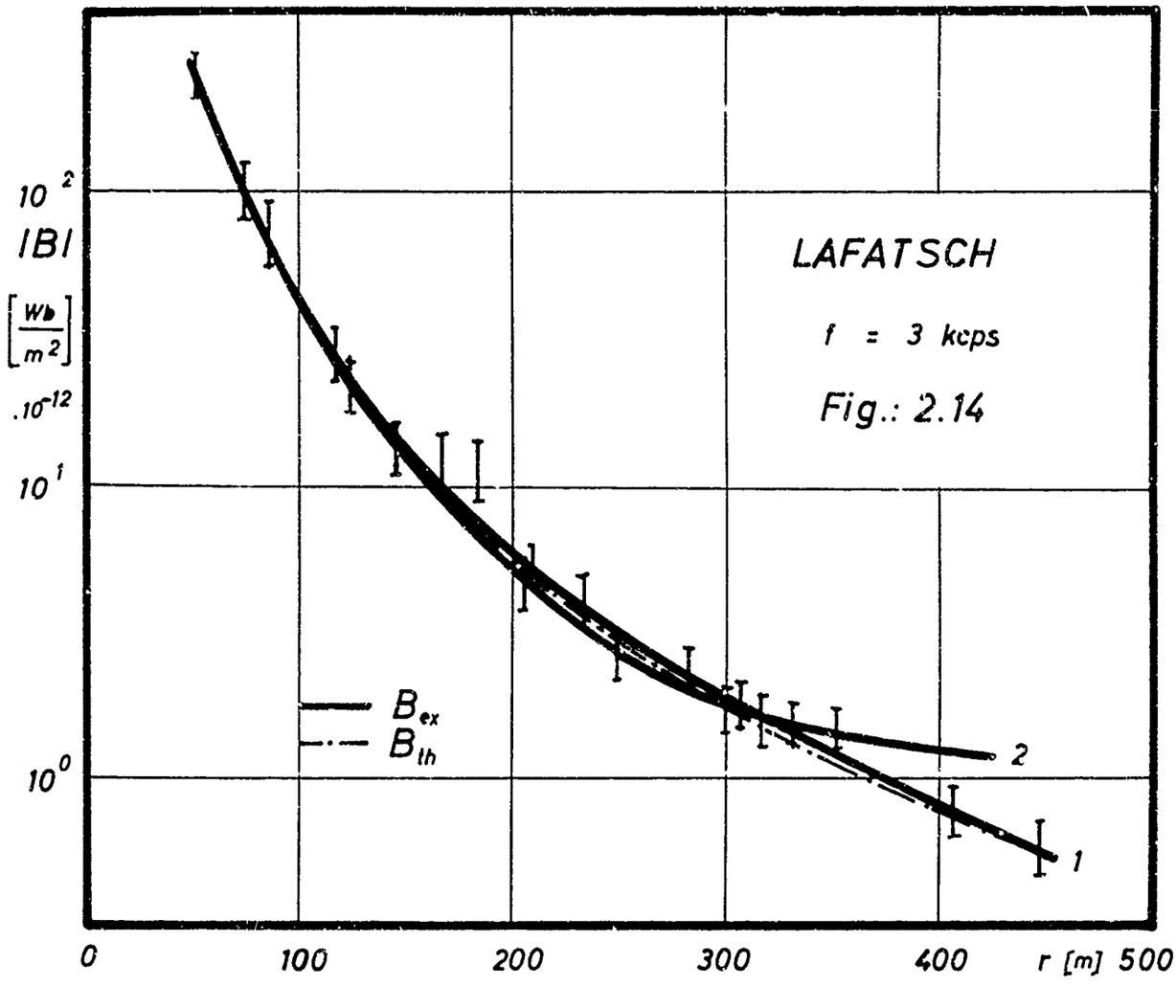
LAFATSCH
f = 3 kcps
Fig.: 2.14
IBI
[Wb/m²]
.10⁻¹²
10²
10¹
10⁰
B_ex
B_th
1
2
0
100
200
300
400
r [m] 500

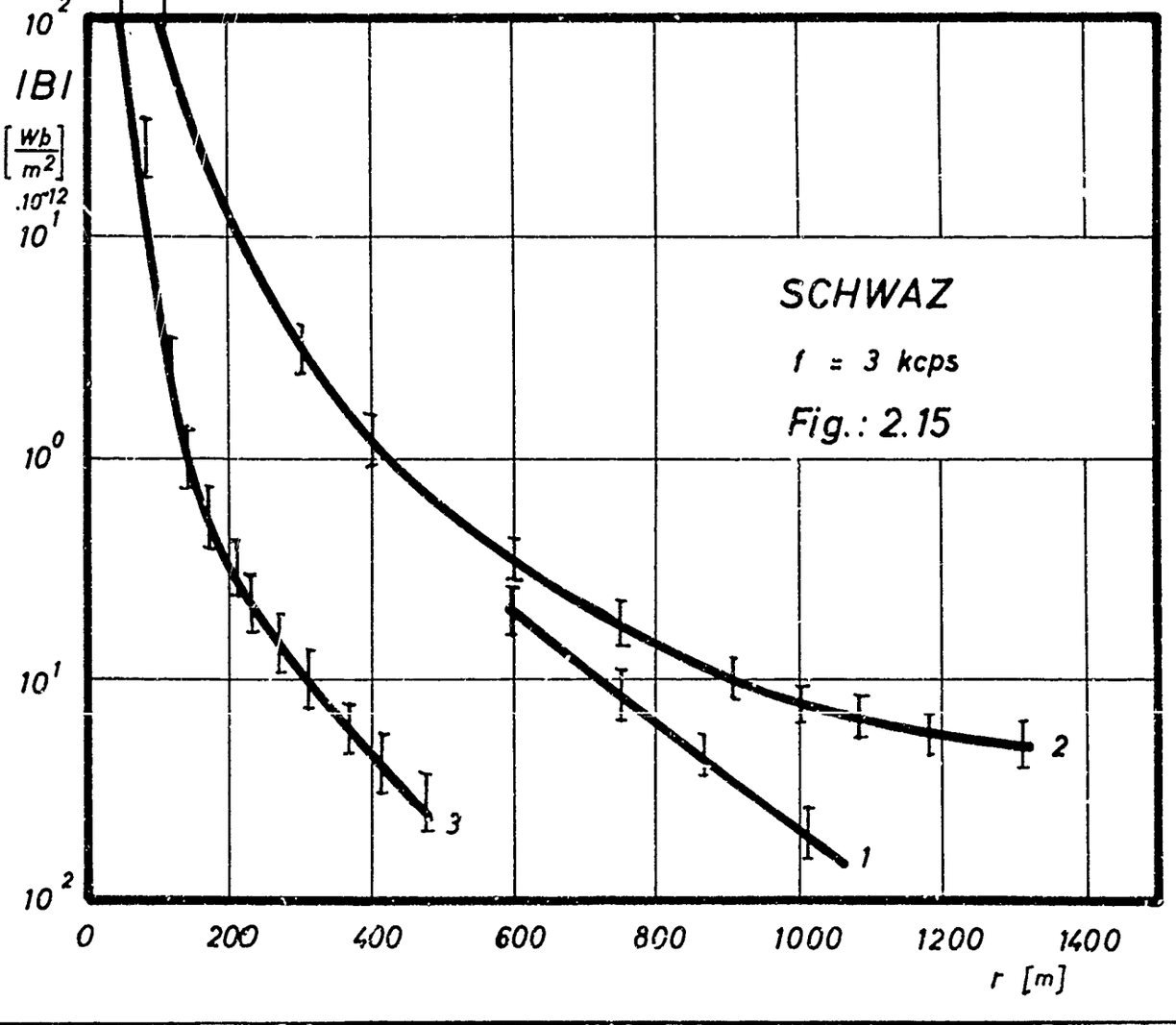
SCHWAZ
f = 3 kcps
Fig.: 2.15
IBI
[Wb/m²]
.10⁻¹²
10²
10¹
10⁰
10¹
10²
1
2
3
0
200
400
600
800
1000
1200
1400
r [m]

pipes and power cables. An 18 m and a 25 m distance at the 1000 m level appeared to be suited best. Although the distances were short, characteristic antenna diagrams could still be measured, as the conductivity was very high, namely 2.10^{-1} mhos/m.

The measurements in Konrad I showed that the voltage read at an angle of $\varphi = 90^{\circ}$ (cf. chapter 2.1.1.) does not always become zero as had been expected according to the theory of the cosine law. An explanation although just a qualitative one, would be the high inhomogeneity of the field, an assumption which seems quite probable [3] at the small distance and the high conductivity. A detailed examination of this effect will be made at higher frequencies.

An evaluation of the antenna diagrams showed that the transition from near field to far field at $2 \cdot 10^{-1}$ mhos/m occurs already at 25 m ($G \sim 1$), whereas at Gertraudi (approximately 10^{-4} mhos/m) the measurements were still made in the near field even at 800 m ($G > 1$). In this case of extremely high conductivity the strong shift in near field - far field transition becomes quite evident. Under these circumstances, effects occur at minimum distances which elsewhere set in at greater distances, being immeasurable because of the small power of the transmitter.

2.2.4. Potassium mine Hansa III, Empelde near Hannover

Whereas in Konrad I the electrical conductivity of rock on average was by three powers higher than in the mines studied so far, the conductivity of the medium used in Hansa III was so small (approximately 10^{-8} mhos/m) that it may be looked upon as being almost an insulator. The measurements were conducted in a large, dry salt stock at the 1000 m level.

Apparently favorable conditions of propagation and measurement, however, could not be used much because of the disturbing influences. Owing to the weak attenuation in the salt body, disturbances caused by the mining railway at higher levels were noted strongly. High static charges caused by

pipes and power cables. An 18 m and a 25 m distance at the 1000 m level appeared to be suited best. Although the distances were short, characteristic antenna diagrams could still be measured, as the conductivity was very high, namely 2.10^{-1} mhos/m.

The measurements in Konrad I showed that the voltage read at an angle of $\varphi = 90^{\circ}$ (cf. chapter 2.1.1.) does not always become zero as had been expected according to the theory of the cosine law. An explanation although just a qualitative one, would be the high inhomogeneity of the field, an assumption which seems quite probable [3] at the small distance and the high conductivity. A detailed examination of this effect will be made at higher frequencies.

An evaluation of the antenna diagrams showed that the transition from near field to far field at $2 \cdot 10^{-1}$ mhos/m occurs already at 25 m ($G \sim 1$), whereas at Gertraudi (approximately 10^{-4} mhos/m) the measurements were still made in the near field even at 800 m ($G > 1$). In this case of extremely high conductivity the strong shift in near field - far field transition becomes quite evident. Under these circumstances, effects occur at minimum distances which elsewhere set in at greater distances, being immeasurable because of the small power of the transmitter.

2.2.4. Potassium mine Hansa III, Empelde near Hannover

Whereas in Konrad I the electrical conductivity of rock on average was by three powers higher than in the mines studied so far, the conductivity of the medium used in Hansa III was so small (approximately 10^{-8} mhos/m) that it may be looked upon as being almost an insulator. The measurements were conducted in a large, dry salt stock at the 1000 m level.

Apparently favorable conditions of propagation and measurement, however, could not be used much because of the disturbing influences. Owing to the weak attenuation in the salt body, disturbances caused by the mining railway at higher levels were noted strongly. High static charges caused by

salt yielded considerable irregular fluctuations in indication. The GBR transmitter which above ground was very strong, could not be received, since the salt-containing ground water layer at a depth of 180 m screens off all signals from above.

Yet, an antenna diagram was measured whose ratio $G = h_r : h_\vartheta = 2$ leads to the assumption of a very low conductivity.

2.2.5. Ore mines of Füsseberg and Georg
(Siegerland, Germany)

From an electric viewpoint, the conditions in these two mines were similar to those at Schwaz or Gertraudi. The iron ore (siderite) mined there occurs in the form of a steep edge heave approximately 10 m thick. The deposit of Füsseberg is straight, whereas in the Georg mine it has the shape of a horseshoe.

The sites of measurement were chosen so that the line connecting transmitter and receiver ran mainly through ore. The influence of the inhomogeneous medium on the propagation of VLF waves could thus be studied. The measured values showed on the whole the same trend as those measured at Schwaz, thus suggesting equal conductivity. Direct current measurements which were made parallel [3] yielded the same conductivity for ore and dead rock, thus explaining the small differences on measuring in front of and behind the ore layer.

The antenna diagrams showed pure minima at $\varphi = 90^\circ$ and were well consistent with the theoretical values obtained for this conductivity value.

2.2.6. Coal mines Oranje Nassau, Heerlen (Netherlands)

The Nassau III mine offered the unique possibility of making measurements in coal. They were made in the direction of the coal seam which is about 2 m thick. For this purpose, the mine management provided a surrounding for transmitter and

receiver that was free of iron, short drifts were lined with wood formwork. Measurements were made at the angles $\vartheta = 0°$ and $\vartheta = 90°$ and at a distance of 300 m and 500 m, respectively. Unexpectedly, the conductivity measurements with direct current showed coal to have a poor conductivity and the rock below was found to have a comparatively high conductivity. Hence, propagation proceeded in the direction of a thin and weakly conductive layer which was bounded by two media of good conductivity. Such a "sandwich" structure which in principle is typical of any coal pit, on account of the results seems to favor the propagation of VLF waves. Various factors apparently affect the propagation: The relation between the seam thickness and the measuring distance in connection with the wavelength which again depends on the conductivity of the surrounding medium, is an essential factor. Also the antenna alignment (angle ϑ) has a different effect as compared to air or homogeneous rock.

At a distance of 500 m, G was found to have the value 0.22 which corresponds to a conductivity of about $1 \cdot 10^{-3}$ mhos/m at a frequency of 3 kcps. A comparison with the d-c conductivity however, cannot be made, since the propagation in the strongly heterogeneous medium cannot be compared with the conditions of our theory. It was not possible to study the variety of effects on the spot with the required accuracy. The preliminary results show, however, that a detailed examination of this alignment would yield highly interesting results.

2.2.7. Mine at Bleiberg, Kärnten (Austria) [15]

In this mine, measurements were mainly made in Wetterstein limestone containing ore inclusions (20 to 30 m) in the form of lead glance and zinc blende which compared to the range of measurement (400 to 800 m) were rather small. The inhomogeneities therefore had only a slight effect on the results of measurement. Fig. 2.16 shows such a profile measure-

ment (curve 1). The dashed curve gives the theoretical decrease in field strength resulting from the mean value of conductivity, approximately 10^{-4} mhos/m. At about 400 m, the transition to rock of somewhat higher conductivity is clearly recognizable.

Curves 2 and 3 give the measurements of the GBR transmitter (16 kcps). The horizontal field strength decrease was plotted for the distance from the shaft mouth (curve 2) and in 2a the cover is also plotted (shortest distance from the earth's surface). Curve 3 gives the decrease in vertical direction. The distance here is not the transmitter - receiver range which has the order of about 1000 km, but the respective distance from the earth's surface. Hence, the much weaker attenuation of the GBR transmitter as compared to our own transmitter can also be explained, since in one case the measurement is made in the far field (approximately plane waves), whereas in the other case the geometry of the field contributes considerably to the attenuation (decrease of the field with $1/r^3$ in addition to absorption).

2.2.8. Mine at St. Gertraudi, Tyrol

(mining charts see [2] and [3])

At Gertraudi, a straight gallery 800 m long was available as a connection between the Großkogel mine and the Kleinkogel mine, which is highly suited as it passes through largely homogeneous dead rock; its elongation of another 500 m in the abandoned Kleinkogel mine is again highly suitable for the measurements. This is the reason why preliminary experiments and measurements were made in this mine from the very beginning of our project work, besides the measurements made at Schwaz.

Let me mention some of the numerous measurements and experiments: Preliminary experiments with adapted transistorized portables; measurements of other long-wave transmitters; primary experiments with our own transmitter at higher fre-

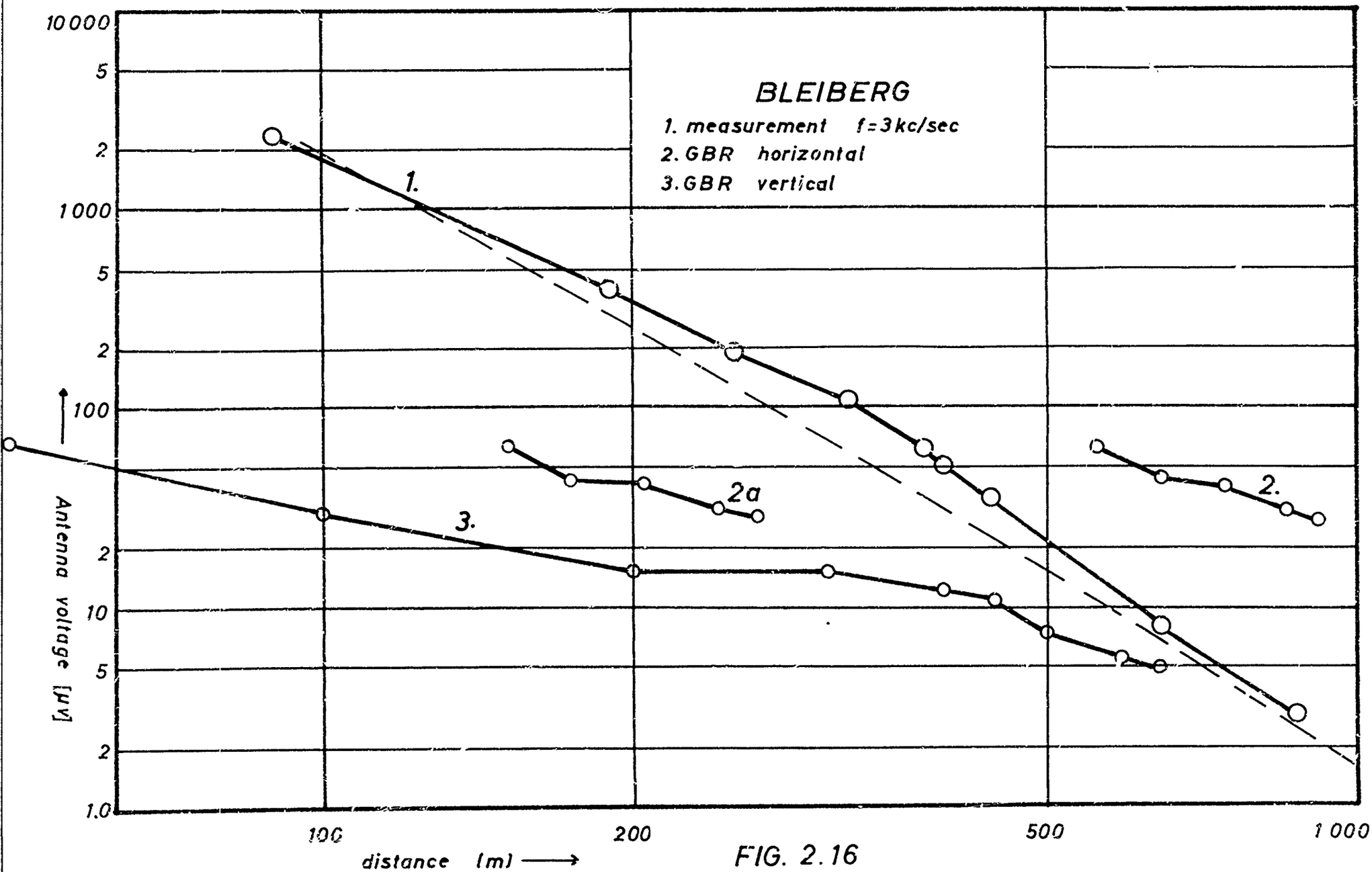
BLEIBERG
1. measurement f=3kc/sec
2. GBR horizontal
3. GBR vertical
1.
2.
2a
3.
10 000
5
2
1 000
5
2
100
2
10
5
2
1.0
Antenna voltage [μV]
100
200
500
1 000
distance (m) ⟶

FIG. 2.16

quencies (about 100 kcps); profile measurements with specially designed transmitting antennas; experiments and measurements with various receiving antennas.

On the preparatory measurements discussed herein, a theory of wave propagation was based which is adapted to the simplified conditions of measurement [2] as has been mentioned in 2.1. From the profile measurements, the conductivity was calculated and found to be of the order of 10^{-4} mhos/m, in some series of measurements, however, only the conductivities above 10^{-4} mhos/m at smaller distances could be excluded. A comparison with the theory at first could only be based on the attenuation relation owing to the absence of accurate calibration factors for transmitting antennas and receiving antennas, i.e., the slopes of the measured curves were compared with the respective theoretical curves by means of a balancing calculation (method of least squares); the agreement with theory was good so that the adapted theory of the transmitting dipole for the near field may be assumed to be correct [2].

The antenna diagrams measured in the direct neighborhood of the transmitting antenna also showed good agreement with the theory for transmitting dipoles.

From the electrical and geological viewpoints, the conditions of measurement in the mines of Schwaz and St. Gertraudi are approximately equal, hence also the similar results of measurements (cf. chapter 2.2.2.).

From the requirement for covering larger distances resulted the necessity of building always larger transmitters and of making the receiving antennas more selective and sensitive. By means of a stationary 1 kw amplifier set up in the mine laboratory [3] (details see chapter 1), distances of up to 7 km could be covered by means of the transmitting antenna SA VIII (dimensions 40 x 40 m.) set up especially for this purpose. As a distance of the above length could not be found within the mine, measurements at the remotest points had

to be made above ground. Owing to the much higher noise level (no screening effect by rock layers), the sensitivity of the receiving antenna could not be used fully so that the corresponding measurements below ground would permit even larger distances [3] .

An improved version of the SA VII transmitting antenna was used for plotting antenna diagrams at frequencies of 3 and 11 kcps. As the distances covered with the SA VII antenna are shorter than those of SA VIII, diagrams were made up to a distance of no more than 820 m. The diagram of Fig. 2.16a clearly shows that the measurement was made in the near field also at greater distances, thus being in good agreement with the theory for the existing conductivity values [4]. In this connection, the change in angular position ψ of the receiving antenna was also studied. The corresponding points are plotted in Fig. 2.13. Here, agreement with the theory is not quite as good, as small inhomogeneities affect the angular position, whereas the influences on the amplitude cannot be measured (cf. chapter 2.1).

2.3. Comparison between experiment and theory

The great number of measurements which were made under different geological conditions were almost all confined to the near field, with the corresponding distance of measurement changing considerably in dependence on the conductivity. It has already been said in chapter 2.1 that propagation at very small distances is quite independent of external influences. The results of measurement therefore are in good agreement with the theory, since the assumptions on which the theory is based, are actually verified (measurements of [1] and partly also of [2]).

For greater distances (measurement still in the near field), the influence of the conductivity σ is already

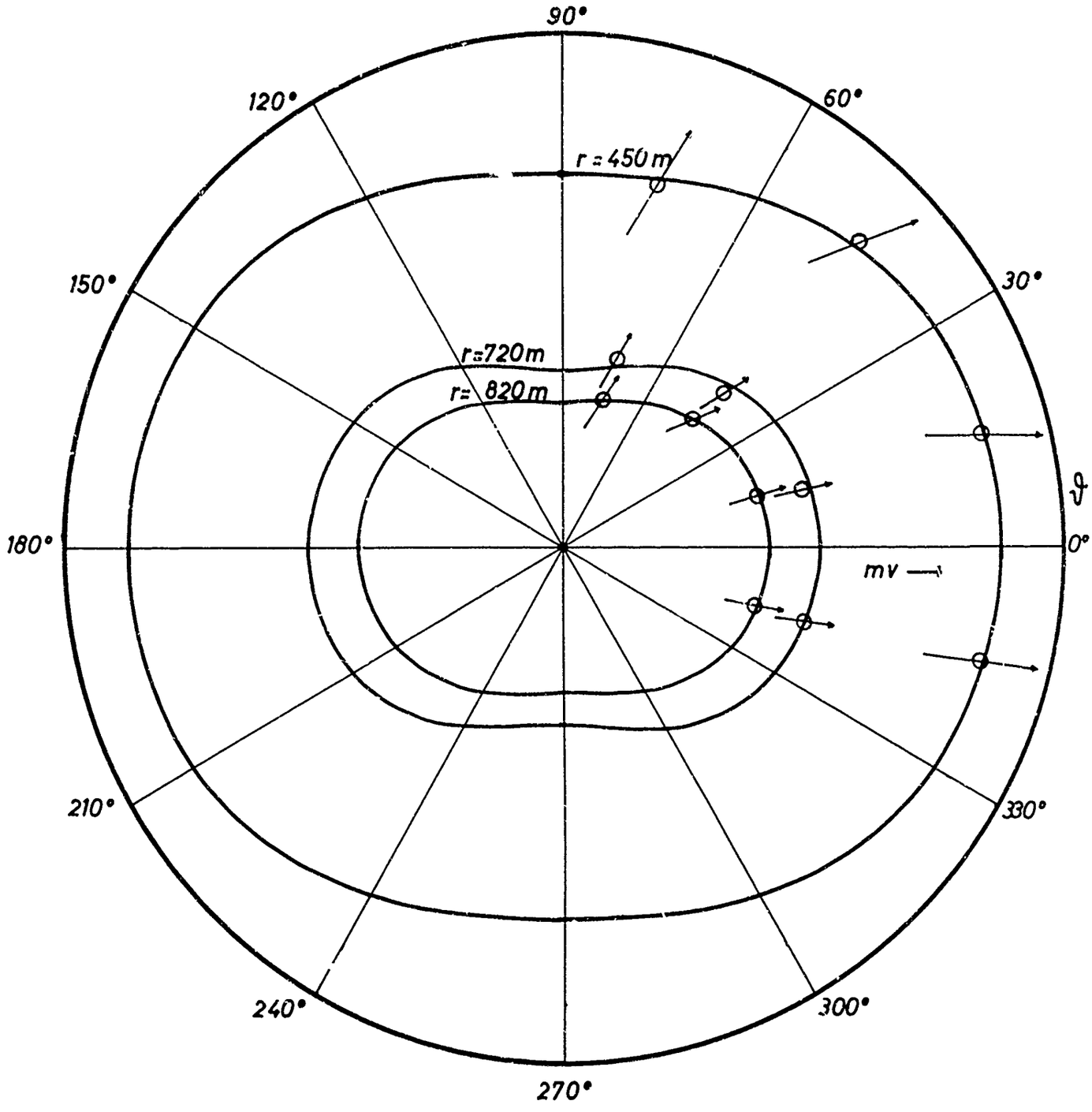

scale :

1 2 5 10

frequency : 3 kcps

FIG. 2.16 a

noticeable; it is therefore used for determining the value of σ. In this case, the results of measurement are satisfactorily explained by the theory (measurements of chapters 2.2.1, 2.2.2, 2.2.4, 2.2.5).

In few cases the conditions of measurement did not at all correspond to the theoretical conditions (measurement in the coal seam, chapter 2.2.6), thus making a comparison impossible.

The measurement in the mine Konrad I (chapter 2.2.3) was made in a medium of extremely high conductivity ($\sigma = 2 \cdot 10^{-1}$ mhos/m), yielding for the first time a result that can be theoretically interpreted in terms of a far field measurement ($G \sim 0.2$).

The most recent measurement over large distances at St. Gertraudi (chapter 2.2.8) offered the possibility of studying also the effects of reflection from the earth's surface and surface waves (cf. Fig. 2.17). A comparison with the theory of [10] (reflection from the earth - atmosphere interface) is only conditionally possible, as the earth's surface in the region of the St. Gertraudi mine is by no means plane, as assumed for the present calculation. Yet, propagation in accordance with the refined theory is quite probable. Summing up the results we may say that the propagation of VLF waves in the near field ($G > 1$) on the whole is described by the theory developed in [1] and [2]. For larger distances, this theory probably is too simple, a correction according to [10] (reflection from the earth's surface) yields better agreement. An influence of the medium in the form of refraction or diffraction of VLF waves at the existing power and frequency of transmitter could not be observed to a useful extent. At present, comprehensive experiments are made at approximately 100 kcps for studying these effects in detail.

2.4. Bearing of a dipole probe
(an example of practical application [20])

From the determined experimental and theoretical results, the possibility of taking a bearing of a transmitting magnetic dipole in a solid medium with high accuracy was derived. From the expressions (2.1), (2.2), and (2.3) (chapter 2.1) it follows that all field lines lie in meridional planes, i.e., every tangent to a field line crosses the dipole axis (cf. Fig. 2.18). This tangential direction is exactly the direction at which maximum voltage is induced in the ferrite-rod direction-finding antenna. In general, this direction does not directly point to the transmitting dipole, as can be seen in the field line diagram of Fig. 2.20a. If the magnetic dipole is displaced along its axis (position B), the direction-finder antenna shows a new maximum direction b at the same point of reception. The two space directions a,b define one meridional plane (two intersecting lines).

For determining another meridional plane, two more field directions are measured from the point II (cf. Fig. 2.19) in the same manner as above (c,d correspond to the positionc C,D). The positions C, D may coincide with A, B, but can be chosen arbitrarily in accordance with the respective conditions. The line of intersection of these two meridional planes is identical with the dipole axis.

The position of the basis line I-II with respect to the dipole axis must be wind-tipped, a parallel position or intersection of the two lines would render the problem indefinitive.

The accurate location of the dipole itself after having found its axial direction by means of the field line diagram (Fig. 2.20 a) is now possible. The direction of field lines is given by the expression:

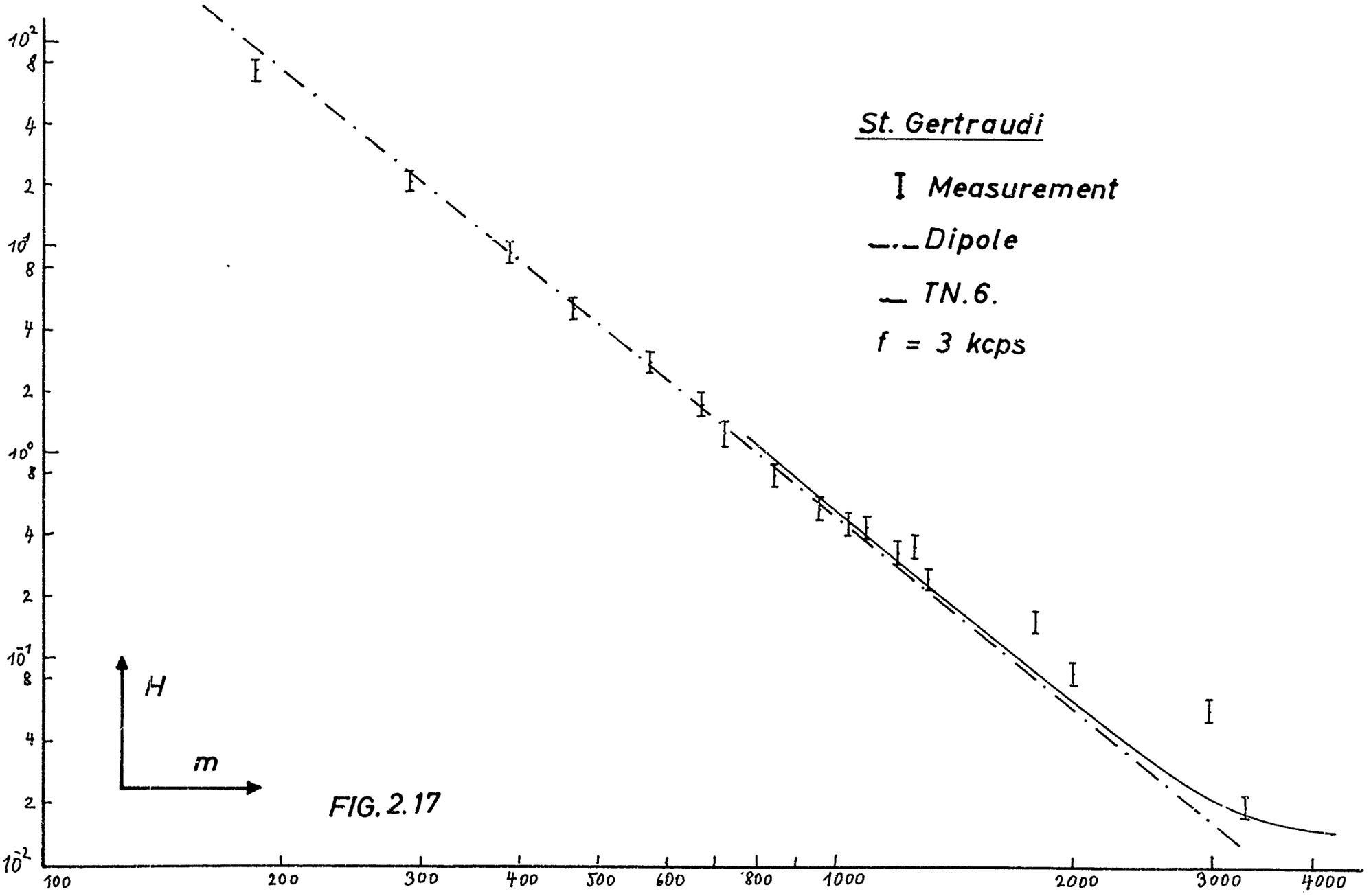
St. Gertraudi
Measurement
Dipole
TN.6.
f = 3 kcps
H
m
10^2
8
4
2
10^1
8
4
2
10^0
8
4
2
10^{-1}
8
4
2
10^{-2}
100
200
300
400
500
600
800
1000
2000
3000
4000

FIG. 2.17

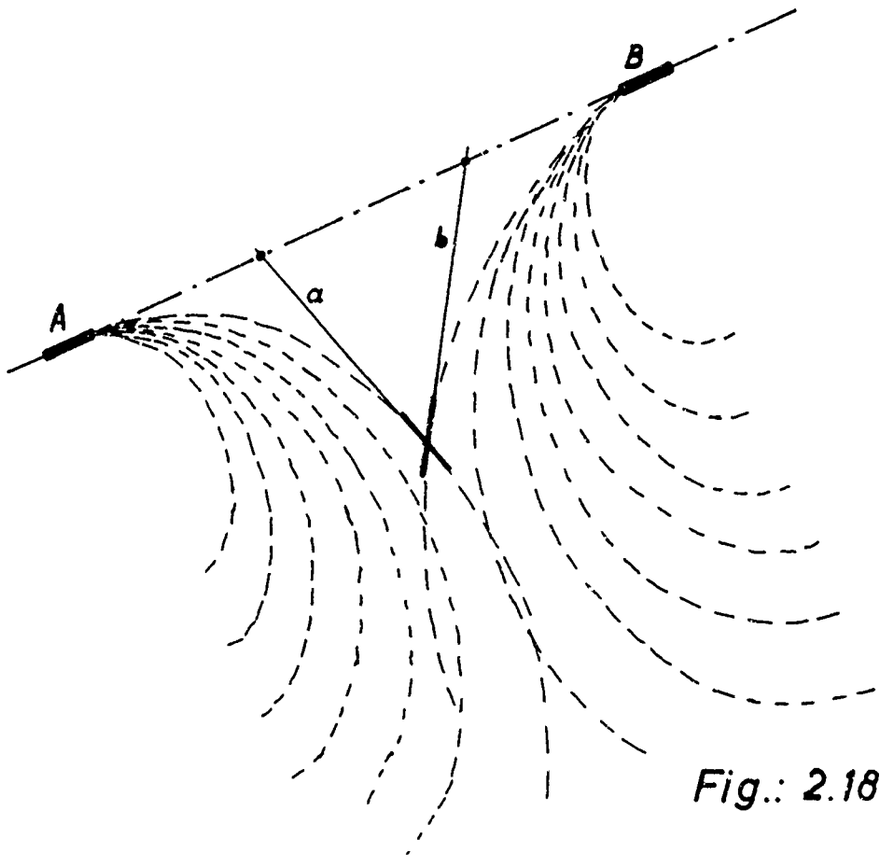

Fig.: 2.18

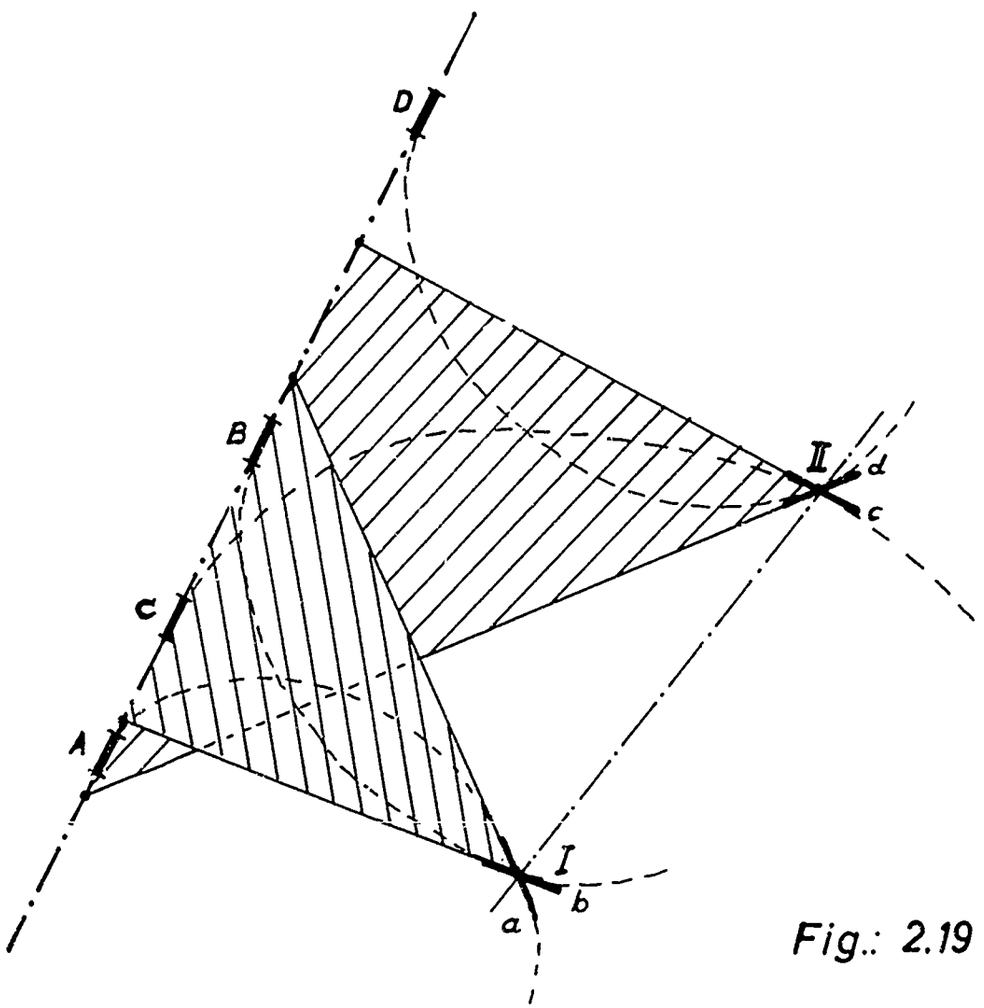

Fig.: 2.19

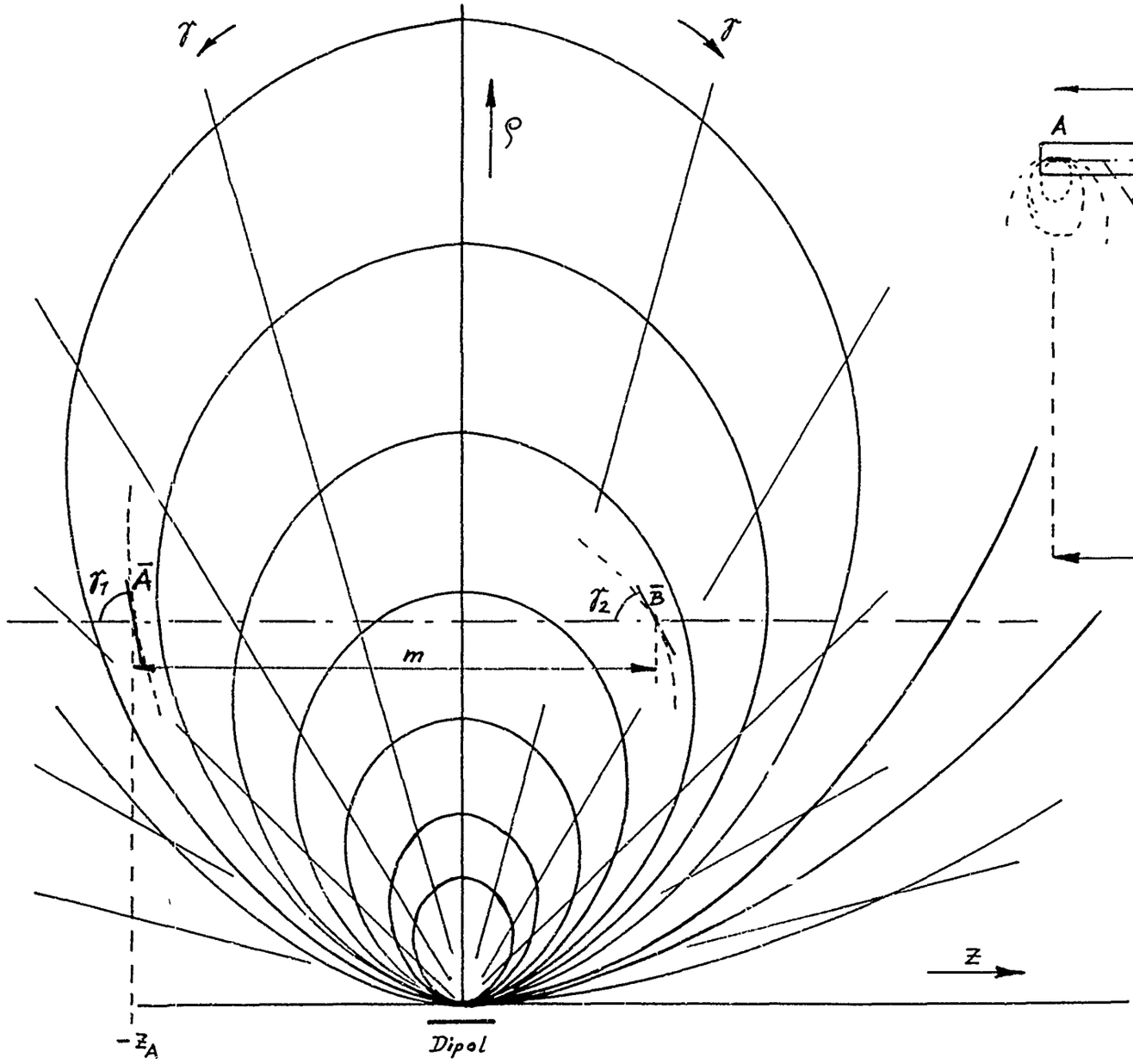

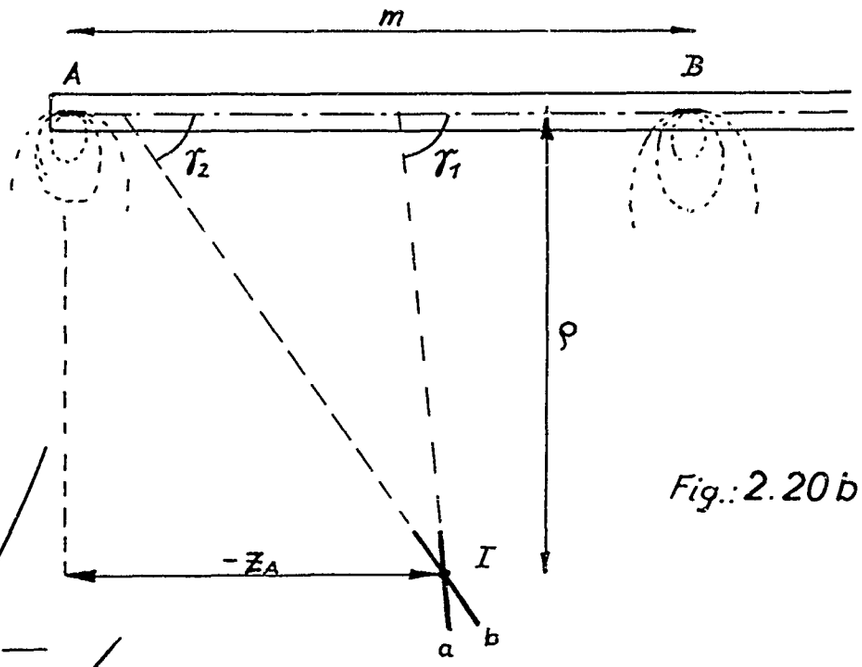

Fig.: 2.20 b

Maßstab beliebig

Fig.: 2.20 b

$$\frac{dr}{r\,d\varphi} = \frac{H_r}{H_\varphi} = \frac{2m\, e^{-\beta_2 r} \cdot \cos\varphi \cdot \frac{1}{r^3}}{m\, e^{-\beta_2 r} \cdot \sin\varphi \cdot \frac{1}{r^3}} = 2 \cot\varphi \qquad (2.15)$$

with the expressions for H_r and H_φ (expressions (2.1) and (2.3), chapter 2.1) being approximated by the first term, in accordance with the problem (measurement over a comparatively short distance).

Integration of the equation (2.15) yields

$$r = a \cdot \sin^2\varphi \qquad (2.16)$$

for the field lines, with a being the parameter of field lines.

Similar to the antenna diagram measurements of chapter 2.1.1, the displacement of the transmitting dipole (Fig. 2.20 d) with the corresponding directions a,h here is represented as a shift of the point $\bar{A},\bar{B}$, thus permitting a full-scale representation of the direction of reception in one diagram of field lines (Fig. 2.20 a). As the angular position of the field lines with respect to one radius vector is always equal and independent of the radius, the scale may be chosen arbitrarily. For a unique determination of position, always two angular positions must be taken into consideration.

The method described above, is suited, e.g., for locating miscarried boreholes in mines. Because of the narrow hole, the magnetic dipole for this purpose usually has the shape of a long and thin coil with an iron core placed at various depths (according to the positions A...D).

In a measurement based on this method, the position of a borehole (54 mm diameter) which was miscarred by 1.6 m in the copper mine of Mitterberg, Salzburg, could be determined with an accuracy of 10 cm [20].

3. Studies on the electrical conductivity of rock

The studies on the propagation of VLF waves also included measurements of the conductivity and dielectric constant of rock. The conductivity measurements on solid rock were made with direct current and alternating current, whereas those on rock samples were made with alternating current only.

3.1. Direct current measurements

The conductivity measurements with direct current followed the principles of the four-electrode configuration. The theoretical fundamentals and the measuring equipment used for this purpose are described in [3] , p. I - 23. The principal aims of direct-current conductivity measurements were the following:

(a) to study how far rock is uniform from an electrical point of view,

(b) to derive the conditions under which the conventional methods of measurement based on the conditions of an unbounded semispace or full space can be applied also in mine galleries,

(c) to determine the absolute value of conductivity.

3.1.1. Inhomogeneity of rock

It could be shown that the socalled Wenner arrangement is well suited for conductivity measurements in mine galleries. For inhomogeneous media, measurements following the Wenner method yield a mean value of conductivity. Therefore it is possible to vary the range covered by the lines of force and thus also the range for which the mean value is taken, by varying the electrode spacing. Measurements at many different points of the mine with small electrode spacings showed that the rock within small ranges (order of 1 - 2 m) is of con-

siderable electrical inhomogeneity. Scattering of the results of measurements about a mean value of conductivity was the greater, the smaller the space covered by the measurement. At electrode spacings of the order of 30 - 40 m, however, good agreement of all measured values was attained. This means that the rock within small ranges shows considerable electrical inhomogeneities, the mean value of conductivity which is decisive also for the propagation of electrical waves over greater distances, is highly significant.

3.1.2. Influence of the gallery cavern on the result of measurement

The conventional methods of determining the electrical conductivity of rock require the measurement to be made on a semi-space or full space. The results measured in a gallery, however, are affected by the gallery itself. The resulting error will be negligible if the field of electric flow in a gallery agrees with the undisturbed field within a large region. Under what conditions this is the case was studied by three different methods:

(a) From an analytical representation of the current distribution between two electrodes in a homogeneous full space it was calculated how large the electrode spacing must be so that only 10% of the total current flows through a circle whose center coincides with the point that bisects the line connecting the electrodes and whose plane is perpendicular to the connecting line, with the radius of the circle being equal to the diameter of the gallery [Ref. 4, chapter 3.1.1.] .

(b) The voltage profile along the line connecting the electrodes and along a straight line parallel to it on the opposite side of the gallery was measured and compared with the voltage profile valid for a homogeneous full space and the corresponding conductivity. The measurement was made such

that a voltage probe was kept at M during the entire measurement, the second one was connected to the points of measurement in between.

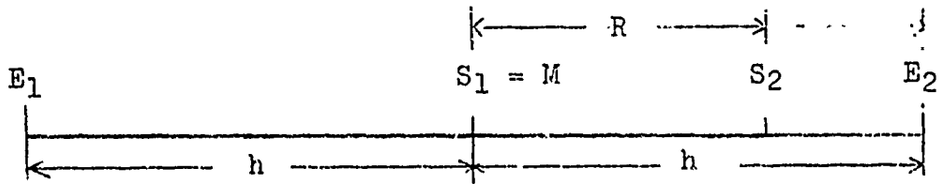

Using the denotations of the figure above we obtain for the conductivity:

$$\sigma = \frac{I}{2\pi U} \cdot \frac{R}{h^2 - R^2} \quad . \qquad (3.1)$$

From the measured voltage values on the electrode side the corresponding conductivity values were calculated and from them the arithmetical mean value $\bar{\sigma}$ was determined. In a diagram, the theoretical curve of the voltage trend was plotted for this mean value, furthermore the measured voltage trend along the line connecting the electrodes and on the opposite side of the gallery (Fig. 3.1). $\bar{\sigma}$ is a suitable scale factor which permits a good comparison of the measured and the calculated results. From a certain electrode spacing onward, the three discussed curves agree well except for deviations due to inhomogeneities. If the value thus obtained is used as a minimum electrode spacing for conductivity measurements, the conductivity value is obtained in good approximation ([4], chapter 3.1.2).

The statement that a correct result for σ is obtained if the discussed curves in the region restricted by the probes are in good agreement, is identical with the statement that the ratio of voltage between the probes on the electrode side and the voltage on the opposite side U_I/U_{II} must be unity. Measuring this ratio, however, we shall find considerable deviations from the value expected according to the geometrical

conditions, because of rock inhomogeneities. If this ratio is determined at numerous sites of measurement for a certain probe distance, the arithmetical mean of all resulting values will come very close to the correct value, since the rock inhomogeneity is completely irregular.

3.1.3. Determination of rock conductivity in a mine gallery. Solution of the respective boundary problem.

The influence of the gallery cavern on the result of a measurement by means of the Wenner method was also studied theoretically. [17]. The results were in good agreement with the measurements.

The problem to be solved is determined by the following data:

$\Delta\Phi = 0$ anywhere in the medium

Φ = const. / R for $r \to \infty$]

$\Phi \approx$ const. $[1/R_1 - 1/R_2]$ near the electrodes,

$\left.\frac{\partial\Phi}{\partial\varrho}\right|_{\varrho=0} = 0$ on the cylinder mantle (R_1, R_2 ... distances from the electrodes).

The resulting solution is a Fourier series:

$$\Phi(a, z, \varphi) = -\frac{I}{2\pi^2 a}\sum_{n=0}^{\infty}\frac{2}{1+\delta_{n,o}}\left\{\int_0^{\infty}\frac{K_n(ma)}{mK_n'(ma)}\sin mh \sin mz\, dm\right\}\cos m\varphi \qquad (3.2)$$

$K_n(ma)$ = modified Bessel functions,

ϱ, z, φ = cylinder coordinates,

h = half the electrode distance

a = radius of cylinder.

This series was computed on an electronic computer for h = 12 m and the angles $\varphi = 0$ and $\varphi = \pi$. The cylinder radius was assumed to be 1 m. The calculation yielded the result that the change in potential trend for the chosen electrode spacing is smaller owing to the cylinder influence, than is the deviation

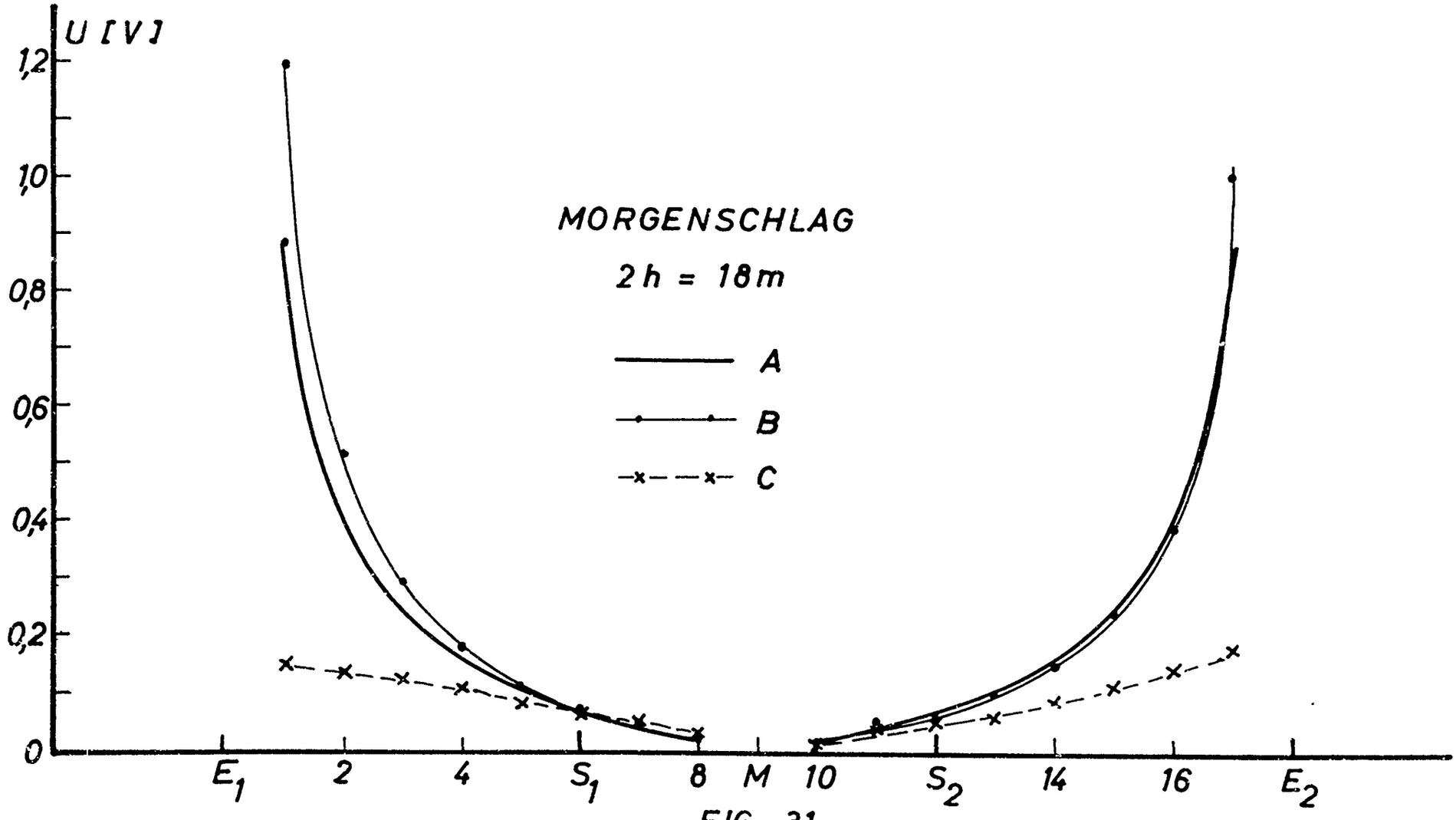
U [V]
1,2
1,0
0,8
0,6
0,4
0,2
0
MORGENSCHLAG
2 h = 18 m
A
B
C
E1
2
4
S1
8
M
10
S2
14
16
E2

FIG. 3,1

of the measured values from the calculated potential trend, due tc the inhomogeneity of rock. Furthermore, the current density was calculated from the expression for the potential and from it the portion of current flowing through a circle with the radius R in the plane z = 0 for different electrode spacings (total current = 1). A comparison of the result with the analogous value for a homogeneous full space suggested the conclusion that the influence of the cylinder can be neglected from an electrode spacing of 2h = 20 m onward.

3.1.4. Results of d-c measurements

Measurements of this kind consistently showed that the distance of probes under the given circumstances (gallery diameter = 1.5 m) must be larger than 7 - 8 m in order to yield a sufficiently accurate result.

Since the voltage is measured by means of a compensating circuit, the relative error of measurement grows smaller the higher the voltage to be measured. Owing to the great probe distance and the resulting high voltage to be measured, the Wenner method proved more suitable than any other conventional arrangement. The electrical conductivity value will only be a mean value because of the inhomogeneity of rock throughout the accessible mines. Here again, the Wenner method proved highly suited, as the influence of small-dimensioned inhomogeneities is comparatively small because of the large probe distance as compared to the electrode spacing. A suitable choice of array will thus yield a value averaged over a large region.

From the discussed values of the U_I/U_{II} ratio, an accurate statement can be made on the inhomogeneity of rock. Especially for small probe distances the values of the U_I/U_{II} ratio scatter considerably (Fig. 3.2). This means that the specific conductivity within a small region changes considerably, whereas the average value determined by means of a four-electrode

configuration is almost constant.

3.1.5. Results of measurements in various mines

With allowance for the discussed conditions, direct-current conductivity measurements were made in numerous mines. The results shall be reviewed briefly hereinafter.

Bleiberg: Shaft Rudolf

In dead rock, values ranging between 0.9 and 1.1 · $10^{-4}\Omega^{-1}m^{-1}$ were measured. The slight difference between the two extreme values suggests that the rock bodies are largely homogeneous, yet the number of measurements made in this connection is too small as to allow a final statement in this direction. Measurements in strongly inhomogeneous ore (zincblende) showed greater fluctuations in conductivity than those in dead rock, the values, however, had the same order of magnitude. Only in comparatively homogeneous zincblende on level 10, the conductivity was much higher (6 · 10^{-2} to 1 · 10^{-3} $\Omega^{-1}m^{-1}$).

Salzgitter, mine Konrad

In this mine, the measurements in ore as well as those in dead rock yielded only slight fluctuations. Rock containing small quantities of ore yielded values between 3 · 10^{-2} and 1 · 10^{-1} $\Omega^{-1}m^{-1}$, measurements in oolithic rock yielded the value 3.1 · $10^{-1}\Omega^{-1}m^{-1}$. The maximum deviations from this value were 9%.

Hannover, potash mine of Empelde

Measurements in dry salt were impossible with the available measuring device because of the low conductivity which was smaller than 1 · 10^{-9} $\Omega^{-1}m^{-1}$.

Siegerland, mines of Friedrich Wilhelm II and Georg

The rock of both mines is strongly inhomogeneous, the ore (siderite) that occurs there is mixed with dead rock. Measurements in dead rock and in ore yielded values of the same order of magnitude; in both cases, however, the values obtained at different sites varied considerably. The measured values

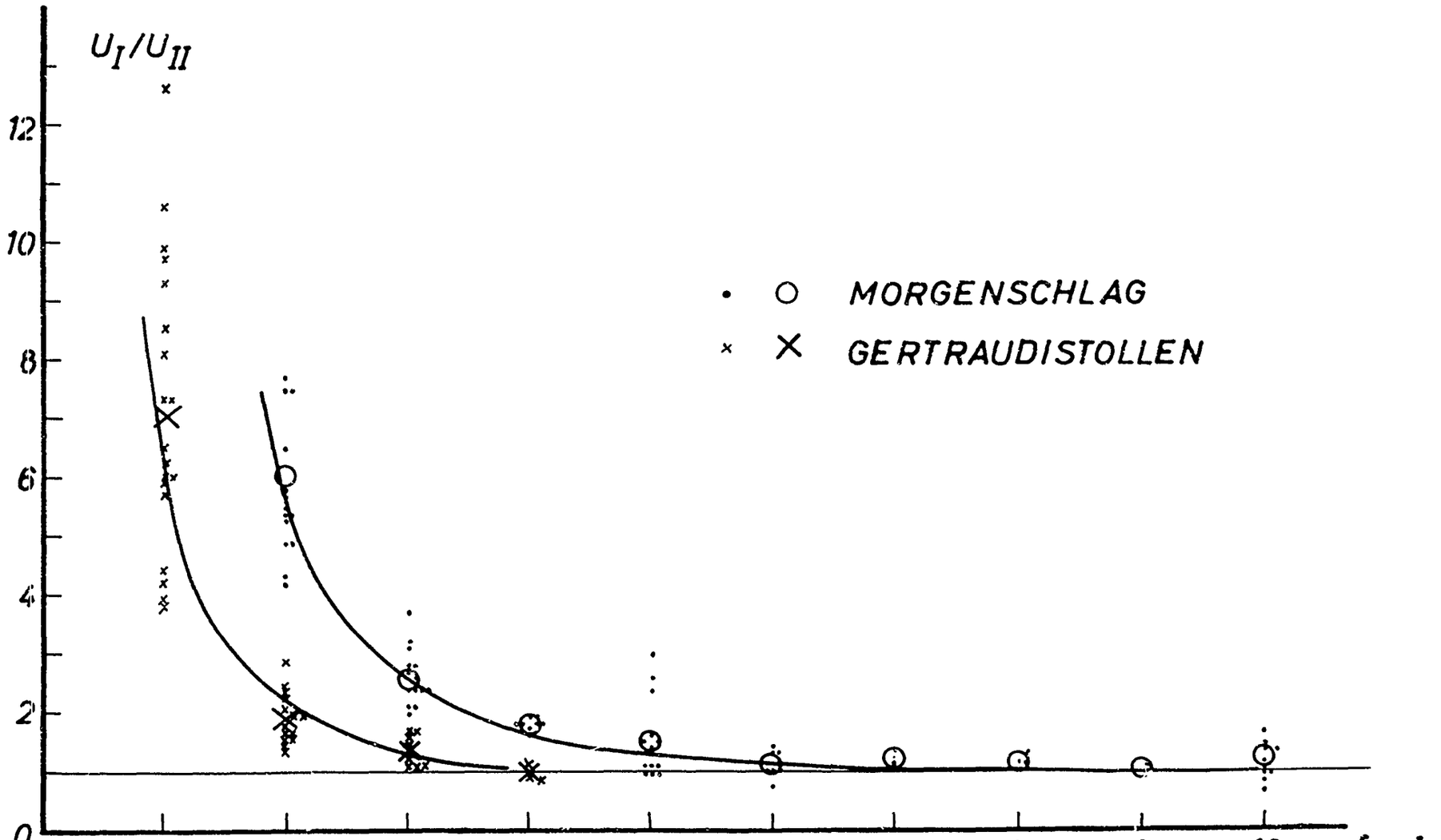
U_I/U_{II}
12
10
8
6
4
2
0
1
2
3
4
5
6
7
8
9
10
a i m l
MORGENSCHLAG
GERTRAUDISTOLLEN

FIG. 3,2

were uniformly distributed over the range between $2 \cdot 10^{-4}$ and $8 \cdot 10^{-3} \Omega^{-1} m^{-1}$.

Heerlen, coal mine of Oranje - Nassau III

Only a small cross section was available for measurements in coal. Therefore the number of measurements is very low.
Results: coal in the direction of seam: $\sigma = 8.0 \cdot 10^{-8} \Omega^{-1} m^{-1}$
coal vertical to direction of seam:
$\sigma = 1.5 \cdot 10^{-7} \Omega^{-1} m^{-1}$.
The slate zone on top of the coal from an electrical viewpoint is largely homogeneous with a conductivity of $5 \cdot 10^{-3} \Omega^{-1} m^{-1}$.

3.2. Frequency dependence of σ and ε of rock

The frequency dependence of the electrical parameters of rock was mainly measured on samples, some measurements were also made on solid rock. The measurements comprised the real part and the imaginary part of the complex dielectric constant:

$$\varepsilon^* = \varepsilon' - i\varepsilon'' . \qquad (3.4)$$

The real part ε' is the relative dielectric constant of the medium, whereas the imaginary part ε'' yields the conductivity according to the following relation:

$$\sigma = \omega \varepsilon_o \varepsilon'' . \qquad (3.5)$$

3.2.1. Measuring device

A Schering-bridge circuit was used for the measurement. This bridge indicates the capacity and loss factor $\tan \delta = \varepsilon''/\varepsilon'$ of the complex unknown impedance.

For the measurements, the specimen was put between the plates of a capacitor. This measuring capacitor can be represented as a parallel circuit of capacitance and resistance. Between the quantities R_p and C_p of the equivalent-circuit diagram and the real part and imaginary part of the complex

dielectric constant there exist the following relations:

$$\varepsilon' = C_p/C_0$$
$$\varepsilon'' = 1/\omega R_p C_0 \qquad (3.6)$$
$$\text{and} \qquad \sigma = \varepsilon_0/R_p C_0,$$

where $\varepsilon_0 = 8.86 \cdot 10^{-12}$ a·sec·v^{-1}m^{-1} is the absolute dielectric constant of the vacuum, C_0 is the capacitance of the measuring capacitor without rock samples.

In most cases it is more favorable to conduct the measurement by means of a substitution method, because of the inevitable wiring capacitance and the restricted measuring range of the bridge. The points that must be taken into account in this connection and the technique of measurement are described in detail in [19] and [25].

3.2.2. Review of possible error sources.

The quantities of ε' and ε'' show a great dependence on frequency and humidity. Various attempts of explaining the frequency dependence have been described in publications. Above all, polarization phenomena on the electrodes are made responsible. It is well-known that two metallic electrodes in a dissociate solution have the same effect as a capacitor of high capacitance, if a current is produced between the plates. The most essential contribution to this capacitance is made by a thin layer on the electrodes, partly owing to a change in concentration on the plates caused by the current, and partly by the resulting concentration potential. For direct current, this capacitance may assume very high values (up to 0.02 f/cm^2). It depends on the electrode material and on the surface of the electrodes. When using alternating current, these processes are of importance only if the ions have time to concentrate on the electrodes during half the period. In his theoretical

studies, Joliffe [26] found that the capacitance decreases with the root of the frequency, using the assumption that the concentration potential alone contributes to the capacitance due to polarization. Various experiments confirm the theoretical result whereas others contradict it. A satisfactory explanation of the frequency dependence of the quantities ε' and ε'' in this manner, however, is impossible.

In a report also dealing with the measurement of electrical rock parameters, Tarkhov [7] states that the frequency dependence of the quantities ε' and ε'' is not observed on rock samples separated from the electrodes by thin mica plates, he therefore assumes the electrode polarization to be responsible for the frequency dependence.

Since the above report has been frequently quoted by numerous authors, the Tarkhov measurement was repeated in order to get an explanation of the influence of electrode polarization on the result of measurement. The sample was separated from the electrodes by two plastic foils. First, the dielectric constant and the loss factor of the insulating material were determined. For ε' the frequency-independent value of $\varepsilon_1' = 1.21$ was obtained, the loss factor being negligibly small.

For the capacitance of a capacitor shown in the diagram, the following value was obtained:

$$C = \frac{\varepsilon_o \cdot F \cdot \varepsilon_1' \cdot \varepsilon_2'}{2d_1\varepsilon_2' + d_2\varepsilon_1'} \qquad (3.7)$$

The fact that the frequency dependence of the capacitance of the measuring capacitor is not observed with the rock sample being insulated from the electrodes by plastic foils, led Tarkhov to the conclusion that the frequency dependence of ε' in rock can be explained by electrode polarization. This conclusion, however, is incorrect. Under the assumption that ε_1' should be constant, the expression (3.7) clearly shows the condition for which the frequency dependence of C vanishes:

$$2d_1 \varepsilon_2' \gg d_2 \varepsilon_1' \ . \qquad (3.8)$$

The measurements described in the present report show that ε' is always very large especially in the range of a great frequency dependence so that the above condition (3.8) is satisfied. Thus we obtain

$$C = \frac{\varepsilon_0 \cdot F \cdot \varepsilon_1'}{2d_1} = \text{const} \ . \qquad (3.9)$$

Measurements of electrical rock parameters on samples may be affected by errors due to possible surface conductivity. Whether or not this is the case has been studied by using a guard ring capacitor for the measurement. In all cases of measurements with and without a guard ring, the same results were obtained; this means that there exists no essential surfa e conductivity. The dependence of electrical parameters on the frequency thus is not due to disturbing effects of measurement, but is an actual property of rock.

3.2.3. Reproducibility of measuring results [16]

As the electrical parameters depend on the frequency and on the water content of the samples, it must be studied how far the humidity values can be reproduced. Since a cooling liquid must be used for drilling and cutting the

samples, the water content frequently varies.

The water content of the samples was determined by weighing, the change in humidity was brought about by long-time storage in an atmosphere of constant humidity. The entire reproducibility examination was made so that the electrical parameters were determined at different humidity values, the water content at first being increased stepwisely, beginning with dried samples, until no weight increase could be observed. Then, the sample humidity was changed in opposite direction, again several measurements of the electrical quantities being made. A good reproducibility of the electrical parameters was obtained in dependence of humidity, but only in thin samples (thickness $\approx$ 4 - 5 mm). In thicker samples, the changes in results are probably due to the fact that the homogeneity of samples regarding their water content is not preserved.

The dependence of the dielectric constant ε' on the humidity decreases as the frequency increases, approaching a constant value. At high humidity values, the frequency dependence is quite distinct, in dry samples, however, it is very low.

The manner in which the conductivity depends on the frequency is hardly affected by the water content. The absolute value strongly depends on the humidity, changes by a factor of 1000 were observed.

3.2.4. Explanation of the frequency dependence by dielectric polarization

An explanation of the observed frequency dependence of the electrical rock properties resulted from a comparison with K.W. Wagner's theory [28] of dielectric polarization.

The most simple mathematical model of dielectric polarization was given by Debye. He assumed the polarization to consist of two portions: one portion P_1 which is assumed

to have the same phase as the external field E, and a portion P_2 with a time displacement by the relaxation time τ with respect to the E field. This model, however, is not sufficient for describing the frequency dependence of electrical data of a number of dielectrics as well as rock. The frequency behavior is represented much better by Wagner's expansion of this theory. For only one relaxation time we obtain the relaxation function

$$\Phi(t) = \frac{k}{\tau} \cdot e^{-t/\tau}, \quad k = \frac{\varepsilon_0' - \varepsilon_\infty'}{\varepsilon_\infty'} \tag{3.10}$$

indicating how the final value of the polarization portion P_2 (not of like phase as E) is attained. Expanding Debye's theory, Wagner assumed that the behavior of numerous dielectrics is determined by an infinite number of relaxation times which are distributed about a dominating relaxation time τ_o ($z = \tau/\tau_o$) according to the probability function

$$W(\tau)d\tau = \frac{k \cdot b}{\sqrt{\pi}} \cdot e^{-b^2 z^2} dz \, . \tag{3.11}$$

Under this assumption we obtain for the relaxation function:

$$\dot{\Phi}(t) = \int_0^\infty \frac{\dot{W}(\tau)}{\tau} \cdot e^{-t/\tau} d\tau = \frac{k \cdot b}{\sqrt{\pi} \cdot \tau_o} \int_{-\infty}^{+\infty} e^{-b^2 z^2 - z - (t/\tau_o) e^{-z}} dz, \tag{3.12}$$

with b being a measure of the width of the distribution function which becomes the wider the smaller b.

For the quantities ε' and ε'' we obtain:

$$\varepsilon' = \varepsilon_\infty' \left[1 + \frac{k \cdot b}{\sqrt{\pi}} e^{-b^2 z_o^2} \int_0^\infty e^{-b^2 u^2} \frac{\cosh (2b^2 z_o - 1)u}{\cosh u} du\right], \tag{3.13a}$$

$$\varepsilon'' = \frac{\varepsilon_\infty' \cdot k \cdot b}{\sqrt{\pi}} e^{-b^2 z_o^2} \int_0^\infty e^{-b^2 u^2} \frac{\cosh 2b^2 z_o u}{\cosh u} \tag{3.13b}$$

with

$$z_o = \ln \omega\tau_o$$
$$u = z + z_o = \ln \omega\tau \ .$$

These equations contain four constants which all have a certain physical meaning: k being a measure of the change in dielectric constant within the frequency range in which a dielectric polarization occurs, ε'_∞ being the dielectric constant of the medium at the upper end of this frequency band, b being a measure of the density of distribution of relaxation times about the prevailing value of τ_o and $f_m = 1/\tau_o$ being the frequency at which the dielectric losses have a maximum. By means of a graphical method described by W.A. Yager [29] which has already been discussed briefly in [4], the results obtained on rock samples have been compared with this theory. Furthermore, the dependence of the constants contained in Wagner's theory on the water content of the samples was studied. A dolomite sample (D III) from the mine of St. Gertraudi whose electrical data were determined for nine different humidity values was treated in detail. It was found out that the studied types of rock have very similar electrical properties, therefore the results obtained for D III shall be discussed first.

3.2.5. Measurements on D III

The nine measurements on the sample DIII were made in two groups: the measurements 1 - 6 were made at low humidity values. It has already been said that the water content was varied by storage in an atmosphere whose absolute humidity was changed. The measurements 7, 8 and 9 followed about two months later. In the meantime, the samples were stored in a damp atmosphere (about 30%) then the water content was increased in the same manner as above (measurements 7 and 8). In order to increase the water content further, the sample

was stored in tap water for another week and then it was superficially dried with blotting paper (measurement 9). Figs. 3.3 and 3.4 show the results of all nine measurements.

Evaluation of the measurements 1 - 8.

The results of the measurements 1 - 9 are shown in table 3.1. All four constants of Wagner's theory could only be evaluated in the measurements 3 - 8, because in Yager's report only a limited range of the parameter values z_o has been dealt with. An exact determination of b and f_m was not possible at the restricted range of measurement of the bridge. For measurement 1, b was approximately estimated and for measurement 2 also f_m.

For b and f_m, a unique dependence on the humidity was obtained: both quantities increase with the water content. This means that the frequency at which the maximum losses occur is displaced toward higher values and that the frequency range in which losses occur becomes narrower.

Also for ε'_∞ and k strong changes were observed owing to the change in the water content of the samples, but a clear relation could not be observed.

Table 3.1

Result of evaluation

Sample D III, C_o = 2.65 pf

d = 6.7 mm

Nr. of measurement	weight	p	b	f_m	ε'_∞	$\varepsilon'_\infty \cdot k$	$\varepsilon'_{\infty exp}$	k
1	34.9518	0	≈ 0.10					
2	34.9523	0.00143	≈ 0.12	≈0.017			9	
3	34.9531	0.00372	0.19	0.36	9.2	256	9.3	27.6
7	34.9542	0.00687	0.20	1.49	17.8	174	10.2	17.0
8	34.9554	0.0103	0.22	9.2	10.0	180	10.2	17.6
4	34.9560	0.0120	0.24	11	11	268	9.6	27.9
5	34.9563	0.0129	0.26	41	16	235	10	23.5
6	34.9569	0.0146	0.29	81	17	200	10.9	18.3
9	35.0157	0.183					10.4	

p = percent by weight of the water contained in the sample.

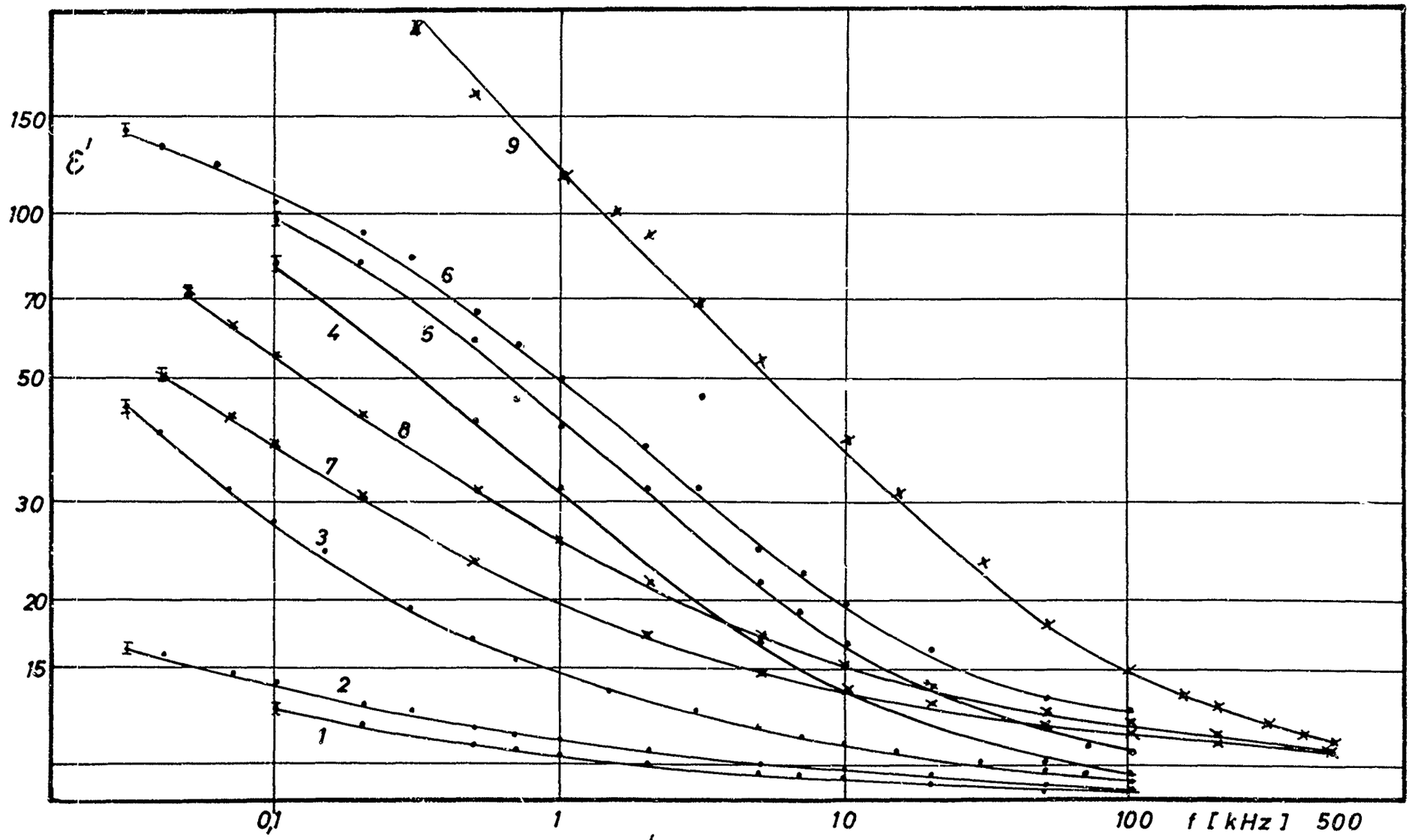

FIG. 3,3 ε', Probe D III, Parameter Feuchtigkeit

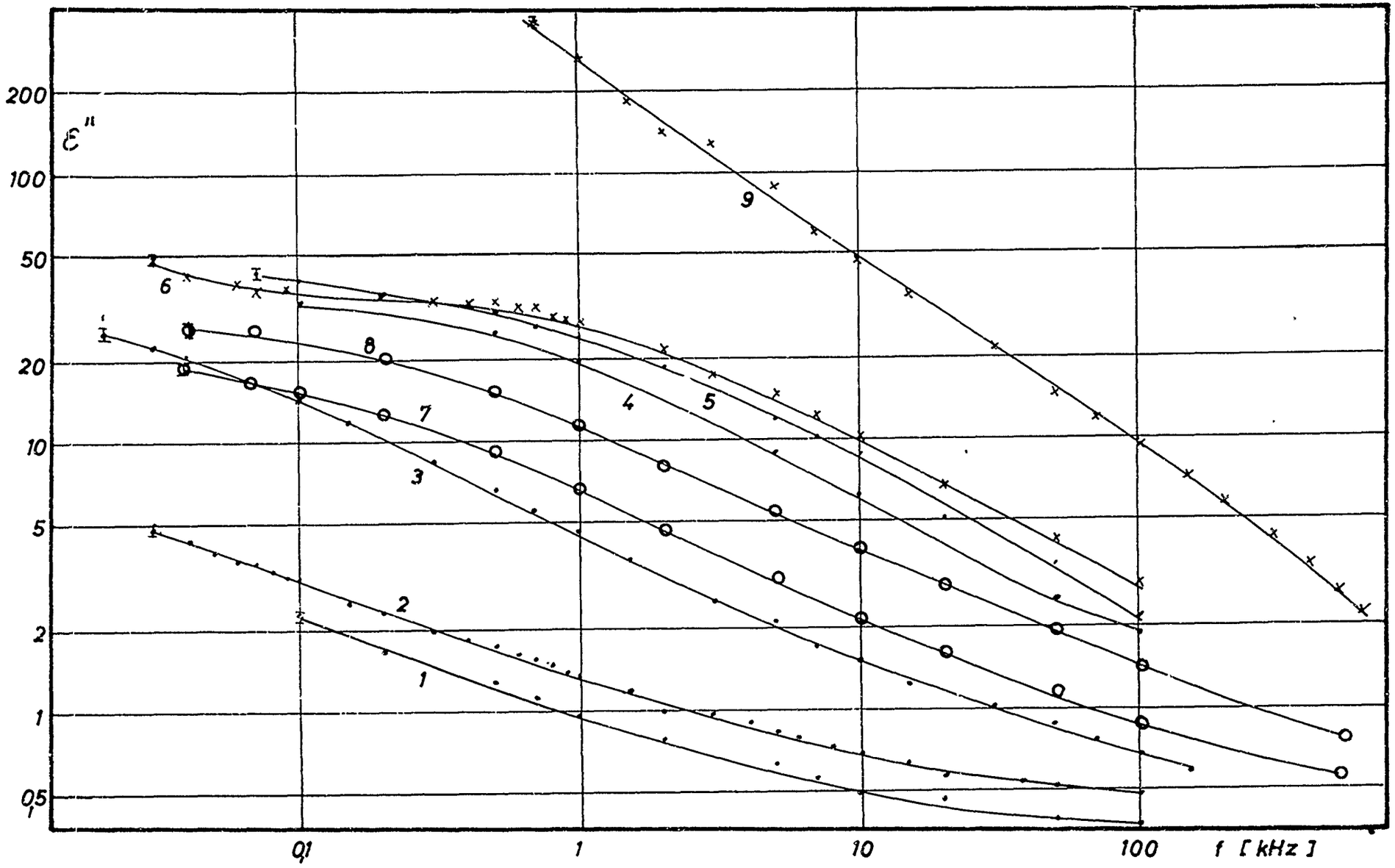

FIG. 3,4 ε'', Probe D III, Parameter Feuchtigkeit

It is striking that ε'_∞ is larger and k is smaller for the measurements 7 and 8 than it is in the other measurements. The reason for this fact so far has not been explained, yet it is quite clear that the long-time storage of the samples used for the measurements 7 and 8 caused a certain change in dielectric constants, whereas the constants which are decisive for the frequency trend of ε'' remain unaffected [3] .

The quality of the reproduction of experimental data by Wagner's theory and the accuracy with which the distribution constant b can be determined were discussed in [4] . Only at very small frequencies, deviations from theory were observed: in general the values are in good agreement.

From the good agreement between the experimental data and the values obtained from Wagner's theory it may be concluded that the dielectric losses observed on the partly moistened rock sample in the concerned frequency range can be explained by polarization phenomena. Because of the complex nature of rock, one relaxation time is not sufficient for describing how the portion of polarization not of like phase as E is attained, but for a satisfactory explanation a distribution of relaxation times about a dominating value must be applied.

Results of measurement 9

The result obtained for measurement 9 on samples largely saturated with water could not be reproduced by Wagner's theory [19]. Since the assumption that the properties of the water contained in the sample are decisive for its electrical properties was quite evident, ε' and ε'' of water were also measured. The values of the mixed body consisting of water and rock (measurement 9) were found to lie between the values of its components. Despite the small portion by volume of water ($\approx$ 0.55%) the frequency dependence of the two quantities is similar to their frequency dependence for water.

This fact and the absence of a frequency dependence typical of Wagner's theory permits the conclusion that the occurring losses are no longer due to dielectric polarization if the pore volume of rock is largely filled with water, but due to line losses, with the charge carriers migrating through the rock without local restrictions. These losses are inversely proportional to the frequency. In solids they contribute essentially to the total losses only at very low frequencies ([30] and [31]).

3.2.6. Measurements on other rock samples

Studies on the frequency dependence of ε' and ε'' were made also in other rock samples: dolomite samples, new red sandstone, ore-containing rock from the mines of Bleiberg in Kärnten, Austria, and Füsseberg in Siegerland, Germany, as well as samples from the oolithic ore of the Konrad mine at Salzgitter.

For the quantities b and f_m a clear dependence on the water content was obtained for all samples, similar to that of D III, not so for the quantities ε'_∞ and k. The highest value of b was obtained for new red sandstone which has the highest porosity of all examined types of rock. In all samples, an essential difference regarding the frequency dependence of ε' and ε'' was observed, depending whether the sample was moistened in parts or saturated with water. Whereas in the first case, an evaluation of the measured results by Wagner's theory was possible, thus explaining the principal contribution to the dielectric losses by polarization phenomena, this was not the case in saturated samples, where the dielectric properties seem to be determined by those of the contained water.

Only the frequency dependence of the values measured on the sample of oolithic iron ore could not be reproduced by a relaxation function for which a distribution of the relaxation

times about a predominating value of τ_o is assumed. Moreover, the form of frequency dependence would suggest the assumption that there exist two different prevailing relaxation times. An exact evaluation in this direction, however, has not been attempted so far. On saturation with water, the frequency dependence of ε' and ε'' of these samples agrees with that for the sample) III so that again the occurring losses on the whole may be classified as line losses [4] .

3.2.7. Measurement of the frequency dependence on solid rock

On solid rock, the resistance R between two metallic electrodes was measured as dependent on the frequency. From it, σ was determined as follows [32]:

$$\sigma = \frac{1}{\pi a R} \cdot \ln \frac{2a}{b} \quad . \qquad (3.14)$$

It must be mentioned that the contact resistance of the electrodes has not been taken into account in the above expression, the measuring technique thus yielding too small an absolute value of conductivity. The impedance between the electrodes was also measured with a Schering bridge. However, only the real part was taken into account, since the earth capacitance of the measuring device can hardly be determined, its elimination by a substitution method is almost impossible when measuring on solid rock. For applying a substitution method, first a balanced bridge is necessary with a hot electrode that is not connected. The measuring bridge here lies opposite a wall with a uniform potential. Balancing with a connected hot electrode, however, leads to an electric-potential gradient along this wall. The earth capacitances of the lines and the instrument casings therefore have different effects on the result of measurement in either case. Since the earth capacitances have the same order of magnitude as the capacitance to be measured, the latter cannot be de-

termined with sufficient accuracy. Yet, the resistance R can be determined as it is independent of the capacitance and of the alignment of lines.

For measurements on solid rock, battery-fed instruments must be used as voltage source and detector. Since one electrode is connected with the bridge screening, the resistance of the electrodes is decreased when using mains-fed instruments owing to the grounding point of the network being connected parallel with it; thus, the existing conditions are not clearly defined.

Results of measurement on solid rock

In all measurements, the dependence of conductivity on the frequency was only small. For measurements on solid rock, the frequency dependence is much smaller than for measurements on saturated samples. Both results, however, cannot be reproduced by Wagner's theory. At low frequencies, σ is consistent with the direct current values measured at the same point.

The absolute conductivity value measured on samples saturated with water is always one to two decades lower than the values measured on solid rock. Since an examination showed that the electrical data of the water used for saturation differ but slightly from those of the water in the mine, the conclusion was drawn from this deviation that the original saturation degree of the samples cannot be restored by submerging the samples in water. A similar conduction mechanism resulted from the similarity in the frequency dependence of samples thus saturated and of solid rock, which differs from the mechanism observed for samples moistened in parts. Whereas for the latter the data of measurement can be well explained by polarization phenomena, a suitable explanation of the frequency dependence for saturated rock (for measurements on samples as well as solid rock) can be given under the assumption that in the frequency range in question line losses constitute the principal portion of all dielectric losses.

4. Mathematical-physical basis for the propagation and excitation of VLF waves

4.1. Introduction

It has already been mentioned that the examination of wave propagation in an underground mine is subjected to numerous restrictions such as, e.g., difficulties of transportation, lack of space, restricted possibilities of setting up antennas, and the points of measurement, etc. Primarily it is of greatest importance to choose the suitable type of antenna for the intended studies. The choice had to be made between linear electric antennas (extended live wire) or current coils. More complex types of antennas and antenna arrays with several elements were not suited, partly because of the small financial means available, and partly because of the above restrictions.

It was possible to record only the near field, since the wavelength λ in the interior of the earth at the used frequencies still has the order of up to 10^4m (depending on the conductivity), whereas below ground the distances of measurement cover only some 10^3m. On the other hand, the distances within which measurements were possible are large as compared to the dimensions of available antennas so that the antenna at these sites could always be looked upon as being a dipole. For this reason, our attention concentrated mainly on the dipole radiation in a conducting medium; its theory was studied in detail and compared to the experiment. A comparison of the performance of an electric dipole with that of a magnetic dipole showed the latter to be superior, a fact which has already been found out by other authors, e.g., [21]. A theoretical explanation of this fact is given in 4.2. Let us only mention that the energy consumption in the immediate

neighborhood of the magnetic dipole is smaller. Therefore preferably frame antennas were used for exciting a VLF field below ground.

In another section, 4.3, the theory of a magnetic dipole embedded in a conducting medium is described in detail. The well-known Hertzian solution for a dipole in free space is expanded for a conducting medium with a complex dielectric constant ε. Problems regarding the validity of the solution for our special case, e.g., allowance for quadrupole radiation, embedment of the dipole in a hollow space, etc. are discussed subsequently. Let me, furthermore mention that comprehensive numerical calculations of the magnetic field strength for wide parameter regions have already been discussed in [1] - [4].

In section 4.3, the space was assumed to be homogeneous and unbounded. In 4.4 the geometry of the actual measuring arrangement is accounted for, and a review is given on the possibilities of calculating the radiation field of magnetic dipoles in a conducting semi-space having a ground - air interface. The studies are made in correspondence with the fundamental studies by Sommerfeld [22] also resulting in a separation of the field into three different portions being due to a direct wave, a wave reflected by the boundary layer, and a ground wave. The latter probably transfers most of the energy over large distances. On checking the experiment, an expansion of the theory to the geometry of a semi-space did not yield any noticeable effects; the space in the range of measurement therefore was assumed to be a full space. Hence, the studies described in [3] were not continued in 1965.

Finally, the conductivity determination also comprised a theoretical estimation of the validity of the Wenner method

when applied to a geometrical position that differs from that of a full space or semi-space. These considerations are summarized in 4.5.

4.2. Comparison between a magnetic dipole and an electric dipole from the viewpoint of energy

First we shall give a brief review of the used electromagnetic parameters

$$i\beta^* = \left[i\omega\mu(\sigma + i\omega\varepsilon)\right]^{1/2} \approx \left[i\omega\mu\sigma\right]^{1/2} =$$

$$= \left(\frac{\omega\mu\sigma}{2}\right)^{1/2}(1 + i) = \beta(1 + i) = \frac{2\pi}{\lambda}(1 + i)$$

β^* = complex propagation constant
σ = conductivity
ε = dielectric constant
ω = angular frequency
μ = magnetic permeability
δ = depth of penetration
λ = wavelength

The wave resistance η is also a complex quantity (vacuum $\eta = \sqrt{\frac{\mu}{\varepsilon}}$).

$$\eta = \sqrt{\frac{\mu}{\varepsilon - i\frac{\sigma}{\omega}}} \approx \sqrt{\frac{i\omega\mu}{\sigma}} = \sqrt{\frac{\omega\mu}{2}}(1 + i) = S(1 + i)$$

Considering these values we obtain the following expressions for an electric dipole in a homogeneous, conducting medium:

$$E_\vartheta = \frac{Il}{4\pi}\frac{e^{-i\beta^* R}}{R}\left[i\omega\mu + \frac{\eta}{R} + \frac{1}{i\omega\varepsilon R^2}\right]\sin\vartheta \qquad (4.1)$$

$$H_\varphi = \frac{Il}{4\pi} \frac{e^{-i\beta^* R}}{R} \left[i\beta^* + \frac{1}{R}\right] \sin\vartheta . \qquad (4.2)$$

For the magnetic dipole:

$$H_\vartheta = \frac{Kl}{4\pi} \frac{e^{-i\beta^* R}}{R} \left[i\omega\varepsilon + \frac{1}{\mu R} + \frac{1}{i\omega\mu R^2}\right] \sin\vartheta \qquad (4.3)$$

$$E_\varphi = \frac{Kl}{4\pi} \frac{e^{-i\beta^* R}}{R} \left[i\beta^* + \frac{1}{R}\right] \sin\vartheta , \qquad (4.4)$$

I = current intensity
K = magnetic flux
l = length of antenna
R, ϑ, φ = polar coordinates in space.

The difference to dipole radiation in vacuo lies in the fact that the term in parentheses in Equs.(4.1) - (4.4) is complex and that furthermore an exponential attenuation occurs. In contrast to air where the antenna may be looked upon as a combination of its ohmic rasistance R_o and its radiation resistance R_R, we here have another energy-consuming resistance, namely that of the surrounding medium. This fact is of much greater influence for an electric dipole than it is for a magnetic one. Calculating the energy flux through a spherical surface with the radius R we obtain for both cases:
electric case:

$$W^e = \frac{8\pi}{3} \left(\frac{Il}{4\pi}\right)^2 \frac{e^{-2\beta R}}{R} \left[\omega\mu\beta + \frac{2S\beta}{R} + \frac{2S}{R^2} + \frac{1}{R^3}\right] \qquad (4.5)$$

(in vacuo $W^e_v = 40\pi^2 \left(\frac{Il}{\lambda}\right)^2$),

or transformed for $R >> \lambda$,

$$W^e_{R>>\lambda} = W^e_v \frac{e^{-\frac{4\pi}{\lambda}R}}{6\lambda} .$$

Magnetic case:

$$W^m = \left(\frac{Kl}{\lambda}\right)^2 \frac{e^{-\frac{4\pi}{\lambda}R}}{6\lambda}\left[1 + \frac{\lambda}{4\pi R}\right] \qquad (4.6)$$

$\left(W_v^m = \frac{\pi}{3\eta}\left(\frac{Kl}{\lambda}\right)^2 \text{ for a vacuum}\right)$.

For $R >> \lambda$ this yields:

$$W^m_{R>>\lambda} = W^m_v \frac{6\lambda}{2\pi} e^{-\frac{4\pi}{\lambda}R} .$$

Let us assume that there exists a radius R_o so that the energy radiation of both dipoles through a spherical surface of this radius is the same. This yields the following relation between the energies W_v^m and W_v^e which thus holds also for the moments Kl and Il of the two dipoles:

$$\frac{W_v^e}{W_v^m} = \frac{18.10^9}{f} \frac{h_e(R_o)}{h_m(R_o)} ,$$

where h_e and h_m express the terms in parentheses in Equs. (4.5) and (4.6), respectively. Under this assumption, the relation $\frac{W^e}{W^m}$ for a second radius R and thus approximately also for $R >> \lambda$ yields:

$$\frac{W^e}{W^m} \approx \frac{h_e(R_o)}{h_m(R_o)} ,$$

an expression which is always smaller than unity.

Owing to ohmic losses, the energy flux of the magnetic dipole is thus weakened by the surrounding medium less than the electric dipole. This fact is discussed in detail in [4].

4.3. The field of the magnetic dipole

The solution of the Maxwell equations for a magnetic dipole at the origin of a polar coordinate system R, ϑ, φ

yields the following expression for the field components:

$$H_R = \frac{Kl}{2\pi}\left(\frac{i\beta^*}{R^2} + \frac{1}{R^3}\right) e^{-i\beta^* R} \cos\vartheta$$

$$H_\vartheta = \frac{Kl}{4\pi}\left(i\omega\epsilon + \frac{1}{\mu R} + \frac{1}{i\omega\mu R^2}\right) \frac{e^{-i\beta^* R}}{R} \sin\vartheta \qquad (4.7)$$

$$E_\varphi = \frac{Kl}{4\pi}\left(i\beta^* + \frac{1}{R}\right) \frac{e^{-i\beta^* R}}{R} \sin\vartheta \,.$$

Since the component E_r vanishes, the field is transversally electric (TE). The electric lines of force describe circles around the z-axis, whereas the magnetic lines of force are located in the meridional plane. As there exists no φ-dependence, all meridional planes are equivalent. At the beginning of 4.2 in connection with the field parameters, approximate expressions have been used for the complex propagation constant β^* and for the complex wave impedance η. These expressions can be used if the imaginary part prevails in the complex dielectric constant

$$\epsilon^* = \epsilon - \frac{i\sigma}{\omega\epsilon_0}$$

so that

$$\epsilon^* \approx -i\frac{\sigma}{\omega\epsilon_0} \,.$$

At a frequency of 3 kcs of the lower boundary of the VLF range, this is the case from about $\sigma \geq 5\cdot10^{-5}$ S/m onward.

The difference between the expressions (4.7) and the wave field in vacuo mainly lies in the fact that an exponential attenuation occurs owing to the complex propagation constant

$$\beta^* \approx \sqrt{\frac{\omega\sigma\mu_0}{\alpha}}\,(1 + i).$$

Furthermore, the complex terms in parentheses of (4.7) bring

about that the radial energy flux through a spherical surface even in the immediate neighborhood of the antenna depends on the radius of this surface; the concept of radiation resistance used for a vacuum thus is useless, since this expression here becomes a position-dependent quantity. It has already been mentioned in 4.2 that this is due to the fact that the energy leaving the antenna is transferred toward infinity by an electromagnetic wave only in parts, whereas part of it is lost already in the neighborhood of the transmitter by heating of the medium. The greater the distance, the smaller the loss portion. In the far field it is given only by exponential attenuation which, because of

$$\beta = \sqrt{\frac{\omega\mu\sigma}{2}}$$

is proportional to the root of frequency and conductivity. At a frequency of 3 kcs, this attenuation factor lies between 10^{-4} and 10^{-2} m^{-1} (cf. [2]), depending on the quantity of conductivity ($\sigma = 10^{-6} - 5 \cdot 10^{-2}$ s/m).

Attenuation is the main reason also for a distortion of the radiation characteristics, again compared with the vacuum case.

The voltage induced in the receiving antenna is proportional to the absolute magnetic field strength at the site of measurement, therefore the measurable quantity is the amount of the expressions in (4.7). We thus obtain the following relation:

$$|H| = (|H_R|^2 + |H_\vartheta|^2)^{1/2} =$$

$$= Me^{-\beta R} \left\{ 4 \cos^2\vartheta \left[\frac{1}{R^6} + \frac{2\beta}{R^5} + \frac{2\beta^2}{R^4} \right] + \right.$$

$$\left. + \sin^2\vartheta \left[\frac{1}{R^6} + \frac{2\beta}{R^5} + \frac{2\beta^2}{R^4} + \frac{4\beta^3}{R^3} + \frac{4\beta^4}{R^2} \right] \right\}^{1/2} \qquad (4.8)$$

M = moment of the antenna.

$$|H_R| = 2Me^{-\beta R}\left\{\frac{1}{R^6} + \frac{2\beta}{R^5} + \frac{2\beta^2}{R^4}\right\}^{1/2} \cos\vartheta$$

$$|H_\vartheta| = Me^{-\beta R}\left\{\frac{1}{R^6} + \frac{2\beta}{R^5} + \frac{2\beta^2}{R^4} + \frac{4\beta^3}{R^2}\right\}^{1/2} \sin\vartheta \qquad (4.9)$$

In these expressions, the displacement current has already been neglected ($\varepsilon \ll \frac{\sigma}{\omega\varepsilon_0}$). The function $|H|$, $|H_r|$, $|H_\vartheta|$ was tabularized in wide parameter ranges as dependent on the distance R and the angle ϑ, being represented in a diagram. In most cases, the curve trend was found to be in good agreement with the measured curves [2], [3] .

In the direct neighborhood of the antenna where the distances of the measuring arrangement are still comparable to the antenna dimensions, the expressions (4.7) are to be looked upon as the first terms of an expansion by spherical harmonics (cf. [2]). Allowing for another term, namely the quadrupole term, we obtain an additional field component:

$$H_R^Q = 3a_Q(3\cos^2\vartheta - 1)\, e^{-i\beta^* R}\left\{\frac{3}{R^4} + \frac{3i\beta^*}{R^3} - \frac{\beta^{*2}}{R^2}\right.$$

$$H_\vartheta^Q = a_Q \frac{3\sin 2\vartheta}{2} e^{-i\beta^* R}\left\{\frac{6}{R^4} \quad \frac{6i\beta^*}{R^3} \quad - \frac{3\beta^{*2}}{R^2} - \frac{i\beta^{*3}}{R}\right\}.$$

If the amount of the field strength is calculated with allowance for these additional expressions, the differences as compared to pure dipole radiation are not noticed from a distance R = 10 m onward. Hence, quadrupole radiation has no essential influence and may thus be neglected.

The effect of the semi-space surrounding the antenna in the form of a secondary field reflected by the boundary layer to the conducting medium can also be neglected. In

accordance with experimental results, a theoretical examination ([2] and [3]) shows no noticeable effects whatsoever.

4.4. Radiation fields of magnetic dipoles under the earth's surface

So far, mathematical and physical studies were made for a transmitting antenna and receiver embedded in a conducting, homogeneous and unbounded medium. This corresponds to reality only so far as the distance between the transmitting and receiving devices in most cases was too small for a reflection by the air - soil interface or the well-known phenomenon of a ground wave being of any importance. Thus, the direct wave was received whose principal term is proportional to $e^{-i\beta^* R}/R^3$. At greater distances (field strengths were recorded up to a distance of 7 km), a deviation of the measured curve from the trend expected in accordance with the theory of (4.3) was evident. The possibility of considering the geometry of a homogeneous semi-space was therefore taken into account and the radiation field of horizontal magnetic dipoles at a certain depth h under a plane surface was calculated by applying the following three methods:

(a) the saddle point method (yields the far field)
(b) a VLF approximations (yields a review of the wave propagation at low frequencies and smaller distances)
(c) by series expansions of the Sommerfeld integrals.

All three methods are characterized by the integral representation of the Hertzian vector. They only differ in the manner the integrals were evaluated. According to Sommerfeld [21] the field is reduced to a two-component vector potential $\vec{\pi} = (\pi_x, 0, \pi_z)$ by the relation:

$$\vec{H}_E = \beta_E^2 \vec{\pi}_E + \text{grad div } \vec{\pi}_E \qquad z > 0$$

$$\vec{H} = \beta^2 \vec{\pi} + \text{grad div } \vec{\pi} \qquad z < 0$$

(the index E refers to the earth).

ad (a):

Satisfying the boundary conditions for z = 0 (earth's surface), we obtain:

$$\pi_{Ex} = \frac{e^{i\beta_E R}}{R} + \frac{i\beta_E}{2} \int_c H_o^{(1)}(\beta_E R \sin\alpha)\, e^{i\beta_E (z+h)\cos\alpha} f(\alpha) \sin\alpha \, d\alpha$$

$$\pi_{Ez} = \cos\varphi \frac{i\beta_E}{2} \frac{\partial}{\partial R} \int_c H_o^{(1)}(\beta_E R \sin\alpha)\, e^{i\beta_E (z+h)\cos\alpha} g(\alpha) \sin\alpha \, d\alpha, \qquad (4.10)$$

where $f(\alpha)$ and $g(\alpha)$ are certain functions obtained from the boundary conditions. The integration path which must encircle a branch line has to be chosen adequately [3] . A saddle point integration [3] yields the following expression for π_E and for the component of the field strength, with the displacement current being neglected (cf. [3]):

$$|H_R| = M \cos\varphi \frac{4\beta_E^2}{\beta^2} \frac{e^{-\beta_E R}}{R^2} \left\{ \left[\frac{\beta^3}{\beta_E} - \beta^2 + \frac{\beta^3}{2\beta_E^2 R} + \frac{6}{R^2} \right]^2 + \left[\frac{\beta^3}{\beta_E} + \frac{4\beta}{R} - \frac{6\beta^2}{\beta_E^2 R^2} \right]^2 \right\}^{1/2}$$

$$|H_\vartheta| = M \cos\varphi \frac{2\beta_E^3}{\beta^4} \frac{e^{-i\beta_E R}}{R^2} \left\{ \left[\frac{\beta^3}{\beta_E} + \frac{3\beta^3}{\beta_E^2 R} - \frac{6}{R^2} \right]^2 + \left[\frac{\beta^3}{\beta_E} - \frac{\beta^4 - 6\beta^2\beta_E^2}{2\beta_E^2 R} \right]^2 \right\}^{1/2} \qquad (4.11)$$

$$|H_\varphi| = \sin\varphi \frac{4\beta_E^2}{\beta^3} \frac{e^{-i\beta_E R}}{R^2} \left\{ \left[\frac{\beta^3}{\beta_E^2 R^2} + \frac{2}{R^2} \right]^2 + \left[\frac{\beta}{R} - \frac{2\beta^2}{\beta_E^2 R^2} \right]^2 \right\}^{1/2},$$

β_o = constant of propagation in vacuo.

The time factor under (a) is assumed to be $e^{-i\omega t}$ in contrast to all other calculations.

ad (b)

Calculation of the dipole field by VLF approximation. The region for which the field strength expressions derived by the saddle point method are valid, is somewhat restricted, since in some parts of the calculation high values of the dimensionless quantity of βR were assumed, equal to those characterizing the far field of a dipole. Thus, the distance from the extreme far field to several wavelengths was covered by separate expressions in order to on the one hand be able to calculate the field strength for all distances, and on the other hand to have a possibility of comparing the near field and the far field which, because of the small distance covered by the measuring transmitter, is of special interest. Starting point again is the vector potential $\vec{\pi}$ which is represented as an integral over the eignfunction $I_o(\lambda\varrho)e^{\mp\mu z}$:

$$\pi_x = M\int_0^\infty e^{\mu(z-h)}\, I_o(\lambda\varrho)\,\frac{\lambda d\lambda}{\mu} + M\int_0^\infty f(\lambda)e^{-\mu(z+h)}I_o(\lambda\varrho)\cdot\lambda$$

$$\pi_z = \int_0^\infty g(\lambda)\, e^{-\mu z}I_1(\lambda\varrho)d\lambda\,\cos\varphi \quad , \qquad (4,12)$$

where $\mu = \sqrt{\lambda^2 - \beta_E^2}$.

With the condition

$$\left(\frac{\sigma}{\omega\,\xi_o}\right)^2 \gg 1$$

being fulfilled, β may be neglected as compared to β_E in the expressions $g(\lambda)$ and $f(\lambda)$, thus yielding:

$$\pi_x = M\int_0^\infty \left[e^{-\mu|z-h|} - e^{-\mu(z+h)}\right]\frac{\lambda I_o(\lambda\varrho)}{\mu}\, d\lambda$$

$$\pi_z = -M \frac{\partial}{\partial x} \int_0^\infty e^{-\mu(z+h)} \frac{2I_o(\lambda \varsigma)}{\mu + \lambda} \, d\lambda \qquad (4.13)$$

The physical situation created by this mathematical approximation can be easily interpreted by the equations (4.13) comprising only fields induced by conduction currents. In the atmosphere such currents cannot exist. Neglecting the displacement currents it follows that the region for which the expressions are valid is restricted to distances within which the conduction currents below ground were mainly induced by primary excitation, not by an induction effect of the displacement currents in the atmosphere, as it would be the case at large ßR, i.e., in the vacuum far field. The resulting expressions are therefore applicable to the near field up to distances of several vacuum wavelengths, thus supplementing the expressions of the saddle-point method in the region of small distances.

The integrals (4.13) can be reduced to well-known integral expressions, thus yielding the following relation for the horizontal components of the magnetic field strength:

$$H_x = M \left\{ ß_E^2 \left[\frac{e^{-iß_E R}}{R} - \frac{e^{-iß_E R'}}{R'} \right] + \frac{\partial^2}{\partial x^2} \left[\frac{e^{-iß_E R}}{R} - \frac{e^{-iß_E R'}}{R'} + \right. \right.$$

$$\left. \left. + \frac{2}{ß_E^2} \frac{\partial^2}{\partial z^2} \frac{e^{-iß_E R'}}{R'} + \frac{\partial}{\partial z} I_o(\alpha) K_o(\gamma) \right] \right\} \qquad (4.14)$$

$$H_y = M \frac{\partial^2}{\partial x \partial y} \left[\frac{e^{-iß_E R}}{R} - \frac{e^{-iß_E R'}}{R'} + \frac{2}{ß_E^2} \frac{\partial^2}{\partial z^2} \left(\frac{e^{-iß_E R'}}{R'} + \right. \right.$$

$$\left. \left. + \frac{\partial}{\partial z} I_o(\alpha) K_o(\gamma) \right) \right] .$$

$$R' = \sqrt{x^2 + y^2 + (z + h)^2} \qquad \alpha = \frac{i\beta_E}{2}(R - (z - h))$$

$$R = \sqrt{x^2 + y^2 + (2 - h)^2} \qquad \gamma = \frac{i\beta_E}{2}(R + (z + h))$$

ad (c):

In the integrals (4.12) of (b), the Hankel functions can be substituted for the Bessel function after changing the interval of integration. Closing the integration path at infinity where a branch line including a pole in the immediate vicinity of the branch point must be avoided, the integration can be reduced to the following integral calculus:

$$U = \frac{e^{-\beta(z+h)\sqrt{ik}}}{\sqrt{ik}}\,\beta \int_c \frac{H_o^{(1)}(\psi\varrho)\psi\,d\psi}{1 - \sqrt{ik}\,M} \tag{4.15}$$

$$K = \frac{\sigma}{\omega\varepsilon_o} \qquad M = \sqrt{\psi^2 - 1}\ .$$

Expanding the nominator which occurs in U, we finally obtain the following expressions:

$$\pi_x = M\left\{\frac{e^{-i\beta_E R}}{R} - \frac{e^{-i\beta_E R'}}{R'} + \frac{ie^{-i\beta R}}{R}\,\frac{e^{-\sqrt{iK}\,\beta(z+h)}}{K}\right\}$$

$$\pi_z = -M\cos\varphi\,\frac{i\sqrt{iK}}{\beta}\,\frac{e^{-i\beta\sqrt{iK}(z+h)}}{\beta}\,\frac{e^{-i\beta R}}{R}\,(1 + i\beta R) \tag{4.16}$$

which lead to the field strength components H_x, H_y and H_z:

$$H_x = \frac{e^{-i\beta_E R}}{R}\left[\beta_E^2 - \frac{i\beta_E}{R} - \frac{1 + \beta_E^2 x^2}{R^2} + \frac{3i\beta_E x^2}{R^3} + \frac{3x^2}{R^4}\right]$$

$$- \frac{e^{-i\beta_E R'}}{R'}\left[\beta_E^2 - \frac{i\beta_E}{R'} - \frac{1 + \beta_E^2 x^2}{R'^2} + \frac{3i\beta_E x^2}{R'^3} + \frac{3x^2}{R'^4}\right]$$

$$+ \frac{e^{-i\sqrt{ik}\,\beta(z+h) - i\beta\varrho}}{\varrho}\left[\beta^2 - \frac{i\beta}{\varrho} - \frac{1 + \beta^2 x^2}{\varrho^2} + \frac{3i\beta x^2}{\varrho^3} + \frac{3x^2}{\varrho^4}\right]$$

$$H_y = \frac{e^{-i\beta_E R}}{R}\left[-\frac{\beta_E^2}{R^2} + \frac{3i\beta_E}{R^3} + \frac{3}{R^4}\right] xy$$

$$-\frac{e^{-i\beta_E R'}}{R'}\left[-\frac{\beta_E^2}{R'^2} + \frac{3i\beta_E}{R'^3} + \frac{3}{R'^4}\right] xy \qquad (4.17)$$

$$+\frac{e^{-\sqrt{iK}\,\beta(z+h)-i\beta\varrho}}{\varrho}\left[-\frac{\beta^2}{\varrho^2} + \frac{3i\beta}{\varrho^3} + \frac{3}{\varrho^4}\right] xy$$

$$H_z = \frac{e^{-i\beta_E R}}{R}\left[-\frac{\beta_E^2}{R^2} + \frac{3i\beta_E}{R^3} + \frac{3}{R^4}\right] x(z-h)$$

$$-\frac{e^{-i\beta_E R'}}{R'}\left[-\frac{\beta_E^2}{R'^2} + \frac{3i\beta_E^2}{R'^3} + \frac{3}{R'^4}\right] x(z+h)\,.$$

This method of numerical evaluation whose validity again depends on the neglegibility of displacement currents, is much simpler than that of (b). The three representations of (a), (b) and (c) are discussed in detail [3] and are compared numerically.

In the theory of conductivity determination by the Wenner method 4.5, it must be found out how far the Wenner arrangement can be applied to the underground geometry, namely a cylindrical cavity. For this purpose, the solution of the following boundary problem for the potential $\bar{\Phi}$ of two electrodes is given in [4] :

$$\Delta\bar{\Phi} = 0 \quad \text{anywhere in the medium}$$

$$\bar{\Phi} = \text{const.}\left[\frac{1}{R_1} - \frac{1}{R_2}\right] \quad \text{near the electrodes,}$$

$$\frac{\partial\bar{\Phi}}{\partial\varrho} = 0 \quad \text{for} \quad \varrho = a$$

$$\bar{\Phi} \to 0 \quad \text{for} \quad \varrho \to \infty\,.$$

For Φ we obtain an integral representation which for $\varrho = a$ assumes the value of

$$\Phi(a,\varphi,z) = - \frac{I}{4\pi a} \sum_{n=0}^{\infty} \varepsilon_n \cos n\varphi \int_0^{\infty} \frac{K_n(m\varrho_o)\, g(z)\, dm}{mK_n'(ma)} \quad .$$

The integrals contained in this expression were evaluated successfully partly by asymptotic representations, partly by numerical calculation, yielding the result that the expressions which are based on the Wenner method [4] are valid for a homogeneous full space if the electrode spacing is sufficiently large as compared to the cylinder radius (= mine gallery).

REFERENCES

[1] 1st Technical Annual Summary Report: On the propagation of VLF waves in solids, 61(052)-490, Dec. 1961

[2] 2nd Technical Annual Summary Report: On the propagation of VLF waves in solids, 61(052)-490, Dec. 1962

[3] 3rd Technical Annual Summary Report: On the propagation of VLF waves in solids, 61(052)-490, Dec. 1963

[4] 4th Technical Annual Summary Report: On the propagation of VLF waves in solids, 61(052)-490, Dec. 1964

[5] Technical Note No. 1: Modeling studies (N. Nessler) 61(052)-490, July 1963

[6] Technical Note No. 2: Attenuation in subsurface signal transmission (H. Scotti and I. Steinacker) 61(052)-490 July 1963

[7] Technical Note No. 3: Determination of rock conductivity from VLF propagation measurements (R. Hommel) 61(052)-490 July 1963

[8] Technical Note No. 4: Horizontal magnetic dipole at the depth h under the earth's surface - Calculation of the radiation field by the integral method (G. Tinhofer) 61(052)-490, August 1963

[9] Technical Note No. 5: Calculation of the dipole field using the VLF approximation (R. Hommel) 61(052)-490 August 1963

[10] Technical Note No. 6: Horizontal magnetic dipole in a conducting earth (G. Tinhofer) 61(052)-490 Nov. 1963

[11] Technical Note No. 7: Propagation of VLF waves in a highly conducting medium (O. Gröbner) 61(052)-490, Dec. 1963

[12] Scientific Report No. 8: Field strength meter for VLF waves (Dr. W. Bitterlich) 61(052)-490 April 1964

[13] Scientific Report No. 9: Current distribution of hemispherical electrodes in a homogeneous semispace (G. Tinhofer) 61(052)-490, May 1964

[14] Scientific Report No. 10: Magnetic dipole antennas for receivers (Dr. W. Bitterlich) 61(052)-490, September 1964

[15] Scientific Report No. 11: VLF measurements in the mine of Bleiberg (O. Gröbner) 61(052)-490, October 1964

[16] Scientific Report No. 12: Reproducibility of measurements of electric rock parameters on specimens (O. Wörz) 61(052)-490, November 1964

[17] Scientific Report No. 13: Determination of rock conductivity in a mine gallery. Solution of the respective boundary problem. (G. Tinhofer) 61(052)-490, April 1965

[18] Scientific Report No. 14: Measuring device for recording the field strength of VLF signals over long periods of time (Dr. W. Bitterlich) 61(052)-490, June 1965

[19] Scientific Report No. 15: On the frequency dependence of the electric parameters of rock (O. Wörz) 61(052)-490 June 1965

[20] Scientific Report No. 16: Bearing technique in the near field of a transmitting dipole in the VLF region (N.Nessler and G. Tinhofer) 61(052)-490, August 1965.

[21] R.K. MOORE, Effects of a surrounding conducting medium on antenna analysis, I.E.E.E. Transactions on antennas and propagation. 1963, No.3.

[22] A. SOMMERFELD, Über die Ausbreitung der Wellen in der drahtlosen Telegraphie. Ann. d. Physik., IV, vol. 28, 1909.

[23] Modeling Studies - Subsurface Propagation, Final Technical Report, 15 March 1962, RA DC-TR-62, ASTIA Nr. AD, SGG Report Nr. 21R-10.

[24] O. GRÖBNER, Thesis, Über die Ausbreitung sehr langer elektromagnetischer (VLF) Wellen im Gestein, July 1964.

[25] O. WÖRZ, Thesis, Über die Dielektrizitätskonstante ε und die Leitfähigkeit σ von Gesteinen, May 1965.

[26] JOLIFFE, C.B., 1923, A study of polarization capacity and resistance at audio frequencies: Physical Rev., v. 22, no. 3, p. 293-302.

[27] TARKHOV, A.C., Widerstand und Dielektrizitätskonstante von Gesteinen in elektrischen Wechselfeldern. VSES. Nauk.-Ozled. Geol. Inst., Mater. Geofiz, No. 12, p. 3-42.

[28] K.W. WAGNER, 1913, Zur Theorie der unvollkommenen Dielektrik, Annalen der Physik, Band 40, 817-855.

[29] W.A. YAGER, 1936, The distribution of relaxation times in typical dielectrics, Physics, v. 7, 434-450.

[30] J.M. STEVELS, Handbuch der Physik XX, The electric properties of glass.

[31] A.B. LIDIARD, Ionic conductivity, Handbuch der Physik XX, p. 311-324.

[32] KRAJEW, Grundlagen der Geoelektrik, VEB Verl. Berlin 1957.

[33] KELLER AND LICASTRO, Dielectric constant and electrical resistivity of natural state cores, Geological Survey Bulletin 1052 - B.

FIRST TECHNICAL ANNUAL SUMMARY REPORT
December 1961

Contents:

SECOND TECHNICAL ANNUAL SUMMARY REPORT
December 1962

Contents:

5. The effect of cavity
6. The transformer and other plans for further theoretical work
7. Plane boundary layer waves
8. Comparison between experiment and theory

III. Experimental part

1. Summary
2. Design and construction of the transmitting station
3. The receiver station
4. Experimental work in the mine
5. Results of the measurements
6. Reception tests with commercial very-long-wave transmitters in the mine
7. On the determination of ε and σ

THIRD TECHNICAL ANNUAL SUMMARY REPORT
December 1963

Contents:

FOURTH TECHNICAL ANNUAL SUMMARY REPORT
December 1964

Contents: